The effect of high sulfate loading on methylmercury production, partitioning, and transport in mining-impacted freshwater sediments and lakes in northeastern Minnesota

A Thesis
SUBMITTED TO THE FACULTY OF
UNIVERSITY OF MINNESOTA
BY

Logan Timothy Bailey

IN PARTIAL FULFILLMENT OF THE REQUIREMENTS
FOR THE DEGREE OF
MASTER OF SCIENCE

Nathan Johnson

February, 2015

© Logan Timothy Bailey 2015

Acknowledgements

This research is part of the Mine Water Research Advisory Panel (MWRAP) project, with funding from the Minnesota Department of Natural Resources Iron Ore and Environmental cooperative research program.

I would like to thank my advisor, Nathan Johnson, for providing me the opportunity to pursue this research, and for the guidance, knowledge, and support he provided during my time as a graduate student. I would also like to thank the members of my thesis committee - Rich Axler, Michael Berndt, and Daniel Engstrom - for their guidance.

This work would not have been possible without the contributions and insight of the following MWRAP research collaborators: Michael Berndt and Megan Kelly from the Minnesota Department of Natural Resources, Nathan Johnson from the University of Minnesota – Duluth, Daniel Engstrom and Jill Coleman-Wasik from the St. Croix Watershed Research Station, and Carl Mitchell from the University of Toronto. I would like to specifically acknowledge the contributions of Carl Mitchell's lab, which handled the mercury-related analysis for this project, and the lab at the St. Croix Watershed Research Station, which performed the sulfide and organic carbon analysis.

I would also like to thank Erin Mittag, Katherine Rasley, Benjamin Von Korff, Amanda Brennan, and Brian Beck for assisting with the field sampling for this project, the Hibbing office of the Minnesota DNR for providing space for lab work during our sampling trips, and my fellow lab mates at UMD, Aaron Mika, Alexandra Dickhaus, Ryan Armstrong, Nick Osmundson, and Kyle Morberg.

Dedication

For my mother Emily, my father Tim, my brother Kyle, and my dear friends Kate and Becca, without your unwavering love and support this thesis would not have been possible.

Abstract

Methylmercury (MeHg) is a highly toxic form of mercury with the ability to bioaccumulate in food webs. The bioaccumulation of MeHg leads to elevated MeHg levels in fish tissue and poses a threat to public health. Thus MeHg concentrations in surface waters – which may be a result of water column MeHg production, or sediment MeHg production and subsequent flux from sediment porewater – are of particular concern. The production of MeHg from inorganic mercury (iHg) is primarily a result of sulfate-reducing bacteria (SRB) activity in anoxic aquatic environments.

Ongoing and historic mining activity on the Mesabi Iron Range (Minnesota, USA) has led to elevated sulfate levels in the downstream waters of the St. Louis River watershed. In an effort to understand the effect of mining-related sulfur-loading on the production and partitioning of MeHg, sediment samples were collected and analyzed from sulfur-impacted and non sulfur-impacted lakes and wetlands within the watershed. Additionally, the water column and inlet and outlet streams of a mesotrophic lake (Lake McQuade) were sampled intensively during summer stratified conditions in order to identify the sources and sinks of MeHg to the lake system and determine the potential for MeHg export downstream.

Results suggest that dissolved sulfide plays a large role in governing MeHg dynamics in sulfate-impacted freshwater sediment. Consistent with previous research, net MeHg production appeared to be inhibited in sediments with dissolved sulfide >60 μM. However, these high concentrations of dissolved sulfide were accompanied by increased

partitioning of MeHg into the porewater phase, potentially increasing the fraction of MeHg available to be transported into surface waters.

Sediment at sulfate-impacted sites was generally characterized by high dissolved sulfide and a low potential for long-term net MeHg production. However, the accumulation of dissolved sulfide in sediment porewaters can be limited by the availability of free labile iron (Fe^{2+}) and consequent iron-sulfide precipitation reactions. In the results presented here, high sulfur-loading at two sites appeared to have consumed the available free labile iron and created conditions which allowed for the accumulation of dissolved sulfide and inhibition of MeHg production in the sediment. However, relatively high sulfur-loading (>100 mg/L) to a third site where iron remains in excess of sulfur in sediment may have led to robust net MeHg production, in absence of inhibitory dissolved sulfide concentrations.

Accumulation of MeHg in the hypolimnion of Lake McQuade occurred during summer 2012 during a time when bottom water sulfate was being consumed. Though some uncertainty remains as to the ultimate source of the MeHg, estimates of MeHg inputs and outputs to the hypolimnion suggest that water column production was a primary source of MeHg to the hypolimnion during the stratified summer months. Following the wet spring months when inputs were dominated by upstream flows, the flux of MeHg across the limnetic surface was estimated to be the primary source of MeHg to the epilimnion during the stratified summer months. However, most of MeHg input to the epilimnion was apparently degraded prior to being exported to the outlet stream. Thus, despite mid-summer accumulation of MeHg in the hypolimnion, the combination of stratification and

substantial degradation in the epilimnion acted to limit export of MeHg out of Lake McQuade.

As a whole, Lake McQuade acted as small net source of MeHg to the surrounding water system during the summer months of 2012. Evidence points to a brief rise in MeHg export immediately following lake turnover in Mid-August due to the release of hypolimnetic MeHg to surface waters during lake mixing.

Table of Contents

List of Tables

List of Figures

List of Figures (cont.)

Appendices:

Chapter 1: Introduction

Study Background

Research Framework

The Mesabi Iron Range in located in the northeastern region of Minnesota, USA, and has been home to iron mining for more than a century (Fig 1.1). One legacy of these mining activities is an expansive landscape of large open pits, tailings basins, and waste rock piles along the northern (upstream) edge of the St. Louis River watershed (Fig 1.2). Sulfate formed by the oxidation of sulfide minerals in the waste rock is transported to downstream wetlands and lakes in headwater tributaries, and eventually into the St. Louis River (Berndt & Bavin 2009). Additionally, pit dewatering activities from active mines regularly discharge water containing sulfate in excess of background levels, resulting in elevated sulfate concentrations in several headwater tributaries (Berndt & Bavin 2009). In many areas, waters with elevated sulfate are often associated with low pH from the production of sulfuric acid; however, significant carbonate geology in the region buffers the pH to above 7 in most mining-influenced waters of the Mesabi Iron Range (Zanko et al. 2008). Iron ore mining remains an important industry in northeast Minnesota, and an expansion of mining activities to target copper, nickel, and PGE-group metals in the Duluth Complex has been proposed in the region.

In order to more fully understand the impact of past, present, and future mining activities on water resources in northeastern Minnesota, the Minnesota Department of Natural Resources (MnDNR) created the Mine Water Research Advisory Panel (MWRAP), a

coordinated research effort involving a number of agencies, institutions, and industrial partners. The intent of MWRAP research is to thoroughly investigate the physical, geochemical, and biological processes that create the link between mine-derived sulfate and the bioaccumulation of methylmercury (MeHg) in downstream ecosystems.

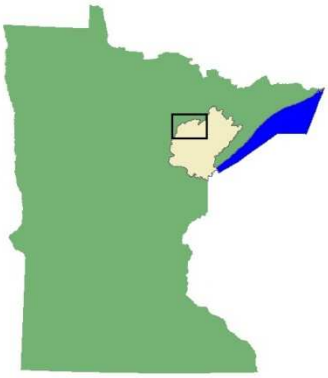

Fig. 1.1. (left) Location of the St. Louis River Watershed in Minnesota, USA. Black rectangle corresponds to location of Fig. 1.2.

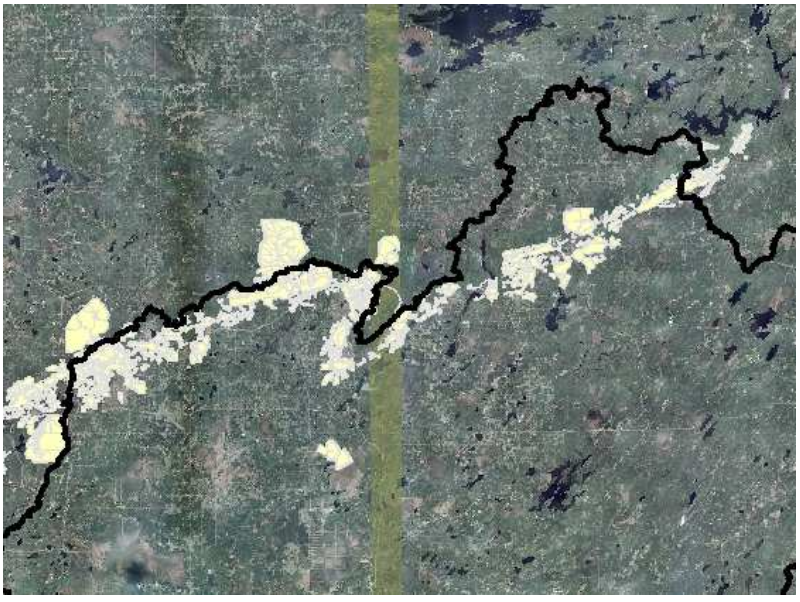

Fig 1.2. Northern edge of the St. Louis River watershed, with lightly shaded regions corresponding to various mining-related landscapes (ore pit, tailings basin, rock stockpile, settling basin, etc.)

Past MWRAP Research in St. Louis River Watershed

Initial research conducted by the MnDNR has provided some context for understanding sulfur and mercury transport and transformations in the St. Louis River watershed (Berndt & Bavin 2009; Berndt & Bavin 2011; Berndt & Bavin 2012b). These studies found that mining activity and the resulting mining-influenced landscape present in the upland reaches of the watershed contribute 20-35 tons/day of sulfate to the St. Louis River (Berndt & Bavin 2012b), enough to account for a majority of sulfate loading to the St. Louis River during many times of the year (Berndt & Bavin 2009). Wetland areas and other reducing zones - such as the anoxic hypolimnia of eutrophic lakes - have been shown to be areas of net sulfate reduction in the St. Louis River watershed (Berndt & Bavin 2012b; Berndt & Bavin 2011).

While net MeHg production within rivers and streams appears to be minimal (Berndt & Bavin 2012a; Berndt et al. 2014), significant net MeHg export from Lake Manganika, a hypereutrophic lake subjected to high sulfate and carbon loading, was observed in summer 2010 (Berndt & Bavin 2011). Mid-summer MeHg concentrations in the outlet stream of Lake Manganika were >2 ng/L, the highest of all sites reported in Berndt & Bavin (2011), and on the high end of surface water observations in several Minnesota rivers studied by Balogh et al. (2006). An investigation of Lake Manganika and several anoxic wetland sites in the St. Louis River watershed found that export of MeHg was not correlated with the net amount of sulfate reduced within a site (Berndt & Bavin 2011), perhaps implying that MeHg production or transport from these areas is influenced by factors other than sulfur cycling. Concentrations of MeHg were strongly correlated with

dissolved organic carbon (DOC) in streams, suggesting that the export of DOC-bound MeHg from lakes and wetlands is a significant source of downstream MeHg (Berndt & Bavin 2012a).

Literature Review

MeHg as an Environmental Toxin of Concern

Mercury (Hg) is a trace metal with known adverse health effects and a pollutant of concern across the globe. Atmospheric deposition of mercury via precipitation is the predominant source of mercury pollution in soils, sediments, and surface waters (Morel et al. 1998). Atmospheric mercury is the result of emissions from anthropogenic sources including fossil fuel combustion, metal production, and waste incineration (Pacyna et al. 2006), as well as natural sources such as volcanic emissions (Pyle & Mather 2003), forest fires (Friedli et al. 2003), and re-emission of mercury from soil and vegetation (Gustin et al. 2000). Anthropogenic sources are responsible for the majority of mercury emissions, having caused atmospheric mercury concentrations to increase by a factor of two or more in the last 100-150 years (Mason et al. 1994).

The form of mercury of greatest environmental concern is methylmercury (MeHg), as it is a highly potent neurotoxin which bioaccumulates in ecosystems (Clarkson 1997). MeHg comprises nearly all (>85%) of the accumulated mercury in fish tissue (Hildebrand et al. 1980; Hsu-Kim et al. 2013) and poses a threat to human health when consumed at rates above the reference dose of 0.1 µg/kg/day (Goyer et al. 2000). As a result, elevated MeHg concentrations in fish tissue have resulted in a statewide fish consumption

advisory in Minnesota and lake impairments across the United States and the world. Because mercury accumulation in biota is known to be dependent on water column MeHg in many situations (Gill & Bruland 1990; Morel et al. 1998), the concentration of MeHg in surface waters used for recreational or sustenance fishing is of particular concern.

Methylation & Demethylation in the Environment

In many aquatic systems, concentrations of MeHg may show little or no correlation with the total amount of mercury present in water or sediment (Benoit et al. 2003). Thus, the processes governing the transformation of inorganic mercury to MeHg (known as methylation) dictate the amount of MeHg produced in the environment. Methylation of inorganic mercury in the environment is the result of microbial activity, primarily the activity of anaerobic sulfate reducing bacteria (SRB) (Compeau & Bartha 1985; Gilmour et al. 1992), although the ability to methylate mercury has also been found to occur in iron-reducing bacteria (Fleming et al. 2006; Kerin et al. 2006) and methanogens (Hamelin et al. 2011). Little was understood about the genetic basis of microbial methylation until Parks et al. 2013 identified a two-gene cluster, genes *hgcA* & *hgcB*, which must be present for a species to be capable of methylation.

The net rate of MeHg production in the environment reflects both the methylation of inorganic mercury (iHg) and the demethylation of MeHg back into inorganic mercury. Demethylation can occur abiotically (Sellers et al. 1996), but has also been shown to result from microbial activity (Oremland et al. 1991). In contrast to methylation, which

is largely driven by SRB, the capability to demethylate is much more widespread and can occur in both aerobic and anaerobic environments (Bridou et al. 2011). The amount of MeHg present in an environment typically reflects the net rate of MeHg production (determined by the methylation rate minus the demethylation rate).

Measurements of methylation and demethylation rates in a particular environment can be accomplished using stable isotope injection techniques (Hintelmann et al. 2000; Mitchell & Gilmour 2008). However, because rates of methylation and demethylation vary seasonally and with changing geochemical conditions, this technique provides an instantaneous measurement that reflects net methylation only under the current conditions. In order to understand net methylation over a longer time frame, %MeHg on the solid phase (the ratio of [MeHg] / [THg]) has been proposed as a proxy to describe recent, time-integrated, net MeHg production (Drott et al. 2008).

Redox reactions follow a sequence based on the "electron tower" of redox couples (Table 1.1). Metabolism of microorganisms will first consume the most energetically favorable electron acceptor, followed by the next most energetically favorable, and so on. This leads to a sequence of reduction zones with depth in aquatic sediment or waters where access to oxygen is limited (Fig 1.3). Most organic-rich, freshwater sediments are characterized by rapid depletion of O_2 (and thus the formation of anoxic conditions) as well as rapid consumption of NO_3^-, Fe^{3+}, and Mn^{4+}, with sulfate reduction typically occurring in the upper 10 cm of freshwater sediments (Holmer & Storkholm 2001). Correspondingly, SRB have been found to be most abundant just below the oxic-anoxic interface in lake sediment (Hintelmann et al. 2000).

Table 1.1. Sequence of microbial mediated redox reduction reactions. Adapted from Stumm & Morgan 1996.

Aerobic Respiration	$CH_2O + O_2 \rightarrow CO_2 + H_2O$
Nitrification	$5CH_2O + 4NO_3^- + 4H^+ \rightarrow 5CO_2 + 2N_2 + 10H_2O$
Nitrate Reduction	$2CH_2O + NO_3^- + 2H+ \rightarrow 2CO_2 + NH_4 + H_2O$
Manganese Reduction	$CH_2O + 2MnO_2(s) + 4H+ \rightarrow CO_2 + 2Mn^{2+} + 3H_2O$
Iron Reduction	$CH_2O + 4FeOOH(s) + 8H+ \rightarrow CO_2 + 4Fe^{2+} + 7H_2O$
Sulfate Reduction	$2CH_2O + SO_4^{2-} + H+ \rightarrow 2CO_2 + HS^- + 2H_2O$
Methanogensis	$2CH_2O \rightarrow CO_2 + CH_4$

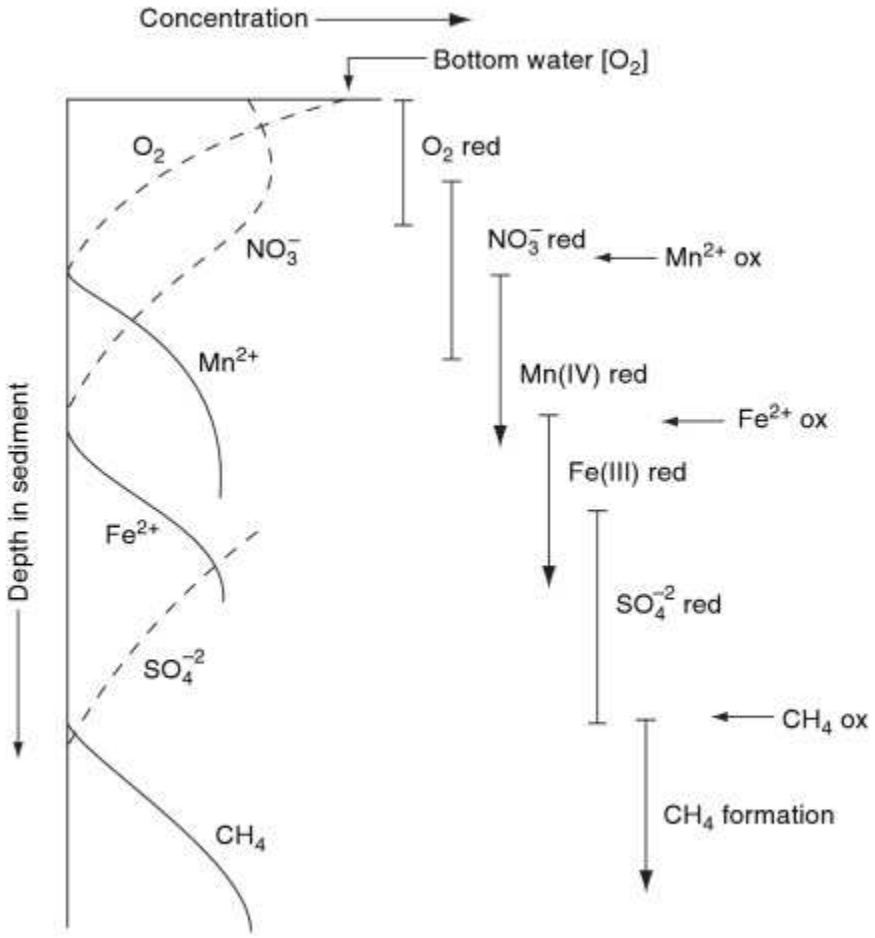

Fig 1.3. Sequence of electron acceptors reduced in sediment profile, following the classic sediment diagenesis model. Figure from Emerson & Hedges 2008.

The metabolism of SRB is dependent on the availability of labile carbon and dissolved sulfate, and the absence of a more favorable electron acceptor. Thus, sulfate has the potential to accelerate the net production of MeHg by promoting the activity of SRB. This relationship of increased MeHg production in response to increased sulfate concentrations has been experimentally observed in sulfate amended wetlands and peatlands (Branfireun et al. 1999; Harmon et al. 2004; Jeremiasson et al. 2006), as well as in the sediment of salt marshes (Langer et al. 2001). Methylation rates have also been shown to be tightly correlated with sulfate reduction rates in laboratory studies (King et al. 1999; King et al. 2000). In addition, depth profiles of methylation rates have been shown to peak at depths corresponding to peaks in SRB population (Devereux et al. 1996).

Mercury Complexes Influencing Methylation & Demethylation

Cellular uptake of inorganic mercury must occur in order for inorganic mercury to be biologically methylated (Choi et al. 1994). Thus, the bioavailability of the inorganic mercury pool in a particular environment is a significant factor determining the potential for MeHg production. The bioavailability of inorganic mercury is determined by the nature of Hg-complexes formed in the vicinity of methylating organisms. The speciation of these complexes is largely determined by the geochemical conditions present. In oxic environments, Hg will typically form complexes with hydroxide or chloride species (Stumm & Morgan 1996), while in anoxic conditions, Hg-complexes with organic matter and reduced sulfur species (Ravichandran 2004). Thus, the geochemical conditions,

particularly the quantity and type of reduced sulfur species, influence the bioavailability of inorganic mercury.

The mechanism responsible for microbial uptake of inorganic mercury remains under debate. Following a model proposed by Benoit et al. (1999), it has been suggested that uptake occurs via passive diffusion of neutral Hg-complexes across the cell membrane. However, it has yet to be confirmed whether this model remains applicable under anoxic, sulfidic conditions (Hsu-Kim et al. 2013). An alternative hypothesis suggests that uptake of inorganic mercury is governed by an active transport process, as has been demonstrated in the sulfate reducer *Desulfovicrio desulfuricans* ND132 (Schaefer et al. 2009; Schaefer et al. 2011).

Complexation of iHg by DOC has been shown to decrease the bioavailability of iHg (Barkay et al. 1997; Ravichandran 2004; Gorski et al. 2008). However, increased concentrations of dissolved organic matter (DOM) have been observed to enhance MeHg production under sulfidic conditions (Eckley & Hintelmann 2006; Graham et al. 2012). Because DOM is believed to be outcompeted as a ligand under sulfidic conditions (Benoit et al. 1999; Benoit et al. 2001c), this enhancement in MeHg production may be a result of DOM acting to stimulate metabolic activity (Eckley & Hintelmann 2006). Alternatively, Graham et al. (2012) proposed that DOM may act to increase iHg bioavailability under sulfidic conditions, and it is often difficult to separate the impacts of DOM's role as a ligand and as a metabolite (Miller 2006; Miller et al. 2007).

In contrast, sulfide has been shown to inhibit Hg methylation at concentrations above 10-100 μM in several studies (Gilmour et al. 1998; Benoit et al. 2001a; Langer et al. 2001; Jay et al. 2002; Drott et al. 2007). This is likely a result of reduced iHg bioavailability rather than a change in microbial activity, since biological sulfate reduction is typically not inhibited below 1000 μM sulfide (Maillacheruvu et al. 1993). Benoit et al. (1999) proposed that this decrease in iHg bioavailability was related to a shift in the predominant mercury species over 10-100 μM sulfide. Other hypotheses have highlighted the influence of colloidal HgS and nanoparticulate HgS on methylation (Zhang et al. 2012) and emphasized the need to consider the role of DOC and sulfide in a kinetic-based approach to Hg speciation (Graham et al. 2012; Hsu-Kim et al. 2013). Irrespective of the underlying mechanism, there is large amount of evidence suggesting that concentrations of dissolved sulfide above 10-100 μM have an inhibitory effect on methylation, which must be taken into consideration when evaluating MeHg in heavily sulfate-impacted freshwater systems.

Methylmercury Partitioning & Mobility

The fraction of total sediment mercury present in the aqueous phase can be described by the linear partitioning coefficient K_D (Equation 1.1).

$$K_D = \frac{Hg_{solid-phase}\left[\frac{ng}{kg}\right]}{Hg_{porewater}\left[\frac{ng}{L}\right]} \quad (1.1)$$

Reported values of $\log(K_D)$ in aquatic sediments have typically ranged from 2.0 – 4.0 for MeHg and 3.5 – 6.0 for iHg (Bloom et al. 1999; Sunderland et al. 2006; Merritt &

Amirbahman 2008; Hammerschmidt et al. 2008). Partitioning coefficients of iHg are typically one to two orders of magnitude larger than those of MeHg under similar conditions, suggesting that iHg has a greater affinity for the solid phase than MeHg (Bloom et al. 1999; Hammerschmidt et al. 2008).

Although the MeHg present in pore fluids represents only a fraction of the total sediment mercury pool, concentrations of dissolved MeHg in porewater are of particular environmental concern. In aquatic sediments, the mobility of aqueous MeHg presents a potential transport pathway from MeHg present in the porewater to the water column. Since there is a strong correlation between water column MeHg concentrations and accumulation of MeHg in biota (Morel et al. 1998), potential sources of MeHg to surface waters are particularly relevant from a public health and water quality management perspective. Because solid-phase mercury is relatively less reactive, microbial methylation occurs primarily in the aqueous phase utilizing dissolved iHg (Benoit et al. 2001b). Thus, the partitioning behavior of iHg can also influence porewater MeHg concentrations.

Geochemical conditions can have a significant impact on partitioning of both MeHg and iHg. Several studies have observed a positive correlation between sediment total organic carbon (TOC) and $\log(K_D)$ of both iHg and MeHg, which translates to a higher fraction of mercury remaining on the solid phase (Hammerschmidt et al. 2004; Sunderland et al. 2006; Hammerschmidt et al. 2008; Gray & Hines 2009), while porewater DOC was negatively correlated with $\log(K_D)$ of iHg and MeHg (Watras 1995b; Gray & Hines 2009). Increases in porewater sulfide concentrations have been shown to lower K_D for

iHg (Bloom et al. 1999; Merritt & Amirbahman 2007; Hammerschmidt et al. 2008) as well as MeHg (Hammerschmidt et al. 2008).

Thus, the quantity of the potentially mobile fraction of bioaccumulative mercury in sediment – porewater dissolved MeHg – is related to a complex set of interrelated geochemical factors: (1) organic carbon on the solid phase, which can bind with mercury and hold it on the solid phase, resulting in lower porewater fractions of both iHg and MeHg in more organic-rich sediments; (2) DOC in porewater, which can both act as a ligand, pulling iHg into the aqueous phase and thus creating a larger pool of mercury available for methylation, and act as a metabolite, stimulating microbial activity which, in areas of active sulfate reduction, may result in increased MeHg production; (3) dissolved sulfide, which, in its role as a ligand for iHg, can enhance iHg solubility but also potentially decrease iHg bioavailability at sulfide concentrations above 10 -100 μM, and in its role as a ligand for MeHg, can increase the fraction of MeHg in the aqueous phase.

Mercury Behavior in the Water Column

Mercury pollution in lakes is particularly significant from a public health perspective, as lakes are often popular fishing destinations and fish consumption is the primary pathway of MeHg exposure in humans (Mergler et al. 2007). There are many possible source and sink pathways of MeHg to and from a lake water column, including atmospheric deposition, hydrologic sources (i.e. inlet streams, outlet streams, direct near-shore runoff, and groundwater seepage), and flux from sediment. Additionally, lake waters can act as both a source and sink of MeHg through production and degradation of MeHg within the

water column. The relative importance of each source and sink mechanism can vary considerably from lake to lake depending on various interrelated hydrologic and geochemical conditions (Rudd 1995). The net effect of these conditions will determine whether a lake acts as net source or sink of MeHg to the surrounding watershed.

Most atmospheric deposition of mercury occurs in the form of inorganic divalent mercury (Morel et al. 1998); however precipitation can still be a measurable source of MeHg to lakes. The amount of MeHg deposited via precipitation differs from region to region, with deposition rates reported in literature ranging from 0.39 – 4.0 mg/ha/yr (Rudd 1995). Direct runoff from surrounding terrestrial areas has been observed to be only a minor source of MeHg to lakes (Sellers et al. 2001; Hines & Brezonik 2007). Loading from upstream sources can vary widely depending on the size and landscape composition of the upstream catchment (Hurley et al. 1995). Several studies have identified wetlands as areas of significant contributors of MeHg to downstream waters (St. Louis et al. 1994; Rudd 1995; Hurley et al. 1995; Branfireun 1996).

Diffusive flux of MeHg from sediment porewater can be a major source of MeHg to lakes and other stagnant surface waters (Langer et al. 2001; Hines et al. 2004; Hammerschmidt et al. 2004). The magnitude of diffusive flux out of the sediment is determined by MeHg concentrations in both the sediment porewater and the overlying water column, as well as physical characteristics of the sediment. Flux of MeHg from sediment porewater in a salt marsh was found to be greater at locations subjected to higher sulfur-loading (Langer et al. 2001). On the other hand, other studies have found little correlation between flux of MeHg and methylation potential of the sediment

(Hammerschmidt et al. 2008), suggesting that partitioning of MeHg off the solid phase and into porewater may be as significant as methylation potential in determining diffusive MeHg flux. Reported estimates of MeHg flux from sediment have ranged from 8 – 174 pmol/m^2/d in saltwater harbor sediments (Hammerschmidt et al. 2004; Hammerschmidt et al. 2008), 390 pmol/m^2/d in high sulfate salt marsh sediment (Langer et. al 2001), and 0.67 pmol/m^2/d in the sediment of a low-sulfate freshwater bog lake (Hines et al. 2004). It has also been suggested that advective flux from groundwater may be a source pathway of MeHg to surface water systems (Stoor et al. 2006).

Production of MeHg within the water column may also be a significant source of MeHg to lakes (Watras et al. 1995a; Eckley et al. 1995; Hines & Brezonik 2007; Watras et al. 2005), though other studies have suggested that in-lake MeHg production has little effect on total MeHg levels (Korthals & Winfrey 1987). Water column methylation in lakes has been shown to occur predominantly in the anoxic hypolimnia of productive lakes, in areas of active sulfate reduction (Furutani & Rudd 1980; Eckley & Hintelmann 2006). Production of MeHg has been observed in the anoxic zones of deep ocean waters (Cossa et al. 2009; Blum et al. 2013), and is also believed to occur within anoxic microenvironments present in oxic marine waters (Monperrus et al. 2007; Sunderland et al. 2009). Periphyton associated with macrophytes have been identified as sites with an especially high potential for MeHg production and bioaccumulation in tropical aquatic systems (Guimarães et al. 2000; Mauro et al. 2002; Correia et al. 2012).

The formation of anoxic hypolimnia in lakes is related to the thermal stratification of lake waters, and commonly occurs in northern temperate lakes, particularly during summer

months. The temperature-density driven isolation of lake bottom waters from the lake surface prevents the bottom waters from being replenished with oxygen, often leading to a depletion of oxygen in productive lakes. In an anoxic hypolimnion, bacteria begin to utilize electron acceptors following the same sequence as in anoxic sediment. Because reduction of iron and manganese represents a relatively minor contribution to carbon metabolism in most lake systems (Matthews et al. 2008), the zone of sulfate reduction begins almost immediately below the oxic-anoxic boundary in lakes with low nitrate loading. Methylation rates have been observed to be greatest at depths corresponding to active sulfate reduction, and the depth of peak methylation rate has been found to follow the depth of the oxycline as it rises and falls in the lake through the summer (Mauro et al. 2002; Eckley et al. 2005; Eckley & Hintelmann 2006).

Accumulation of MeHg has been observed in the hypolimnia of several freshwater lakes over summer months (Watras et al. 1995a; Regnell et al. 1997; Eckley et al. 2005), suggesting that the anoxic zones of a lake can act as a net source of MeHg. However, hypolimnetic MeHg is often sequestered in the bottom waters due to the thermal-density gradient and must be transported through the thermocline in order to reach the epilimnion or downstream waters. This relative isolation between limnetic layers can create a situation where robust MeHg accumulation may occur in the hypolimnion, yet the lake as a whole still acts as a net sink for MeHg (Sellers et al. 2001).

Degradation of MeHg in the water column can occur in two ways: abiotically through photodegradation at the water surface (Sellers et al. 1996; Sellers et al. 2001), or as a result of microbial demethylation (Oremland et al. 1991). Unlike Hg methylation, which

is largely confined to biologically-driven production in anoxic waters, demethylation of MeHg can result from the activity of both aerobic and anaerobic bacteria and therefore can occur in all areas of the water column (Bridou et al. 2011). Studies of demethylation in anoxic waters have reported low rates of demethylation – e.g. Compeau & Bartha (1984) (0.02 d^{-1}) and Eckely et al. (2005) (0.03 – 0.05 d^{-1}) – or failed to measure rates above the detection limit (Eckley & Hintelmann 2006; Acha et al. 2012). Aerobic bacteria have been proposed as important demethylators (Winfrey & Rudd 1990; Matilaninen & Verta 1995; Schaefer et al. 2004), though little research has been done to quantify microbial demethylation rates in oxic lake waters, and other studies have suggested that photodegradation may instead be the primary pathway for MeHg degradation in surface waters (Sellers et al. 2001; Hammerschmidt & Fitzgerald 2006; Lehnherr et al. 2012). Thus, although water column degradation may be a significant sink of MeHg in lakes, the relative importance of microbial demethylation and photodegradation is not yet fully understood.

Study Objectives

Mining activity in the Mesabi Iron Range has contributed to elevated sulfate in the St. Louis River and several upstream tributaries, with sulfate concentrations as high as 1000 mg/L observed in mining-impacted tributary waters (Berndt & Bavin 2009). Evidence of a link between sulfate reduction and MeHg production (Compeau & Bartha 1985; Gilmour et al. 1992) has raised concerns about the impact of past, present, and future mining activities on the region's water resources. The scope of mining activities in the region, and size of the sulfur loading associated with these activities (>20 metric tons per

day, Berndt and Bavin 2012b), necessitates thorough and timely management solutions. However, interactions of sulfur and mercury cycling are complex and can be influenced by a number of geochemical and hydrological conditions. Previous MeHg-related research in the sulfate-impacted St. Louis River has focused on measurements of stream chemistry in the river's main stem and mining- and non-mining- influenced tributaries. This study expands previous research by moving into the anoxic zones of wetlands and lakes impacted by elevated sulfate in order to investigate the role of sulfate in driving mercury-related processes and to identify with more precision where MeHg is produced and how it might be exported downstream.

The high sulfate concentrations that characterize mining-impacted tributaries in the St. Louis River watershed exceed the range of sulfur levels upon which much of literature in freshwater mercury-sulfur geochemistry is based. Research of mercury-related processes at similarly high sulfur concentrations has mostly been limited to brackish or saltwater systems (e.g. research work in the Florida Everglades, Chesapeake Bay). The effects of sulfate-loading on MeHg production in freshwater sediments has been investigated through sulfate addition experiments in several studies (Branfireun et al. 1999; Harmon et al. 2004; Jeremiasson et al. 2006), however most of these studies have been conducted at comparatively lower sulfate concentrations (<100 μM). Thus, a greater understanding of mercury-related processes in heavily sulfate-impacted freshwater systems is needed in order to address mercury and sulfur cycling in the mining-impacted areas of the St. Louis River watershed.

Anoxic wetlands and the anoxic zones of lakes have been identified as areas of MeHg production in the St. Louis River watershed, however the ability of these areas to export MeHg downstream is of greatest concern. Budgets of MeHg on watersheds and freshwater lakes have been conducted in several studies, however the relative importance of various sources and sinks of MeHg to a watershed have been shown to vary greatly depending on the hydrologic characteristics of the waterbody and the surrounding watershed (Rudd 1995). Investigating MeHg export in environments favorable for MeHg production and determining the role of sulfate in these transport processes will help identify areas that may be sources of MeHg to downstream waters.

Proposed expansion of mining activity in the region has raised the possibility of new and long-term sources of sulfur loading, some of which could potentially be discharged to low-sulfate waters and sediments. The effect of high sulfate loads on these systems may be different than the effect of similar loading to historically sulfate-impacted water bodies. Thus, an understanding of mercury processes in sites "transitioning" from low historic sulfate loading to high sulfate loading may be useful for evaluating and managing new and/or long-term sulfur loading from future mining activity. To gain insight on potential MeHg production and export to downstream systems in a "transition" site, intensive water column sampling and a MeHg mass balance analysis was conducted in Lake McQuade, which has recently been subjected to intermediate sulfur loads in excess of historic loading levels.

Within the context of a larger initiative to understand MeHg production, transport, and bioaccumulation that is described in the reports and literature associated with the MN

DNR's Mine Water Research Advisory Panel (MWRAP), this thesis focuses on "*Geochemical factors influencing methylmercury production and partitioning in sulfate-impacted lake sediments"* (Chapter 2) and "*Sources and Sinks of Methylmercury in Lake McQuade"* (Chapter 3). Investigation of MeHg production and export from sulfur-impacted wetlands, also performed as a part of this study, is presented in a separate report (Johnson et al. 2014).

Chapter 2: Geochemical factors influencing methylmercury production and partitioning in sulfate-impacted freshwater sediments

Site Description

Surficial sediment from two lakes and two wetlands that receive a range of sulfate loads (5 – 600 mg/L surface water sulfate) were investigated in this study. All sites were located in the upper reaches of the St. Louis River watershed in northeastern Minnesota, USA, an area influenced by historic and ongoing iron and taconite mining activity (Fig 2.1).

Lake Manganika (N 47.49°, W 92.57°) is a hypereutrophic lake of maximum depth ~25 feet and surface area ~0.67 km^2, subjected to high sulfur and organic carbon loading from two inlets: discharge from a taconite pit dewatering operation, and a stream receiving discharge from a local municipal wastewater treatment plant. Surface water sulfate concentrations range from 200-600 mg/L and excessive algal growth has historically been observed from May to September. Thermal stratification at 8-10 feet below the water surface was observed in Lake Manganika from spring until late summer 2012, leading to sulfide accumulation in bottom waters to concentrations of 1-2 mM.

Lake McQuade (N 47.42°, W 92.77°) is a mesotrophic lake with a maximum depth ~20 feet and surface area ~0.68 km^2. Lake McQuade had surface water sulfate concentrations between 30-120 mg/L in 2012; however, consistent with sulfate concentrations in the inlet river, surface water sulfate observations exceeded 300 mg/L during summer 2013. Lake McQuade also became stratified in early summer (limnetic surface between 8-10

feet), with an anoxic hypolimnion present until mid-September. Bottom water sulfide concentrations remained below 20 μM in Lake McQuade during summer 2012.

The Long Lake Creek wetland (N 47.42°, W 92.56°) is a ~0.14 km^2 sulfate-impacted sub-boreal peatland located downstream from mining activities with typical sulfate concentrations in the open-water between 200-300 mg/L. However in some years, including 2011 and 2012, fall season pumping of mine-pit water increased sulfate concentrations to above 500 mg/L at the wetland inlet between the months of September and November. The periphery of the LLC wetland is dominated by typical fen/bog vegetation (sedges, woody shrubs, and mosses) that grades to a cattail (*Typha*) margin fringing an open-water pool through which Long Lake Creek flows.

The West Two River wetland (N 47.465°, W 92.77°) is a large sedge peatland comprised of organic-rich sediment and peat, fringing the northern margins of a small pond. The pond is situated on a side-tributary of the West Two River with little mining activity in upstream areas. Open water sulfate concentrations in the wetland pond are typically less than 5 mg/L.

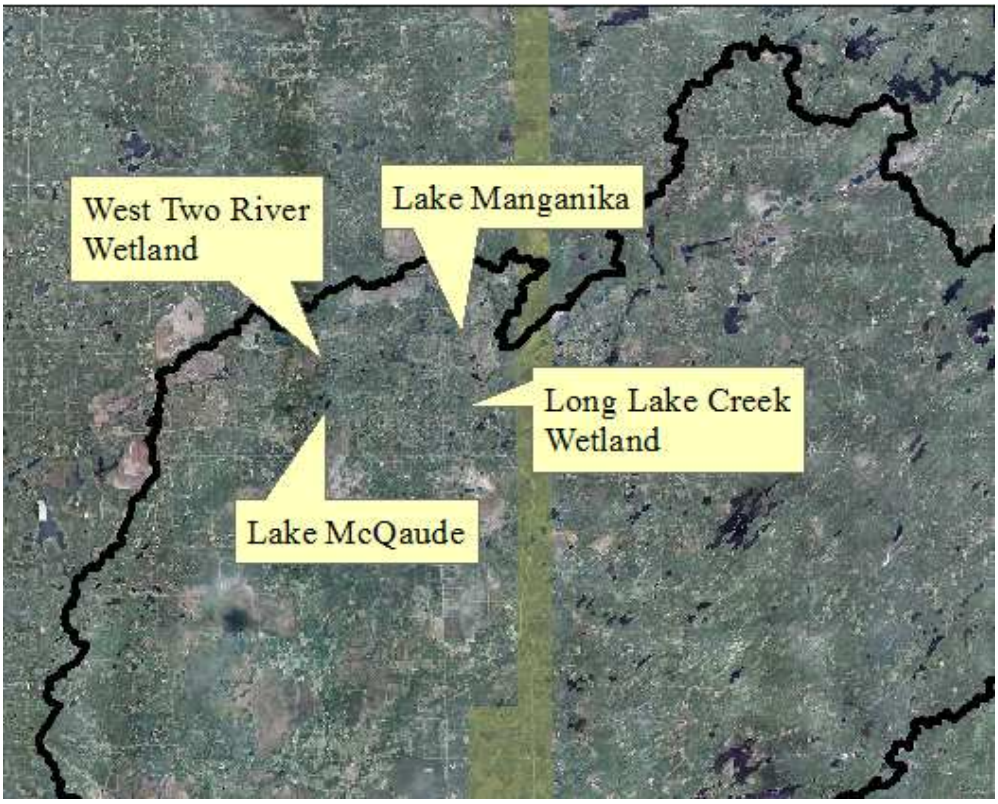

Fig 2.1. Location of field sites in the St. Louis River watershed, Minnesota, USA

Methods

Sampling Design

Field samples were collected on four sampling trips, occurring in the months of May, July, and October 2012 and June 2013. Due to the late persistence of winter conditions in 2013, the June 2013 sampling date reflects late spring conditions (similar temperature and hydrology to May 2012). Sediment was collected from lake sites at two locations: a deeper basin location (>15 feet) and a shallower basin location (8-10 feet). The shallower locations corresponded with depths very near the limnetic surface through most of the summer, while the deeper locations were within the anoxic hypolimnion throughout most of the summer. The deeper sampling locations were labeled as 'Mng 1' and 'McQ 1'; the shallower sampling locations were labeled as 'Mng 2' and 'McQ 2'. At wetland sites, sediment was collected from a single location in the near shore open water area with little emergent vegetation (2-3 feet water depth at Long Lake Creek, 4-6 feet at West Two River).

Sampling Methods

At each sample location, replicate sediment cores were collected using a HTH Teknik gravity corer (70-mm polycarbonate core tube) and composited to obtain sufficient sediment volume for both solid-phase analysis and pore-water extraction. One set of replicate cores from each location was sub-sectioned into 0-2, 2-4, & 4-8 cm depth intervals and composited to concurrently investigate depth trends. Two additional sets of

cores at each location were composited to create samples that comprised only the top 4 cm of sediment.

In order to minimize oxidation of anoxic sediments during sample collection, handling, and allocation, oxygen-free nitrogen gas (N_2) was used to purge the head space in collection jars while the cores were being extruded and composited, and collection jars were immediately placed in an oxygen-free environment upon completion of core sectioning. Porewater was extracted from sediment samples using a 5 cm rhizon sampler (tension lysimeter with polyvinylpyrrolidine/polyethersulfone membrane, Seeberg-Elverfeld et al. 2005) with a nominal filter size of 0.2 microns attached to acid-washed, mercury and oxygen-free, evacuated borosilicate glass serum bottles. Samples for analysis of solid-phase constituents were allocated from homogenized samples and preserved independently of porewater samples and remained in oxygen free conditions for the entirety of the allocation and preservation procedure.

Chemical Analysis

Zinc-preserved sediment samples were stored frozen and analyzed for acid-volatile sulfide (AVS) at the St. Croix Watershed Research Station (SCWRS) using standard method 4500-S^{2-} (Eaton 2005). Weakly extractable metals (WEM), including Fe, Al, Mn, Zn, Ca, K, Mg, & Na, were extracted from freeze-dried sediment samples in 0.5N HCl, heated to 80-85 ºC for 30 minutes and quantified on a PE SCIEX ELAN 6000 ICP-Mass Spectrometer. For analyses using wet sediment samples, measured concentrations were normalized to the sediment dry weight, which was determined by quantifying

sediment bulk density and water content (ASTM D2216-10). Sediment total carbon (TC) and total nitrogen (TN) was measured on a Thermo Electron Flash EA 1112 Elemental Analyzer using freeze-dried sediment samples. Ignition tests were used to quantify sediment organic and mineral composition (ASTM D7348).

Porewater samples for anion analysis were acidified with concentrated HCl to pH<3 and bubbled with N_2 gas for 15 minutes to remove dissolved sulfide. An occasional non-acidified duplicate sample was also used for chloride analysis. Sulfate (SO_4^{2-}), nitrate (NO_3^-), phosphate (PO_4^{2-}), and chloride (Cl^-) were quantified via ion chromatography (Method 300.1, USEPA 1997) on a Dionex ICS 1100 system. Porewater samples for dissolved sulfide ($H_2S + HS^-$) analysis were filtered into an evacuated serum bottle preloaded with ZnAc and NaOH preservative and quantified using an automated methylene blue method (4500-S^{2-} E, Eaton 2005). Porewater ferrous iron (Fe^{2+}) was quantified photometrically using the Phenanthroline Method (3500-FeB, Eaton 2005). Porewater ammonium was analyzed colorimetrically (SCWRS laboratory) using the phenolate method (Lachat QuikChem method 10-107-06-1-B). Dissolved organic carbon (DOC) and dissolved inorganic carbon (DIC) were quantified on a Teledyne-Tekmar Torch Combustion TOC Analyzer. Porewater DOC samples were analyzed for specific ultraviolet absorption (SUVA) at 254nm (Weishaar et al. 2003) and spectral slope ratio (Helms et al. 2008) on a Varian Cary 50 scanning UV-Vis spectrophotometer to provide an indication of aromaticity and relative molecular weight, respectively. Correction for iron color (Poulin et al. 2014) was not included when analyzing DOC samples in this study. Porewater temperature, pH, and ORP were measured in undisturbed cores with

electrodes (Thermo Fisher Orion pH meter with automatic temperature correction and platinum electrode with Ag/AgCl reference).

Methylation and Demethylation Rate Potentials and Mercury Analysis

Potential rates for Hg methylation and MeHg demethylation were assessed via enriched stable isotope incubation techniques (Hintelmann et al. 2000; Mitchell & Gilmour 2008). Potential methylation and demethylation rate constants were measured by injecting sediment cores with a mixture of stable isotope-enriched $^{200}Hg^{2+}$ and $Me^{201}Hg^{+}$ (94.3% $^{200}Hg^{2+}$ and 84.7% $Me^{201}Hg^{+}$) and equilibrated with anoxic, filtered pore water. Sediment cores were spiked through injection septa spaced at 1 cm intervals on the core tubes using a 100 μL gastight syringe. Cores were incubated at in-situ temperatures for approximately 5 hours, and frozen upon completion of the assays. Generation of enriched $Me^{200}Hg^{+}$ and loss of enriched $Me^{201}Hg^{+}$ was measured via ICP-MS detection.

Sediment samples for mercury analysis were freeze-dried and homogenized. For total mercury (THg) analysis (including detection of enriched isotopes), samples were microwave digested in concentrated nitric acid. Digestates were diluted with deionized water and ~0.5% by volume of BrCl was added to oxidize all Hg in the sample to Hg(II). After allowing the sample to react overnight, THg was characterized following the USEPA method 1631 (USEPA 2002) using a Tekran 2600 automated Hg analysis system, with the final detection of Hg by ICP-MS. The Tekran 2600 system automates Hg reduction by addition of $SnCl_2$ and dual gold trap amalgamation of vapor. Rather than standard detection via fluorescence spectroscopy, the Tekran is hyphenated to the

ICP-MS, and the amalgamated Hg vapor is released into the ICP-MS for isotope detection. Determination of MeHg was accomplished by isotope-dilution techniques (Hintelmann & Evens 1997) using samples distilled according to the methods of Horvat et al. (1993), but with the addition of a different enriched MeHg spike ($Me^{199}Hg$). All analyses used calculations from Hintelmann & Ogrinc (2003) to account for the <100% enrichment of isotopes in calculating enriched ^{200}Hg and ^{201}Hg concentrations for THg and MeHg, as well as in calculating ambient THg and MeHg levels from the dominant naturally occurring ^{202}Hg isotope.

Porewater samples for mercury analysis were preserved by adding 0.5% by volume trace metal concentrated HCl. Samples were analyzed for THg according to USEPA method 1631 (USEPA 2002), using a Tekran 2600 automated mercury analyzer, and for MeHg by isotope-dilution ICP-MS following distillation, as explained above for sediment samples.

Clean hands protocols were utilized for all mercury samples throughout sample handling, preservation, and analysis. Filtration blanks were routinely collected and analyzed and typically had less than 0.3 ng/L THg and 0.01 ng/L (detection limit) MeHg.

Final concentrations of mercury isotopes were used to calculate methylation and demethylation rates (Equation 2.1 & 2.2). The ratio of k_{meth}/k_{demeth} was used as a metric for in-situ net MeHg production rate. Inorganic mercury (iHg) concentrations were calculated by subtracting the MeHg concentration from the THg concentration for both dissolved and sediment phases.

$$k_{meth} = \frac{[Me^{200}Hg]/[T^{200}Hg]}{incubaction\ time} \tag{2.1}$$

$$k_{demeth} = \frac{([T^{201}Hg] - [Me^{201}Hg])/[T^{201}Hg]}{incubation\ time} \tag{2.2}$$

Data Analysis

In order to characterize mercury concentrations and geochemical parameters in surficial sediment at each sampling location, a weighted average of measurements from three independent core samples (each comprised of several composited cores) between 0-4 cm depth was used (Equation 2.3). This approach applies to all reported values in both solid phase and porewater samples except for those related to the direct analysis of depth dependent trends.

$$\frac{\frac{1}{2}(A_{0-2} + A_{2-4}) + B_{0-4} + C_{0-4}}{3} \tag{2.3}$$

Because the timescales for methylmercury production and partitioning are not known with certainty, equilibrium conditions in the sediment cannot be assumed. In place of true equilibrium partitioning constants, an apparent partitioning coefficient (K_D^*) is reported for mercury species (MeHg and iHg), defined by the ratio of in-situ solid-phase concentration (per kg units) to in-situ porewater concentration (per liter units) (Equation 2.4).

$$log\ K_D^*(A) = log\left(\frac{[A]_{solid}}{[A]_{pw}}\right) \tag{2.4}$$

Results & Discussion

Geochemical Context of Sites

Total, solid-phase mercury concentrations in the lake and wetland sediments studied were between 50 and 300 ng/g – typical of unimpacted lakes in the region (Wiener et al. 2006) – except at the shallow site of Lake Manganika (Mng2), which had by far the highest mercury levels, averaging 773 ng/g (Fig 2.2a). Solid phase MeHg concentrations typically comprised less than 2% of the solid phase total mercury present in the sediments (Fig 2.2a & 2.2d). Porewater concentrations typically ranged from 2 – 12 ng/L for THg and 0.1 – 2 ng/L for MeHg (Fig 2.2b & 2.2c).

Analysis of depth-interval samples showed that the highest concentrations of MeHg were present in the top 4 cm of sediment. Of the MeHg in the surface 8 cm of sediment, 73% of all porewater MeHg and 66% of all solid phase MeHg was in the top 4 cm (data not shown). In contrast, approximately half of all THg in the surficial 8 cm was present in the top 4 cm in both the porewater (58%) and the solid phase (47%). A similar vertical distribution of mercury species observed in another northern Minnesota lake was interpreted to be reflective of net demethylation over time in depositional lakes (Hines et al. 2004). Since total mercury was distributed relatively evenly with depth in the sediment, the processes leading to net MeHg production must exert a greater influence in the top 4 cm in order for the predominance of MeHg to be present in the top 4 cm. These depth profile observations establish that a characterization of each sample over the 0-4

cm interval captures the most important processes influencing mercury dynamics in the surficial sediments investigated in this study.

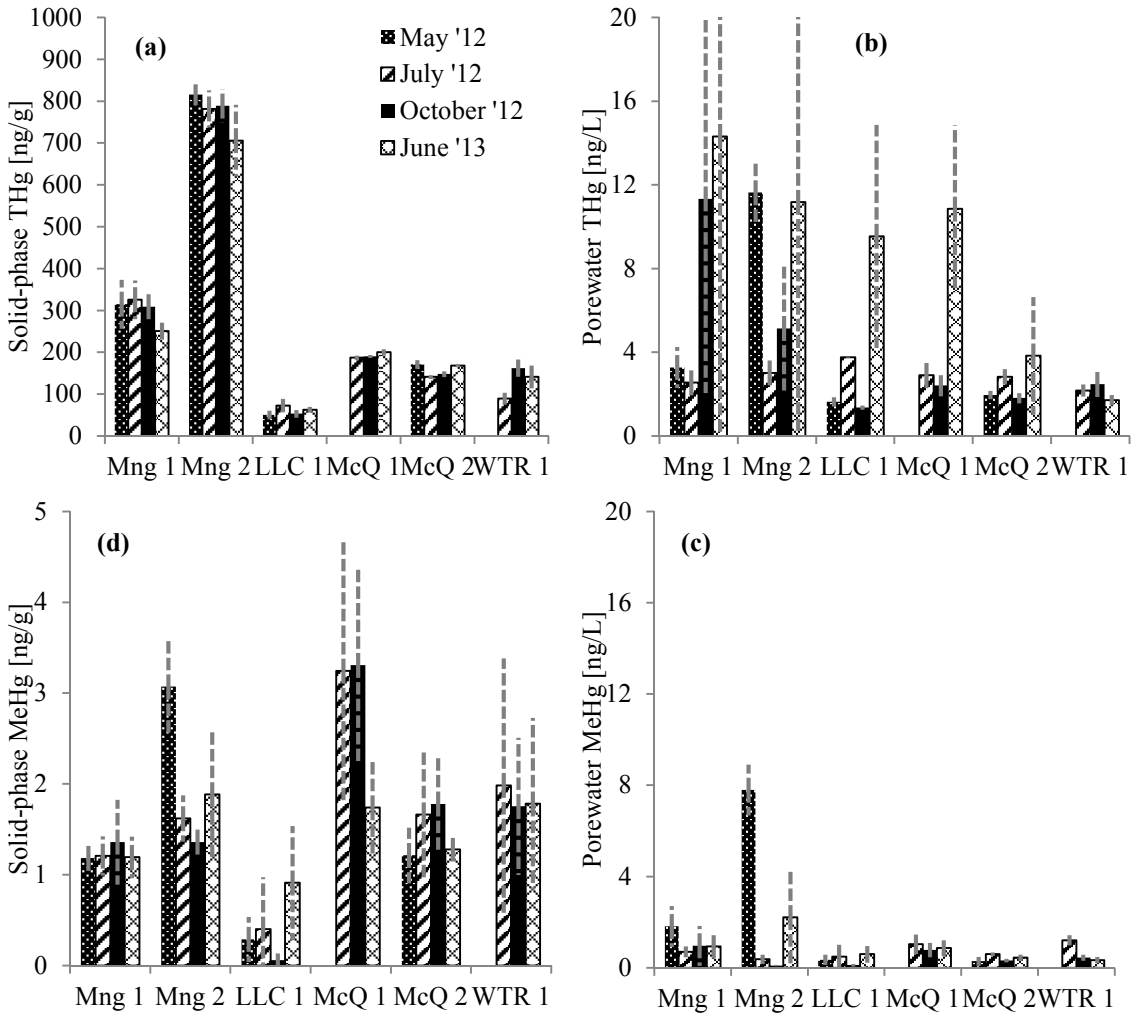

Fig. 2.2(a-d). Mercury concentrations in the surficial sediments at each sampling location (clockwise from top left): (a) total mercury in the solid phase, (b) total mercury in porewater, (c) MeHg in porewater, (d) MeHg in the solid phase. Gray dashed lines represent one standard deviation of triplicate samples.

Concentrations of porewater sulfide reflect a combination of the degree of sulfur loading, net sulfate reducing activity, and the amount of iron available to complex sulfide. Dissolved sulfide concentrations were elevated in the sediment porewaters of both sites historically subjected to heavy sulfur loading, exceeding 1200 µM in Lake Manganika sediments and 200 µM in the open water wetland sediments of Long Lake Creek. By contrast, dissolved sulfide in Lake McQuade and West Two River sediments was observed between 2 and 22 µM (Fig 2.3). Surface water sulfate concentrations of McQ and LLC (Chapter 3 of this thesis; Johnson et al. 2014) were often comparable, though a large difference in porewater sulfide was observed (Fig 2.3).

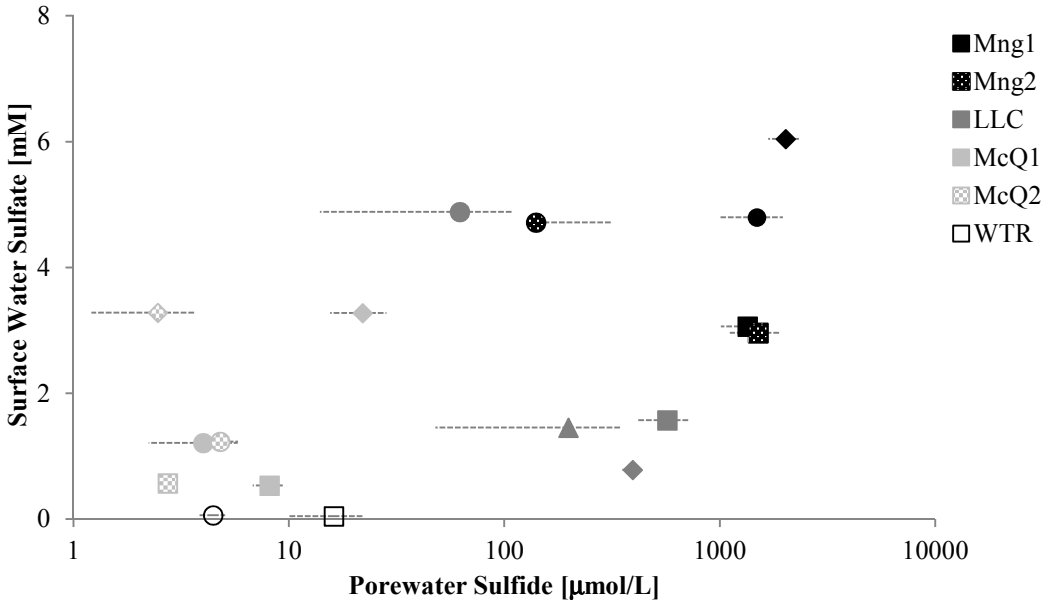

Fig 2.3. Surface water sulfate v. porewater sulfide (log scale). Symbols are shaded according to the degree of sulfur loading at the corresponding site, with the least sulfur-impacted (WTR) represented with no shading (open symbol) and the most sulfur-impacted shaded black (Mng). Symbol shape corresponds to the time of sampling: May 2012 (triangle), July 2012 (square), October 2012 (circle), and June 2013 (diamond). Gray dashed lines represent one standard deviation of triplicate samples.

Molar ratios of sediment iron and AVS (Fe_{WEM}:AVS) ranged between 0.75 and 1.1 in sediments from Mng and LLC and 2.0 to 4.1 in sediments from McQ and WTR (Fig 2.4). These differences are consistent with a net sulfur accumulation from historic sulfur-loading at Mng and LLC and a depletion in the pool of available free iron able to remove sulfide from sediment porewaters. Porewater observations were consistent with precipitation reactions between aqueous sulfide and iron species (Fig 2.5). Porewater ferrous iron concentrations were less than 10 µM at sites with low Fe_{WEM}:AVS ratios but frequently exceeded 50 µM at sites with higher Fe_{WEM}:AVS ratios (Fig 2.4). This suggests that in sites with less historic sulfur loading, iron remains in stoichiometric excess with respect to sulfur and that the availability of uncomplexed Fe^{2+} prevents sulfide from accumulating in the porewaters (Fig 2.5) as a result of sulfate reduction.

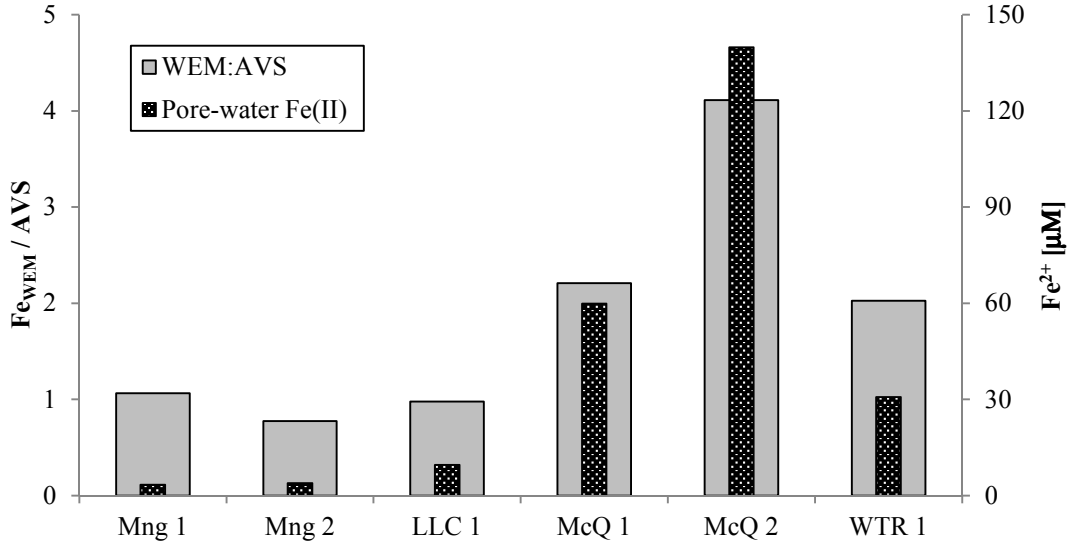

Fig. 2.4. Ratio of extracted Iron to AVS, overlaid with porewater iron (II) concentrations. From July 2012 data.

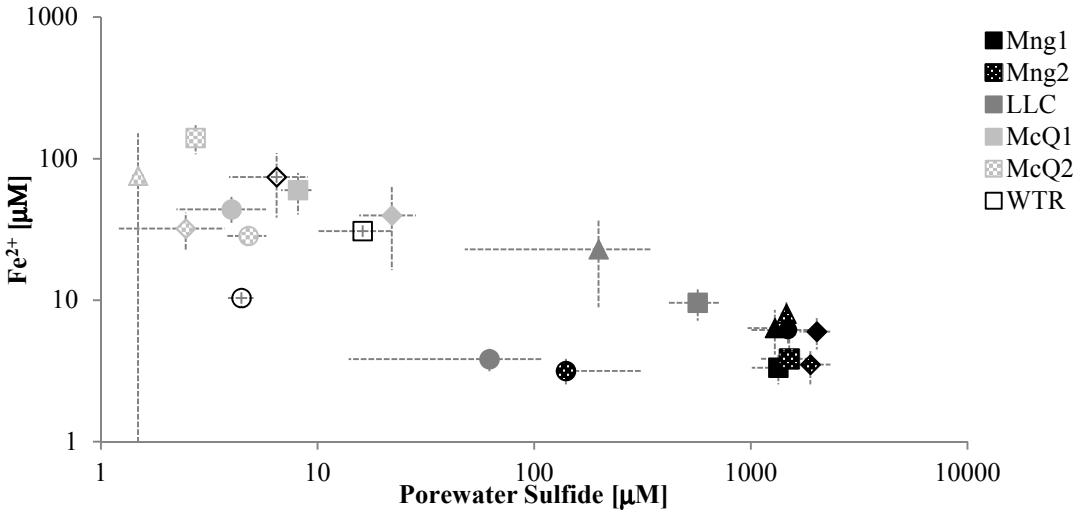

Fig 2.5. Concentrations of porewater ferrous iron and porewater sulfide. Symbols are shaded according to the degree of sulfur loading at the corresponding site, with the least sulfur-impacted (WTR) represented with no shading (open symbol) and the most sulfur-impacted shaded black (Mng). Symbol shape corresponds to the time of sampling: May 2012 (triangle), July 2012 (square), October 2012 (circle), and June 2013 (diamond). Gray dashed lines represent one standard deviation of triplicate samples.

Factors Influencing Methylmercury Production

Previous research has suggested that solid phase %MeHg ([MeHg]/[THg]) is an effective proxy for long term methylation potential in sediments (Drott et al. 2008). In the wetland and lake sediments of this study, solid phase %MeHg was positively correlated with net methylation potentials determined experimentally using stable isotopes (R^2=0.46), implying that the short-term net methylation rates quantified during this study reflect historic net methylation rates (Fig 2.6). When compared to other sites in this study, the low-sulfur wetland, WTR, had consistently high net methylation potentials relative to %MeHg in the solid phase, suggesting that the high instantaneous rates of net methylation measured in WTR sediment may not be reflected in a longer-term accumulation of MeHg in the solid phase.

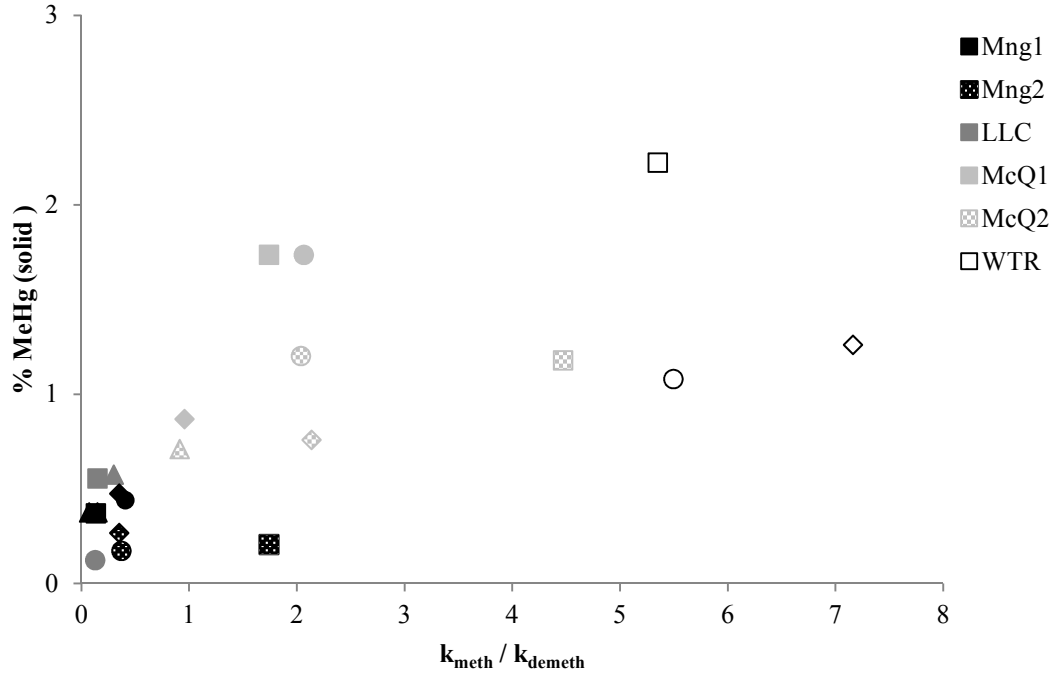

Fig. 2.6. Comparison of solid phase %MeHg, which represents long-term methylation potential, with experimentally measured net methylation rates. Symbols are shaded according to the degree of sulfur loading at the corresponding site, with the least sulfur-impacted (WTR) represented with no shading (open symbol) and the most sulfur-impacted shaded black (Mng). Symbol shape corresponds to the time of sampling: May 2012 (triangle), July 2012 (square), October 2012 (circle), and June 2013 (diamond).

The relationship between coincident measurements of %MeHg on the solid phase and dissolved sulfide in porewater (Fig 2.7) was consistent with previous research suggesting that net MeHg production is inhibited by high levels of dissolved sulfide (Benoit et al. 2001b). At sulfide concentrations <25 µM, solid-phase %MeHg ranged from 0.7% – 2.2% and appeared to increase with increasing sulfide. The June 2013 sample at McQ1 was the only exception to this trend, though surface water sulfate concentrations in Lake McQuade were higher than 300 mg/L at this time. At sulfide concentrations >60 µM, solid phase %MeHg was consistently below 0.6% with one exception (LLC in June 2013) and no trend was apparent between solid phase %MeHg and sulfide.

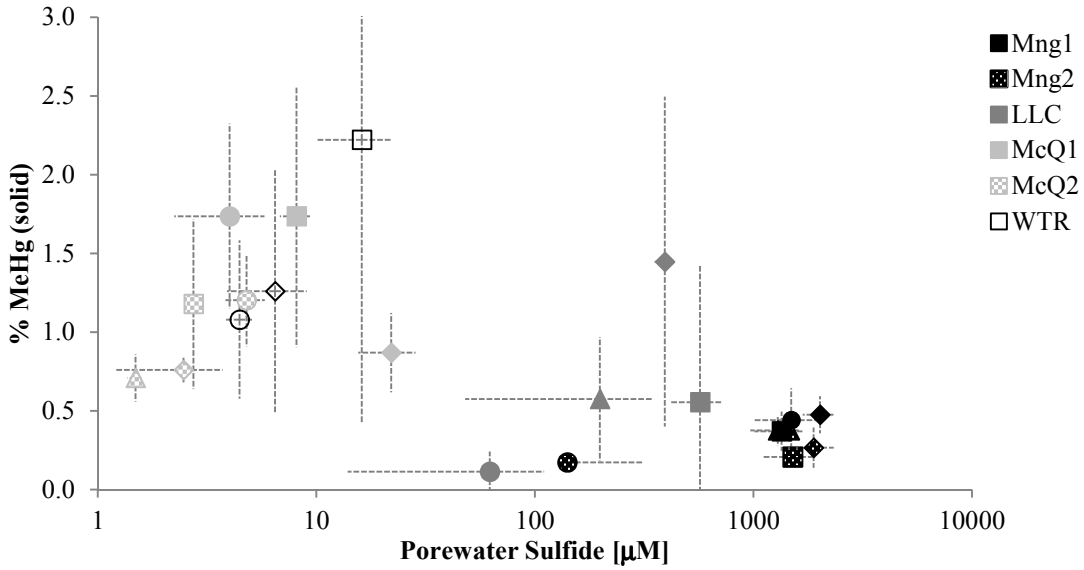

Fig. 2.7. Solid phase %MeHg, which represents long-term methylation potential, across a range of porewater sulfide concentrations. Symbols are shaded according to the degree of sulfur loading at the corresponding site, with the least sulfur-impacted (WTR) represented with no shading (open symbol) and the most sulfur-impacted shaded black (Mng). Symbol shape corresponds to the time of sampling: May 2012 (triangle), July 2012 (square), October 2012 (circle), and June 2013 (diamond). Gray dashed lines represent one standard deviation of triplicate samples.

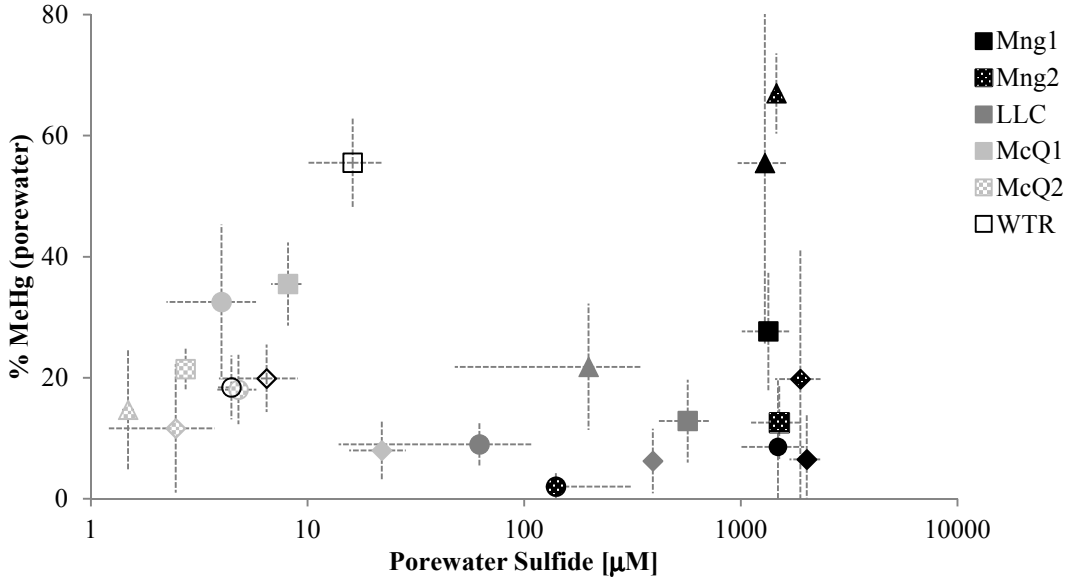

Fig. 2.8. Porewater %MeHg values across a range of porewater sulfide concentrations. Symbols are shaded according to the degree of sulfur loading at the corresponding site, with the least sulfur-impacted (WTR) represented with no shading (open symbol) and the most sulfur-impacted shaded black (Mng). Symbol shape corresponds to the time of sampling: May 2012 (triangle), July 2012 (square), October 2012 (circle), and June 2013 (diamond). Gray dashed lines represent one standard deviation of triplicate samples.

While %MeHg in the solid phase is often considered a proxy for long term net methylation potential, in-situ porewater %MeHg also reflects transport processes and partitioning behavior of MeHg and iHg as well as production and accumulation of MeHg on the solid phase. At dissolved sulfide concentrations less than 25 μM, porewater %MeHg displayed a trend similar to that of solid phase %MeHg, showing a positive trend with dissolved sulfide in all but the June 2013 McQ1 sample (Fig 2.8). However, in sediments with sulfide concentrations >60 μM, and especially in those >1000 μM, porewater %MeHg was not consistently low as it was on the solid phase. In the presence of elevated dissolved sulfide, porewater %MeHg ranged from 2.0% to as high as 67.0% (Fig 2.8).

Using solid phase %MeHg is a proxy of long term net methylation potential, the uniformly low solid phase %MeHg observed in samples with >60 μM dissolved sulfide suggests that little net MeHg production and accumulation had been occurring in these sediments. Dissolved sulfate was present in the surficial sediments of Mng at 0.04 – 0.61 mM, and LLC at an average of ~0.2 mM (though concentrations exceeded 5.0 mM in October 2012) (Appendix B). Thus, the surficial sediment at both heavily impacted sites contained sulfate concentrations sufficient to drive sulfate reduction at some times of the year, suggesting that low net MeHg production in these sediments can not be attributed to sulfate-limited reducing activity. Alternatively, the high concentrations of dissolved sulfide may have had an inhibitory effect on methylation, as has been suggested by several previous studies regarding the effect of dissolved sulfide concentrations on MeHg production (Gilmour et al. 1998; Benoit et al. 2001a; Drott et al. 2007).

The relationship between solid phase and porewater %MeHg was markedly different between the lower and higher sulfide regimes (Fig 2.9). At dissolved sulfide <25 μM, %MeHg in the porewater and on the solid phase were strongly correlated ($R^2 = 0.92$), implying that the accumulation of MeHg on the solid phase is a primary influence governing %MeHg in the porewater under these conditions. In contrast, there was no apparent relationship between porewater and solid phase %MeHg at dissolved sulfide concentrations >60 μM ($R^2 = 0.04$), implying that long term net methylation potential is not a primary influence governing %MeHg in the porewater. Instead, partitioning and/or transport processes may influence porewater %MeHg at these sulfide concentrations.

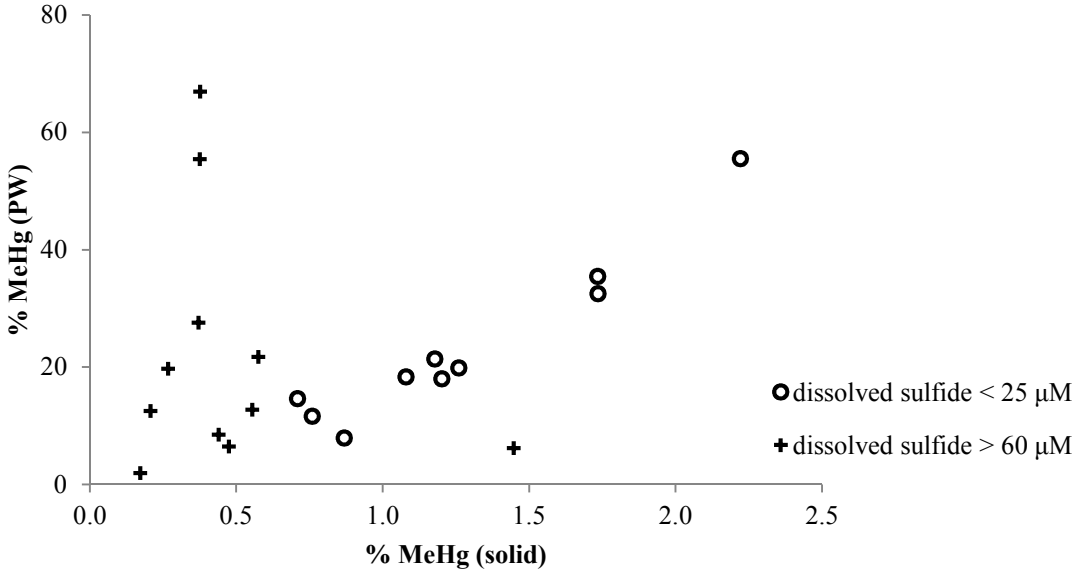

Fig. 2.9. Comparison of solid phase and porewater %MeHg values, with data points separated into two groups based on porewater sulfide concentration

Factors Influencing Mercury Partitioning

Apparent MeHg partition coefficients (Equation 2.3) displayed little variability at dissolved sulfide concentrations <25 μM, with $\log K_D^*$ ranging from 3.2-3.7 and averaging 3.5 (Fig 2.10). At >60 μM dissolved sulfide, partitioning coefficients were more variable and generally lower, with an average $\log K_D^*=3.11$, signifying a greater relative proportion of MeHg in the porewater versus the solid phase. This suggests that higher sulfide concentrations may correspond with increased relative partitioning of MeHg into the porewater, which is consistent with previously reported findings (Hammerschmidt et al. 2008; Berndt & Bavin 2011). Though more variable at higher sulfide, apparent partitioning coefficients for iHg did not show any apparent trend with porewater sulfide (Fig 2.11) which suggests that the influence of sulfide on porewater %MeHg is not related to solid-liquid partitioning of iHg. Instead, the effect of dissolved sulfide on porewater %MeHg appears related to changes in MeHg production (as observed at low sulfide concentrations <25 μM) or changes in MeHg partitioning (as observed at sulfide concentrations >60 μM). Previous studies in freshwater systems at low sulfur conditions have often used porewater %MeHg as an estimation of net methylation (Jeremiason et al. 2006; Mitchell et al. 2008; Coleman-Wasik et al. 2012). While the results of this study at low dissolved sulfide concentrations are consistent with this assumption, at higher dissolved sulfide concentrations this assumption may not be appropriate.

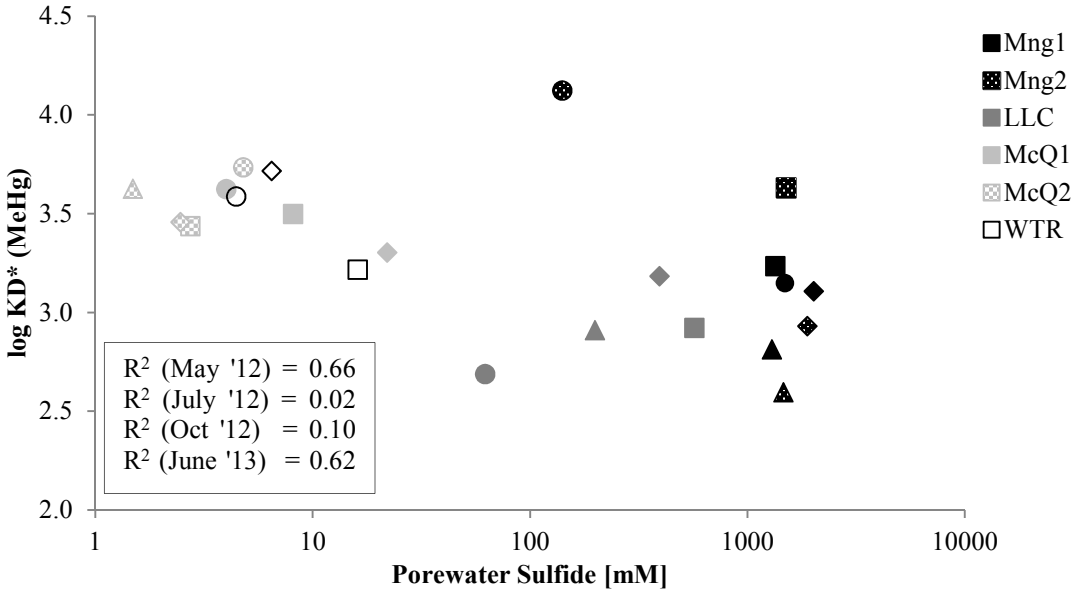

Fig. 2.10. Measured effective MeHg partitioning coefficient across a range of porewater sulfide concentrations. Symbols are shaded according to the degree of sulfur loading at the corresponding site, with the least sulfur-impacted (WTR) represented with no shading (open symbol) and the most sulfur-impacted shaded black (Mng). Symbol shape corresponds to the time of sampling: May 2012 (triangle), July 2012 (square), October 2012 (circle), and June 2013 (diamond).

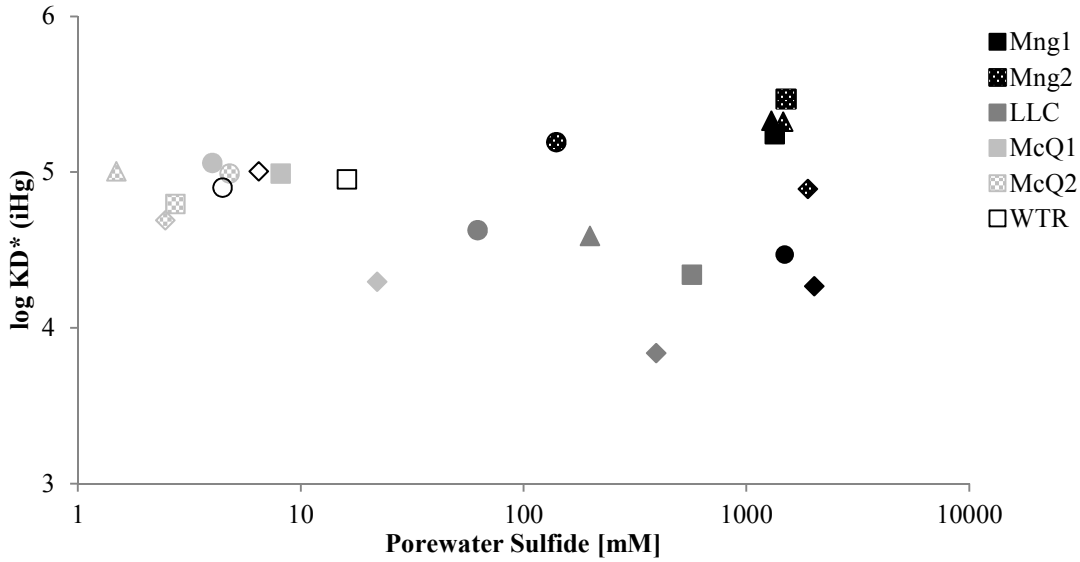

Fig. 2.11. Measured effective iHg partitioning coefficient across a range of porewater sulfide concentrations. Symbols are shaded according to the degree of sulfur loading at the corresponding site, with the least sulfur-impacted (WTR) represented with no shading (open symbol) and the most sulfur-impacted shaded black (Mng). Symbol shape corresponds to the time of sampling: May 2012 (triangle), July 2012 (square), October 2012 (circle), and June 2013 (diamond).

The trend of decreasing apparent MeHg partitioning coefficients was observed across a three order of magnitude range of increasing pore water sulfide concentrations and displayed seasonal variability. Correlations were strongest in samples collected in late spring conditions (May 2012 & June 2013, Fig 2.10). These seasonal differences in apparent porewater partitioning may be related to a dynamic balance between the influence of methylation and demethylation reactions and solid-liquid interactions. Warmer temperatures during summer months correspond with increased biological activity and likely more rapid rates of methylation and demethylation in sediment pore fluids, which could make instantaneous measurements of porewater MeHg less dependent upon partitioning from the solid phase. By contrast, spring conditions, following months of relatively less biological activity under cold temperatures, may be more strongly influenced by equilibrium conditions between the solid and porewater phases. With less influence from methylation and demethylation on porewater MeHg, the presence of sulfide in spring could act to pull additional MeHg into the pore fluids from the MeHg pool on the solid phase. Additionally, because the kinetics of mercury-ligand binding is on the order of days (Miller et al. 2009), it is possible that summer and fall data captured mercury partitioning at a time when equilibrium with the solid phase was not fully realized due to active and rapid reactions in the pore fluids.

Organic carbon has been proposed to play an important role in mercury partitioning in sediments, due to its ability to bind to dissolved mercury (Berndt and Bavin 2012) and to stabilize nanocolloidal HgS crystals (Gerbig et al. 2011; Zhang et al. 2012). No significant trend was observed between MeHg $\log K_D$* and DOC (Fig 2.12), although the

absolute concentration of MeHg in sediment porewater generally increased with increasing DOC (except in sediments of Lake Manganika) (Fig 2.13). This lack of correlation remained when apparent partitioning coefficients of MeHg were compared to SUVA and slope ratio, suggesting that either DOC was not a primary ligand for MeHg in sediment porewaters or that these parameters did not adequately predict mercury-ligand strength. It should be noted, however, that the locations sampled in this study possessed a relatively narrow range of porewater DOC concentrations relative to the observed range in dissolved sulfide (Figs 2.7-2.11).

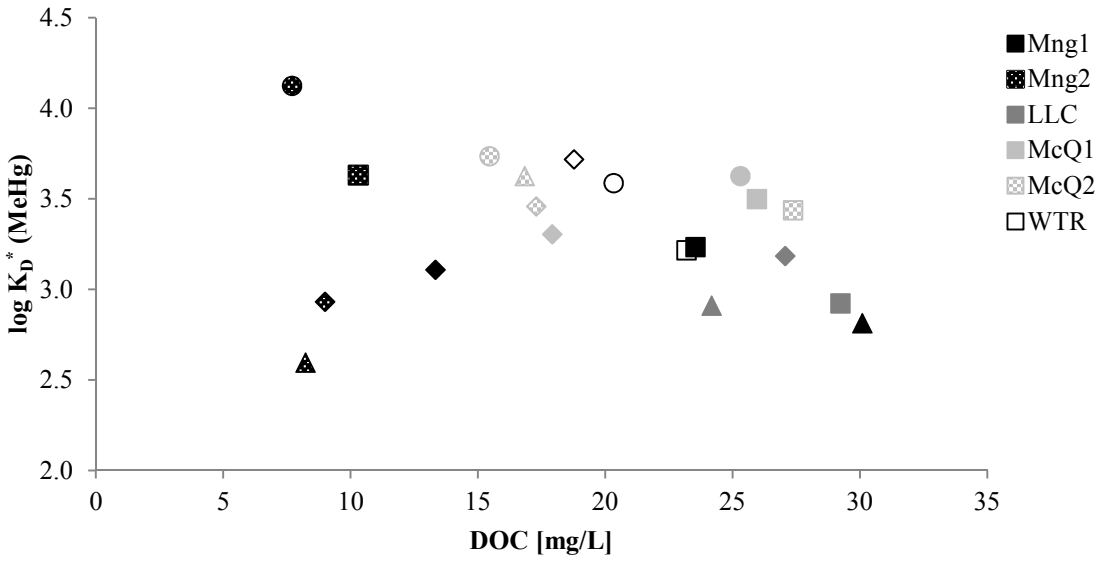

Fig. 2.12. Measured effective MeHg partitioning coefficient as a function of DOC concentration. Symbols are shaded according to the degree of sulfur loading at the corresponding site, with the least sulfur-impacted (WTR) represented with no shading (open symbol) and the most sulfur-impacted shaded black (Mng). Symbol shape corresponds to the time of sampling: May 2012 (triangle), July 2012 (square), October 2012 (circle), and June 2013 (diamond).

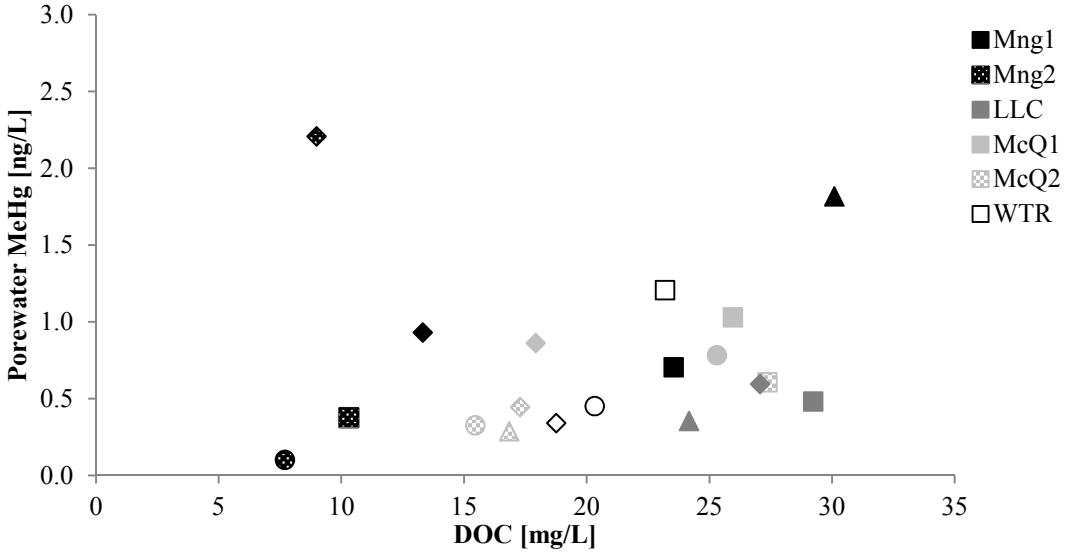

Fig. 2.13. Comparison of porewater MeHg and DOC concentrations. Symbols are shaded according to the degree of sulfur loading at the corresponding site, with the least sulfur-impacted (WTR) represented with no shading (open symbol) and the most sulfur-impacted shaded black (Mng). Symbol shape corresponds to the time of sampling: May 2012 (triangle), July 2012 (square), October 2012 (circle), and June 2013 (diamond).

Conclusions

Consistent with previous research (Gilmour et al. 1998; Benoit et al. 2001b; Ravichandran 2004), results of this study suggest that the net production and partitioning of MeHg in sulfate-impacted freshwater sediments are governed by processes related to the concentration of dissolved sulfide in sediment porewater. Our interpretation is that the MeHg dynamics observed in this study are related to the dual role of dissolved sulfide in controlling porewater MeHg by acting as a ligand for both inorganic- and methyl-mercury. As a ligand for MeHg, dissolved sulfide can act directly to increase partitioning from the solid phase into porewater, while in its capacity as a ligand for inorganic mercury, sulfide can inhibit MeHg production at concentrations >10-100 μM.

In sediments with <25 μM dissolved sulfide, net MeHg production appears to be the dominant process influencing %MeHg in both the porewater and solid phase. In contrast, sediments with >60 μM dissolved sulfide appear to experience inhibited net MeHg production, resulting in limited accumulation of MeHg on the solid phase. At these relatively high concentrations, however, sulfide may also act to increase MeHg partitioning into the porewater. Sulfide's role as a methylation inhibitor will likely have the greatest influence under warm temperatures and active biological conditions (summer/fall). As a result, the effect of sulfide on MeHg production and MeHg partitioning may both be important influences on porewater MeHg during warm summer conditions. Under colder temperatures and more sluggish biological activity (winter/spring), the inhibiting behavior of sulfide on net MeHg production is likely to have less of an impact, and porewater MeHg could be influenced more significantly by partitioning behavior resulting from sulfide's role as a ligand for MeHg.

Though dissolved sulfide concentrations are governed by a number of factors, the presence of ferrous iron can act to limit sulfide concentrations. In many situations, the potential for sulfide accumulation in sediment porewater is primarily dependent on whether iron is present in excess of sulfur at the site. At sites where free iron (uncomplexed with sulfide) has not been depleted, porewater sulfide may not be present in large enough concentrations to either inhibit methylation or have an important impact on MeHg partitioning. Instead, MeHg production is likely governed by rates of microbial sulfate reduction. At sites where free iron has been depleted, dissolved inorganic sulfide could accumulate to concentrations sufficient for it to act as an important ligand,

inhibiting methylation but potentially increasing partitioning of MeHg into the aqueous phase.

It should be noted that while the sites subjected to historic sulfate loading (Mng & LLC) were both characterized by high porewater sulfide concentrations and inhibition of methylation, these conditions arose because free iron had already been depleted in the sediment due to the duration of historic sulfur loading. High sulfate loading to previously unimpacted sediments (such as Lake McQuade) may not consume the pool of available free iron for a number of years. This could stimulate SRB activity in the absence of sulfide inhibition of methylation, potentially resulting in robust net MeHg production.

These findings could have important implications for efforts to reduce MeHg concentrations in heavily sulfur-impacted freshwater systems, such as those impacted by mining activity in Northeastern Minnesota. This study suggests that high sulfur loading can influence porewater MeHg concentrations through at least two different mechanisms. In addition, the influence of sulfide on MeHg production and partitioning could vary seasonally in locations experiencing a large temperature variation and may not be confined to biotic processes.

Understanding the connection between heavy sulfate loading and MeHg concentrations on a watershed-scale involves determining how much MeHg is being produced, where MeHg production is occurring, and how MeHg is transported within the watershed. Thus, in order to successfully manage mining-related sulfate loads in northeastern Minnesota in a way that minimizes the production and bioaccumulation of MeHg, it is

necessary to understand the role of sulfate on mercury-related processes in various geochemical and hydrological settings. To better understand mercury-related processes in heavily sulfur-impacted surficial sediments, the influence of inorganic sulfur on MeHg during seasons with low biological activity and in areas with sulfide concentrations high enough to inhibit methylation should continue to be investigated. Additionally, further investigation into the relative loads of iron and sulfur in the context of long-term sulfate loading could provide insight into the management of sulfur in unimpacted systems. A better understanding of seasonal distributions in site specific geochemical conditions, particularly the presence of dissolved sulfide and free iron, is required in order to more fully understand the impacts of high sulfate loading to freshwater sediments.

Chapter 3: Sources and sinks of methylmercury in Lake McQuade

Site Description

Lake McQuade (N 47.42°, W 92.77°) is a mesotrophic lake located in the upper reaches of the St. Louis River watershed in northeastern Minnesota, USA, in a watershed influenced by historic and ongoing taconite-ore mining activity (Figs 1.1 & 1.2). It has a maximum depth of ~20 feet and surface area of ~0.68 km^2 and, in summer 2012, had surface water sulfate concentrations in the range of 30-120 mg/L owing to upstream inputs of mining-influenced water. Inlet and outlet streams at Lake McQuade are located in close proximity on the northeastern edge of the lake. Though a narrow pinch point separates the southern basin of the lake, which contains the lake's deepest point (Fig 3.1), surface water chemistry differed very little between the northern and southern basins during summer/fall 2012. The deeper southern portion of Lake McQuade was thermally stratified by mid-June in 2012 (limnetic surface between 8-10 feet), experienced partial mixing in August, and reached stable, well-mixed conditions by mid-September.

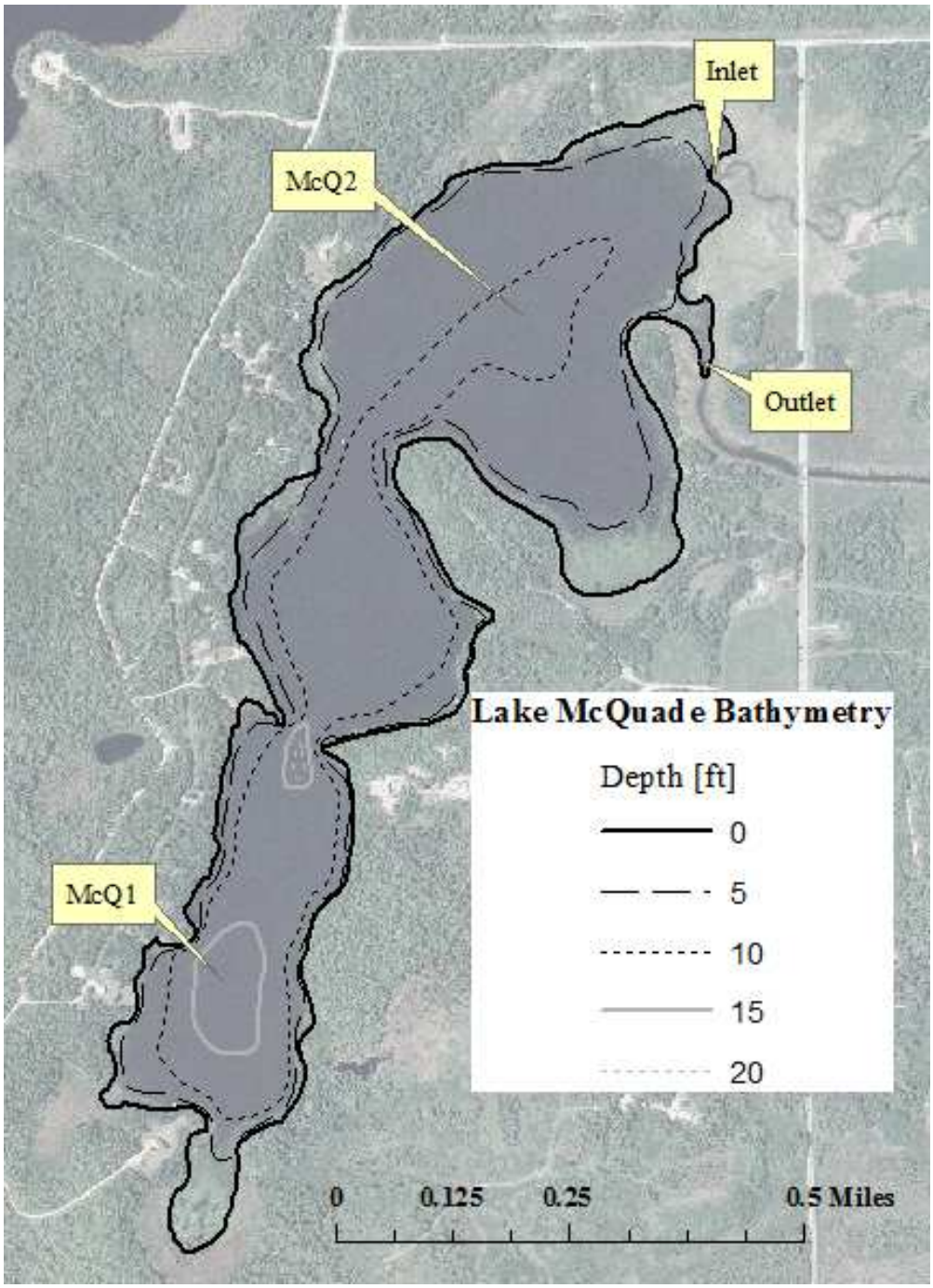

Fig. 3.1. Map of sampling locations and bathymetry contours at Lake McQuade.

Methods

Sampling Design

Water samples were collected periodically throughout the summer at two locations within the lake (Fig 3.1). The shallower location in the northern basin (McQ2) had a water depth of 8-10 feet, which was very near the limnetic surface depth for most of the summer. The deeper location in the southern basin (McQ1) had a water depth of 15 feet, with 5-6 feet of anoxic bottom waters typically present during the stratified season. Surface water and bottom water samples and depth profile measurements of temperature, pH, and dissolved oxygen were collected at both sampling locations every 2-3 weeks from May to October 2012, and once in June 2013, totaling ten sampling trips. Water samples were analyzed for total- and methyl- mercury as well as a host of geochemical parameters (Appendix A).

A more intensive water column sampling scheme was employed at the deep sampling location once a month in June, July, August, and October 2012. Samples were collected at 4-6 discrete depths spaced 2-5 feet apart in order to construct a profile of mercury and related water chemistry from the surface, through the thermocline, into the hypolimnion, and down to near the lake bottom. Sediment and porewater samples were also collected and analyzed during these intensive water column sampling events (Chapter 2 of this thesis).

In order to evaluate net import and export of chemicals from Lake McQuade, water samples from inlet and outlet streams were collected approximately biweekly throughout the summer and fall of 2012 and analyzed for total- and methyl- mercury as well as other

geochemical parameters (Appendix A). The collection procedure and filter size used to collect water samples from inlet and outlet streams for THg and MeHg analysis differed from those used to collect lake water column samples. A comparison of the procedures and a discussion of their implications are included in Appendix C. Samples for isotopic analysis of sulfur and oxygen in molecules of sulfate were also collected at inlet and outlet streams and within the water column (Kelly et al. 2014).

Sampling Methods

Raw (unfiltered) water samples were collected into mercury-free 1 liter PETG bottles using a peristaltic pump with Teflon tubing. After purging the pump line, samples were pumped from depth into the collection bottle, ensuring the pump line discharged below the surface of the accumulating fluid. Bottles were completely filled (within 3 minutes) to minimize gas exchange and oxygen exposure. Filtered samples were obtained from the raw water collection bottles within 6 hours of collection, using 10 cm Rhizon© samplers (polyvinylpyrrolidine/polyethersulfone membrane, Seeberg-Elverfeld et al. 2005) with a nominal filter size of 0.2 µm. In-situ redox conditions were maintained by attaching the Rhizon© sampler to Teflon tubing connected to a stainless steel hypodermic needle. After flushing the sampling assembly with 2-5 mL of sample, the sample was drawn into a pre-evacuated, acid-washed, mercury and oxygen-free, evacuated borosilicate glass serum bottle by piercing the needle through a 1 cm thick butyl rubber stopper (Bellco, Inc). To minimize exposure to oxygen during filtration, raw water samples were sealed with custom bottle caps that allowed nitrogen gas to continuously

purge the head space. Bottles ranged in size from 10 mL to 125 mL and filled within 1 – 10 hours.

Water column depth profiles (3 foot depth interval) of temperature, pH, and dissolved oxygen were measured in-situ at both sampling locations using a Hydrolab S5 sonde (Hach Hydromet) calibrated immediately prior to use.

Chemical Analysis

Filtered water samples for anion analysis were acidified with concentrated HCl to pH < 3 and bubbled gently with N_2 gas for 15 minutes to remove dissolved sulfide. A non-acidified duplicate sample was split from a portion of samples for chloride analysis. Sulfate (SO_4^{2-}), nitrate (NO_3^-), phosphate (PO_4^{3-}), and chloride (Cl^-) were quantified via ion chromatography (Method 300.1, USEPA 1997) on a Dionex ICS 1100 system. Water samples for dissolved sulfide ($H_2S + HS^-$) analysis were filtered into an evacuated serum bottle preloaded with ZnAc and NaOH preservative and quantified using automated methylene blue method (4500-S^{2-} E, Eaton 2005). Dissolved ferrous iron (Fe^{2+}) was quantified photometrically using the Phenanthroline Method (3500-FeB, Eaton 2005). Ammonium was analyzed colorimetrically using the phenolate method (Lachat QuikChem method 10-107-06-1-B). Dissolved organic carbon (DOC) and dissolved inorganic carbon (DIC) were quantified on a Teledyne-Tekmar Torch Combustion TOC Analyzer. DOC was characterized by analyzing samples for specific ultraviolet absorption (SUVA) at 254nm (Weishaar et al. 2003) and spectral slope ratio (Helms et al.

2008) on a Varian Cary 50 scanning UV-Vis spectrophotometer. Correction for iron color (Poulin et al. 2014) was not included when analyzing DOC samples in this study.

Water Column Methylation and Demethylation Rate Potentials & Mercury Analyses

For mercury analysis of lake water column samples, filtered water samples were preserved by adding concentrated trace metal HCl to a final concentration of 0.5%. Clean hands protocols were utilized for mercury samples throughout sample handling, preservation, and analysis. Potential rates for Hg methylation and MeHg demethylation were assessed via enriched stable isotope incubation techniques (Eckley & Hintelmann 2006; Mitchell & Gilmour 2008). Potential methylation and demethylation rate constants were measured by amending unfiltered water samples with a mixture of stable isotope-enriched $^{200}Hg^{2+}$ & $Me^{201}Hg^{+}$ (94.3% $^{200}Hg^{2+}$ and 84.7% $Me^{201}Hg^{+}$) that was pre-equilibrated with filtered site water within 1 hour. Spiked samples were incubated in the dark at in-situ temperatures for approximately 24 hours, and then frozen to finish the assays. The generation of enriched $Me^{200}Hg^{+}$ and loss of enriched $Me^{201}Hg^{+}$ was quantified via ICP-MS detection. Incubations took place in completely-filled, mercury-free, 250 mL PETG bottles fitted with a 1 cm thick butyl rubber stopper through which isotopes were injected using a gastight syringe.

For THg analysis (including detection of enriched isotopes), ~0.5% by volume of BrCl was added to the water samples to oxidize all Hg in the sample to Hg(II). After allowing the sample to react overnight, THg was characterized following the USEPA method 1631 (USEPA 2002) using a Tekran 2600 automated Hg analysis system that was hyphenated

with an Agilent 7700x ICP-MS for detection of individual Hg isotopes. Determination of MeHg was accomplished by isotope-dilution (Hintelmann and Evans 1997), using water samples distilled according to the methods of Horvat et al. (1993), but with the addition of a different enriched MeHg spike ($Me^{199}Hg$). All analyses used calculations from Hintelmann and Ogrinc (2003) to account for the <100% enrichment of isotopes in calculating enriched ^{200}Hg and ^{201}Hg concentration in THg and MeHg, as well as in calculating ambient THg and MeHg levels from the dominant naturally occurring ^{202}Hg isotope. Inorganic mercury (iHg) concentrations were calculated by subtracting the MeHg concentration from the THg concentration.

Sediment Flux Estimates

Estimates of methyl- and inorganic- mercury diffusive fluxes from lake sediment utilized filtered bottom water samples and filtered lake sediment porewater samples (Chapter 2). Diffusive flux was estimated following a method employed in similar studies (Gill et al. 1999; Hammerschmidt et al. 2004), using an equation derived from Fick's first law and assuming no bulk water movement (Equation 3.1), where diffusive flux (J) is a function of the change in concentration across the sediment-water interface (SWI), sediment porosity (ϕ), tortuosity (θ^2), and the diffusion coefficient of the chemical in water (D_w).

$$J = -\left(\frac{\varphi D_w}{\theta^2}\right)\frac{\partial C}{\partial z} \tag{3.1}$$

The methods used to estimate each variable in the diffusive flux equation are included in Appendix E.

Mass Balance of MeHg

A MeHg mass balance analysis was conducted on both the epilimnion and the hypolimnion of Lake McQuade to quantitatively assess the various sources and sinks of MeHg to and from the lake. The lake layers were modeled as two distinct, well-mixed systems (Fig 3.2), with exchange between the layers occurring across the limnetic surface. Methods used to estimate exchange across the limnetic surface were based on transient observations of thermal gradients, and are described in detail in Appendix F4. Both layers are subjected to exchange with sediment porewater in proportion to their surface area. Inlet and outlet streams flow into and out of the epilimnion but are hydrologically isolated from the hypolimnion during thermal stratification. In addition to mass flows across boundaries, methylation and demethylation in the water column were included as potential internal sources or sinks of MeHg.

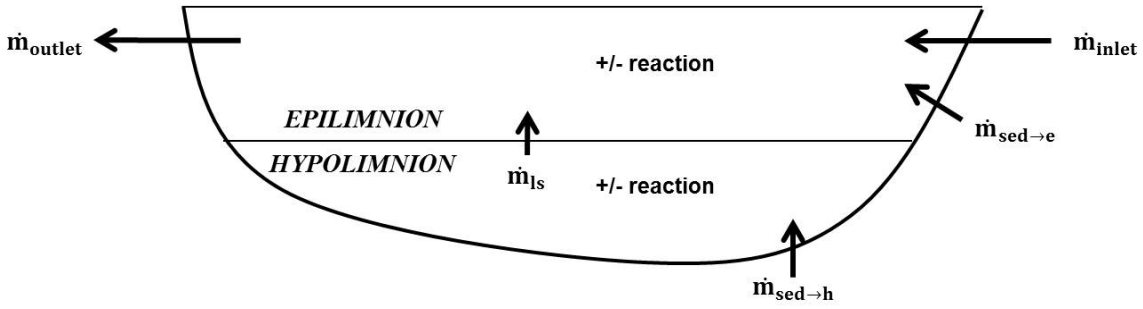

Fig 3.2. Generalized schematic for modeling of Lake McQuade under stratified conditions, describing mass flows across boundaries into and out of the hypolimnion and epilimnion, as well as sources and sinks within the layer.

Mass balance equations on the epilimnion (Equation 3.2) and hypolimnion (Equation 3.3) describe the rate of MeHg accumulation/loss in both layers.

$$\sum \dot{m}_e = \dot{m}_{inlet} + \dot{m}_{sed|e} + \dot{m}_{ls} - \dot{m}_{outlet} - k_{demeth|e} \tag{3.2}$$

$$\sum \dot{m}_h = \dot{m}_{sed|h} - \dot{m}_{ls} + k_{meth|h} - k_{demeth|h} \tag{3.3}$$

Input and output mass flows of MeHg are defined by Equations 3.4 - 3.8. In the interest of quantifying processes contributing to a buildup of MeHg in bottom waters, daily mass flows were calculated (Equations 3.4 – 3.8) for each date between 6/25 (earliest sampling date of McQuade bottom waters) and 8/7 (the last sampling date before mid-August lake turnover). These daily mass flows were then averaged to obtain a single mass flow rate characterizing the low-flow, mid-summer stratified season. An explicit description of all terms used in equations 3.4 – 3.8 and numerical values used to define these terms are included in Appendix F3 & F5.

$$\dot{m}_{inlet} = QC_{in} \tag{3.4}$$

$$\dot{m}_{outlet} = QC_{out} \tag{3.5}$$

$$\dot{m}_{ls} = \frac{K_z A_{ls}(C_e - C_h)}{(z_{BW} - z_{ls})} \tag{3.6}$$

$$\dot{m}_{sed|h} = J_{sed|h} A_{sed|h} \tag{3.7}$$

$$\dot{m}_{sed|e} = J_{sed|e} A_{sed|e} \tag{3.8}$$

To determine rates of accumulation and/or degradation within each layer, the total mass of MeHg in the hypolimnion and epilimnion was estimated at each sampling date.

Estimates applied the measured surface water and bottom water concentrations to the estimated volume of the epilimnion and hypolimnion respectively (Appendix F5). The estimated mass of MeHg on 8/7 was compared to the estimated mass on 6/25 to calculate an average bulk accumulation or degradation rate in both layers over the stratified period.

The contributions of internal sources and sinks of MeHg (i.e., water column methylation and demethylation) are the only mass balance terms not estimated using field data. Mass flows of MeHg calculated from field observations were subtracted from the observed accumulation/loss of MeHg mass to estimate the net production or loss within each layer. Though a water column methylation and demethylation rate measurement was made in June 2013, this net estimation was not able to be separated into individual production and degradation terms, since most samples from summer 2012 were collected under different geochemical conditions than samples collected in June 2013.

Chemical Modeling

Though MeHg mass balances were performed on an average basis using the terms described above, an explicit, numerical model was developed to describe the spatial and temporal changes of sulfate and magnesium in Lake McQuade. The general model framework is derived from the mass balance equations on the epilimnion (Equation 3.2) and the hypolimnion (Equation 3.3), describing the total mass flow of a chemical for both layers of the lake. The model was fit to empirical observations to estimate lake residence time and net sulfate loss in Lake McQuade from late-June to mid-August. Methods outlining model operation are located in Appendix F1.

Field Results

Water Column Sulfate

Lake McQuade was thermally stratified by early-June in 2012 (Fig 3.6a) with undetectable dissolved oxygen concentrations (<0.2 mg/L) present in the bottom waters until mid-September (Fig 3.3a), though a perturbation in the thermal structure of the lake suggests at least partial mixing occurred in mid-August (Fig 3.6f). The limnetic surface was typically shallow enough to create anoxic conditions above the sediment surface of McQ2 (water depth = 8-10 ft) until mid-August (Fig 3.4a).

Hypolimnetic sulfate concentrations at McQ1 declined from 0.16 to 0.04 mM between late-June and early-August during a time when sulfate was steadily increasing in the surface waters (Fig 3.3c), suggesting sulfate was lost from the hydrologically isolated hypolimnion during late June and July. Bottom water concentrations of nitrate were negligible through June, July, and August (Fig 3.3d). The lack of more energetically favorable electron acceptors in the bottom waters suggests that conditions were favorable for sulfate reduction. Despite this, sulfide concentrations in the hypolimnion remained low throughout the year (typically <5 μM) (Figs 3.3e & 3.4e), which could reflect limited sulfate reduction. Alternatively, the presence of aqueous ferrous iron at 10 – 25 μM in hypolimnetic waters during July and August (Fig 3.3i) suggests that sulfide-iron(II) precipitation reactions may have limited the accumulation of dissolved sulfide in bottom waters.

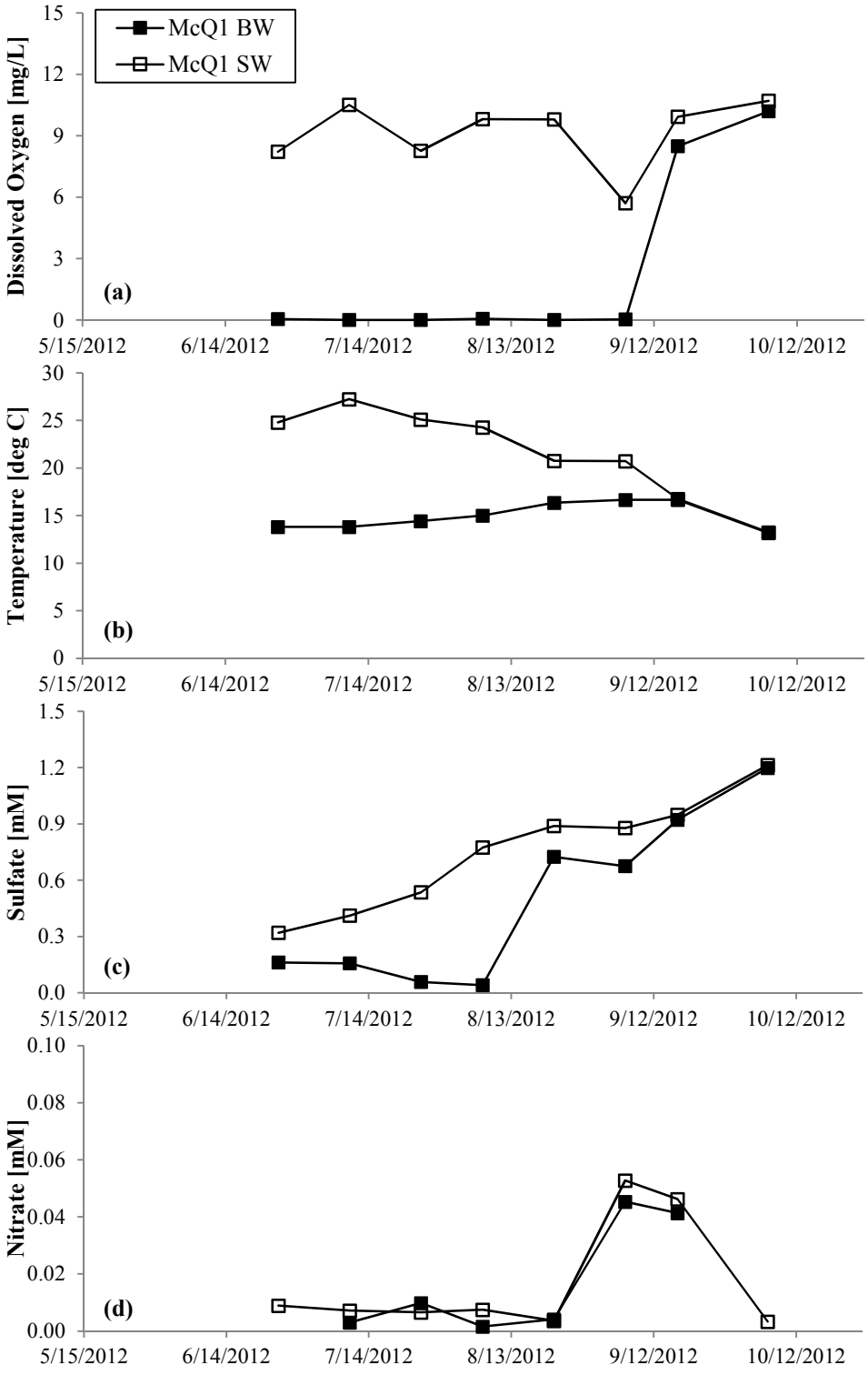

Fig 3.3(a-d). Time-series of McQ1 (deep site) surface and bottom water samples measured for: (a) dissolved oxygen, (b) temperature, (c) sulfate, (d) nitrate

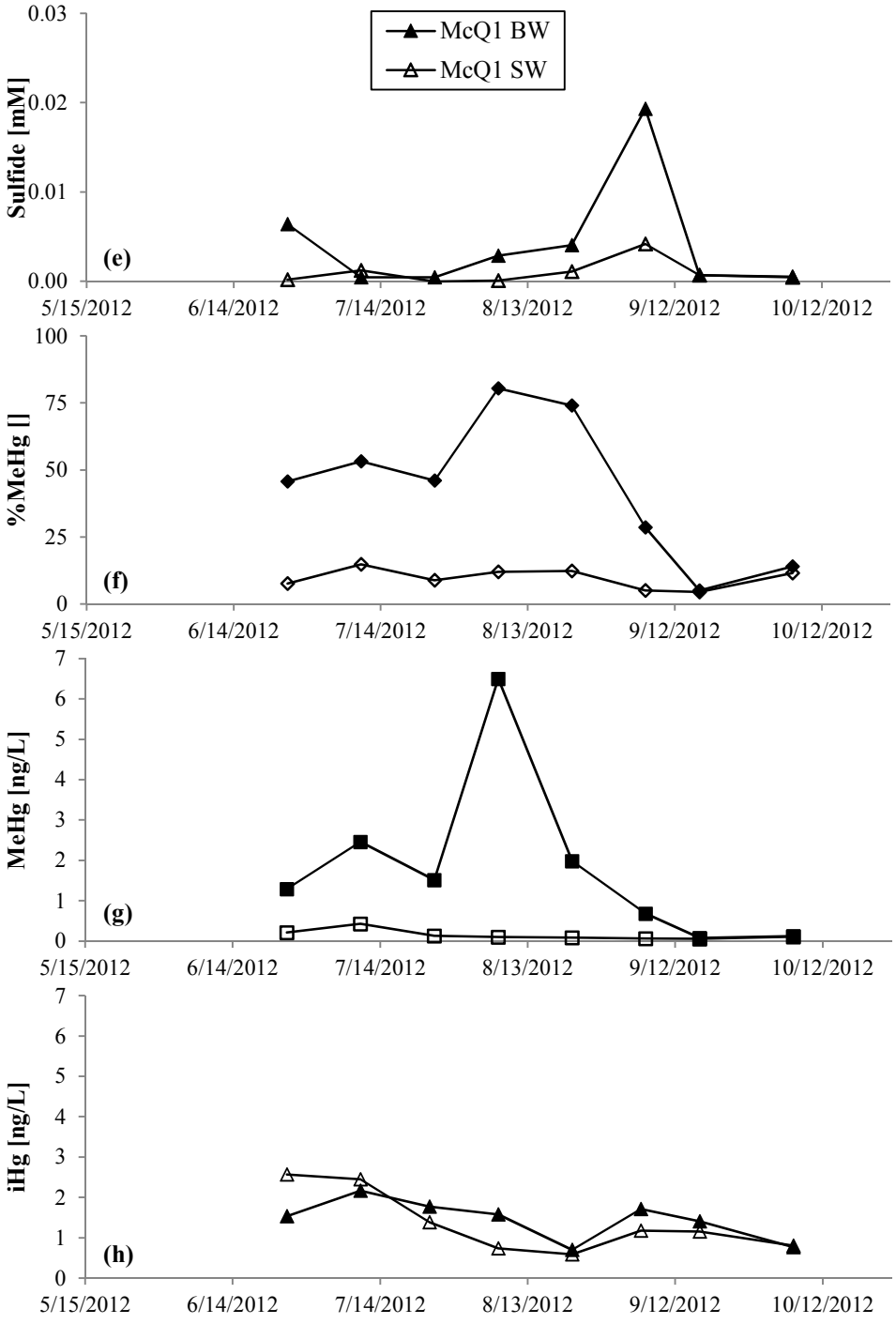

Fig 3.3(e-h). Time-series of McQ1 (deep site) surface and bottom water samples measured for: (e) dissolved sulfide, (f) %MeHg, (g) MeHg, (h) iHg

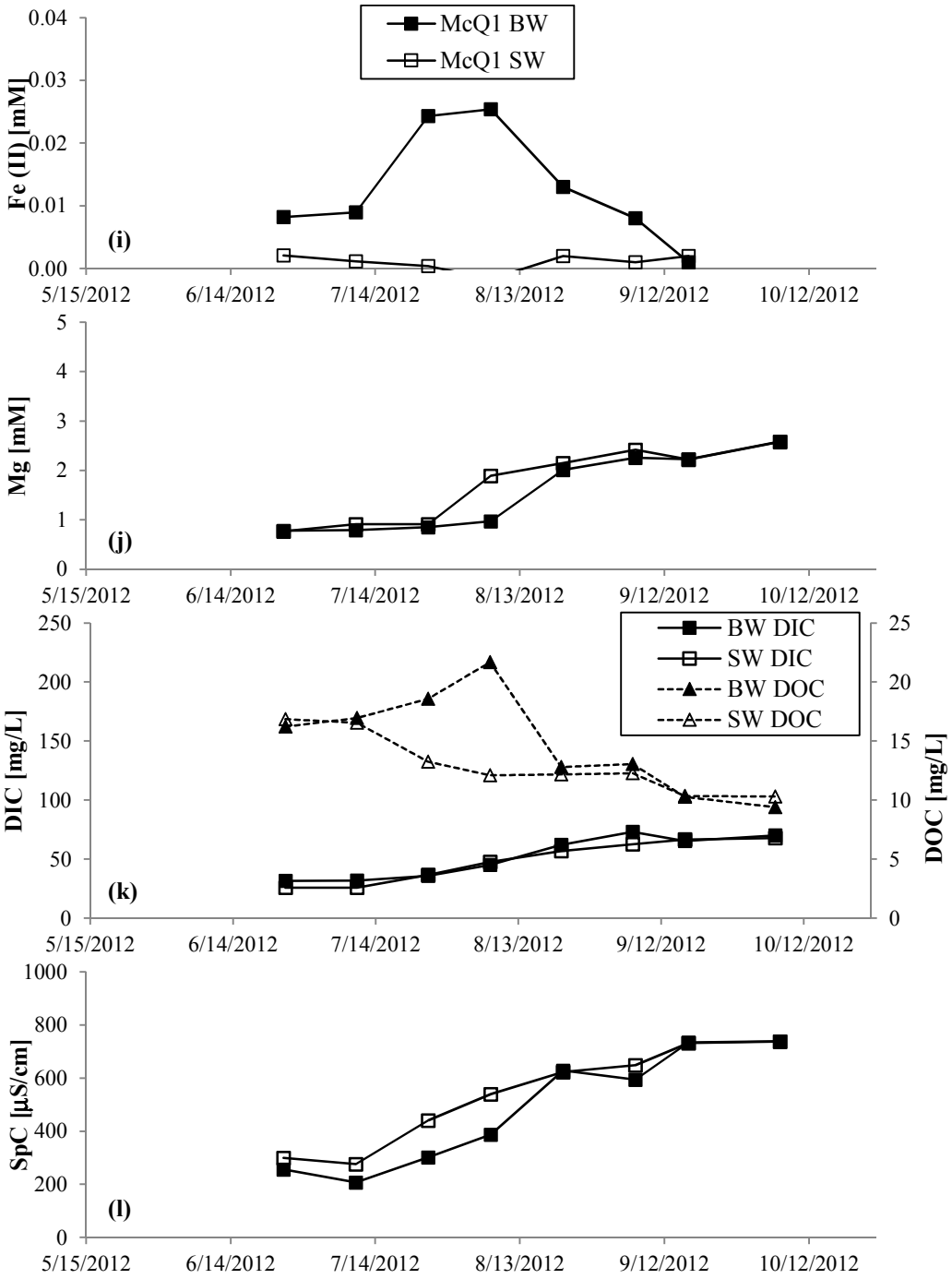

Fig 3.3(i-l). Time-series of McQ1 (deep site) surface and bottom water samples measured for: (i) ferrous iron, (j) magnesium, (k) DOC and DIC, (l) specific conductivity

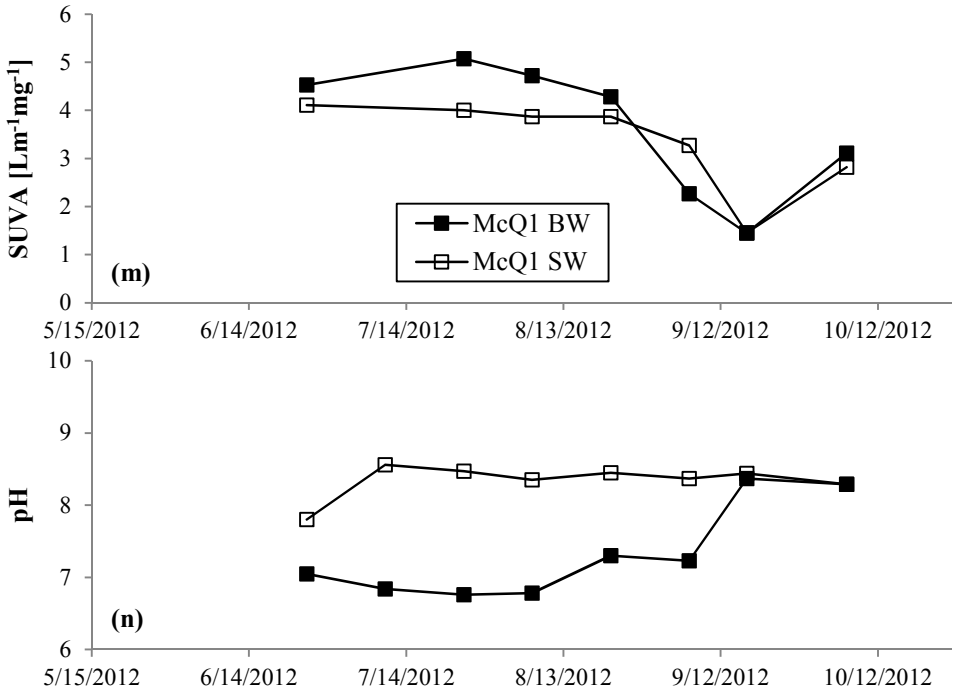

Fig 3.3(m-n). Time-series of McQ1 (deep site) surface and bottom water samples measured for: (m) SUVA, (n) pH

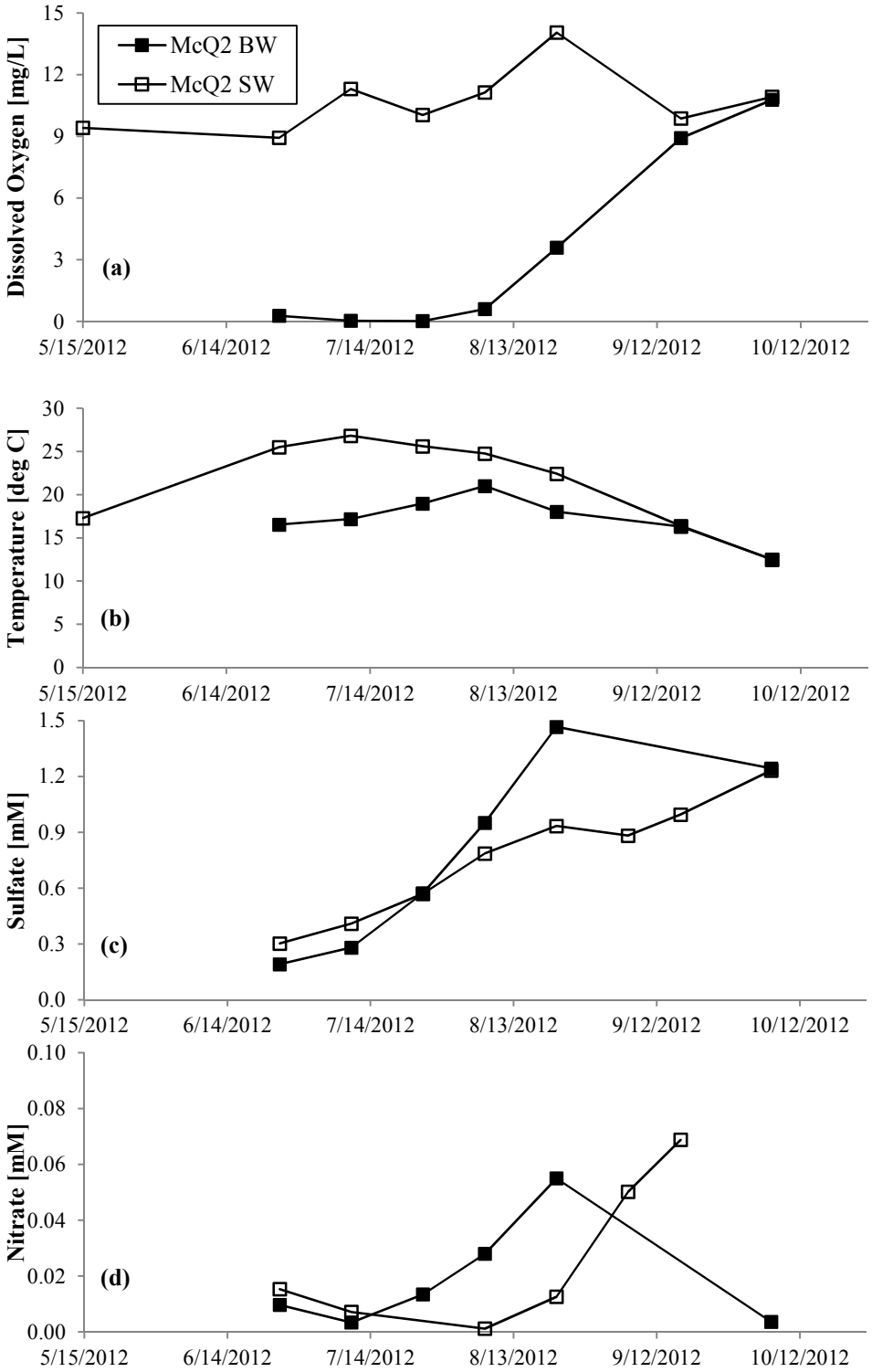

Fig 3.4(a-d). Time-series of McQ2 (shallower site) surface and bottom water samples measured for: (a) dissolved oxygen, (b) temperature, (c) sulfate, (d) nitrate

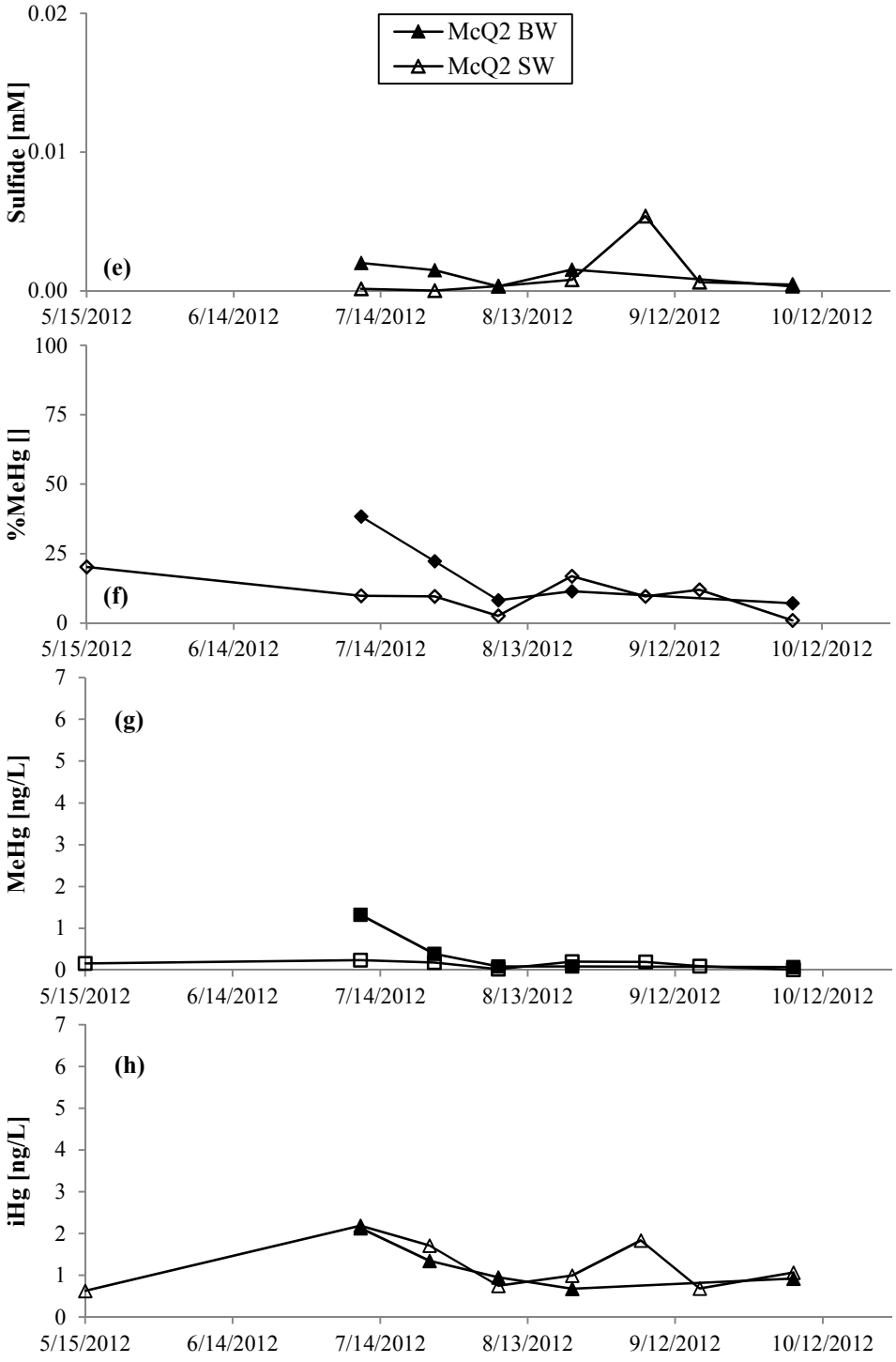

Fig 3.4(e-h). Time-series of McQ2 (shallower site) surface and bottom water samples measured for: (e) dissolved sulfide, (f) %MeHg, (g) MeHg, (h) iHg

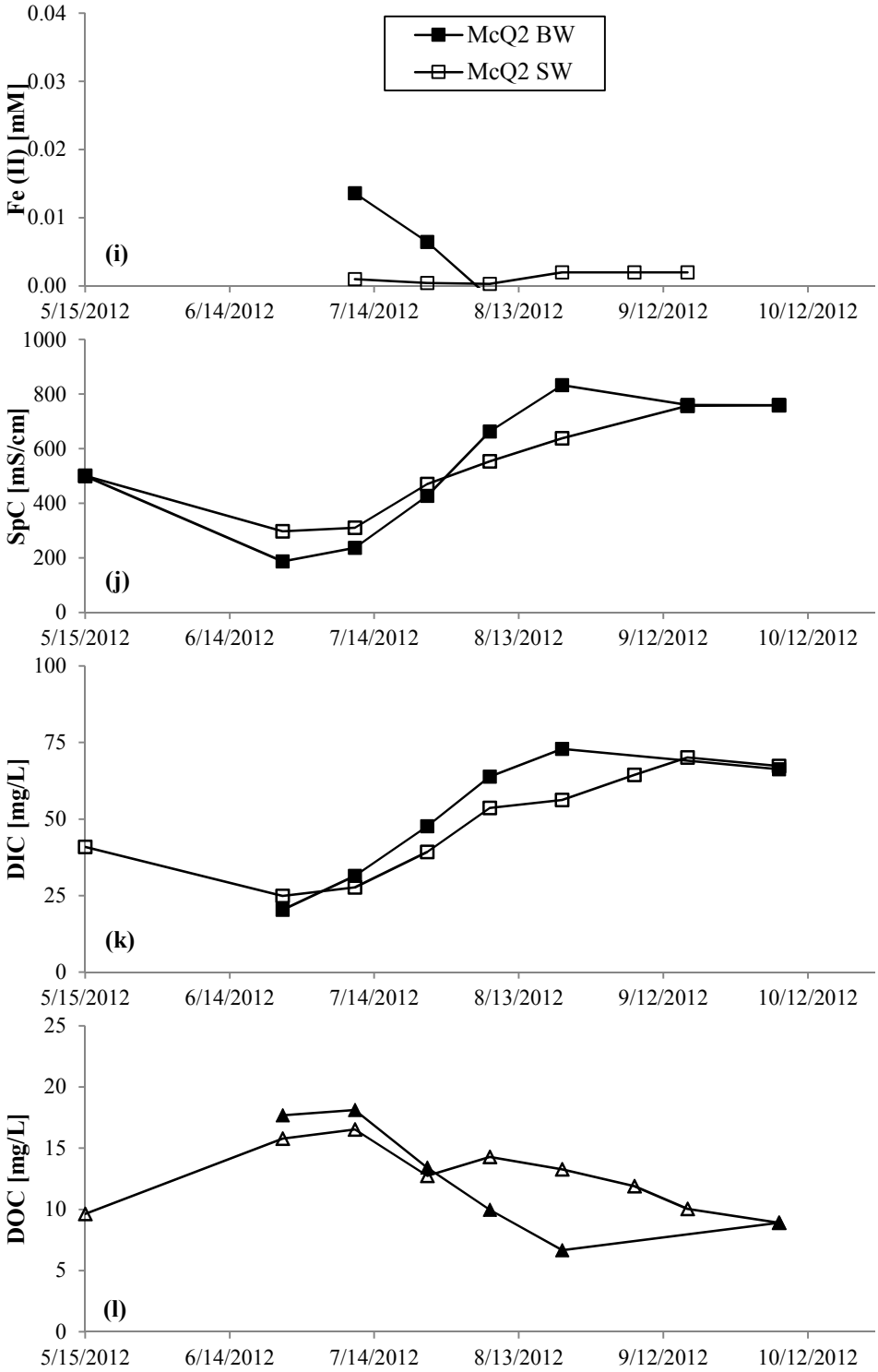

Fig 3.4(i-l). Time-series of McQ2 (shallower site) surface and bottom water samples measured for: (i) ferrous iron, (j) specific conductivity, (k) DIC, (l) DOC

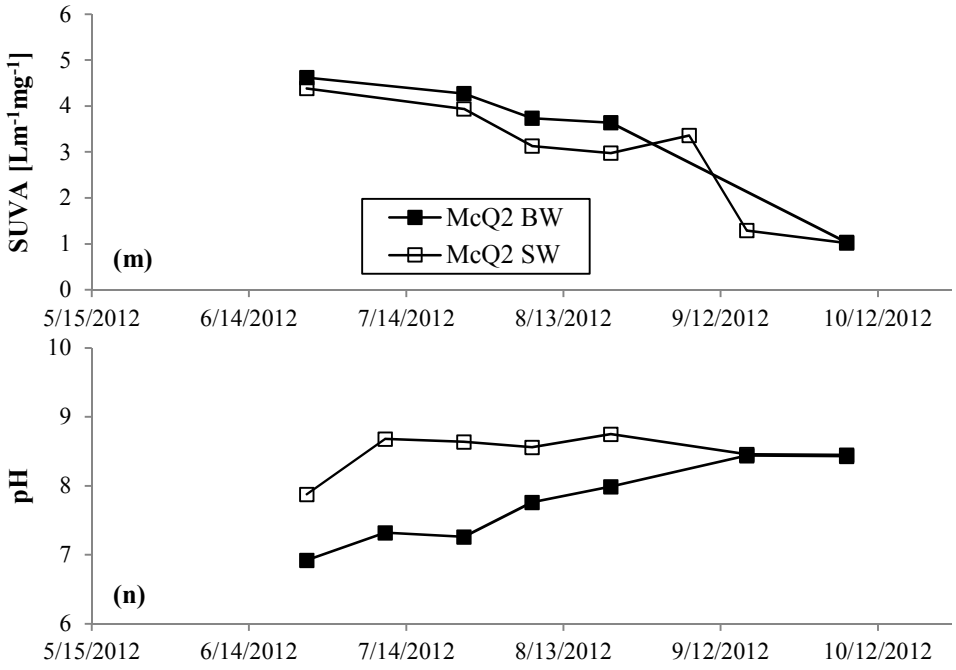

Fig 3.4(m-n). Time-series of McQ2 (shallower site) surface and bottom water samples measured for: (m) SUVA, (n) pH

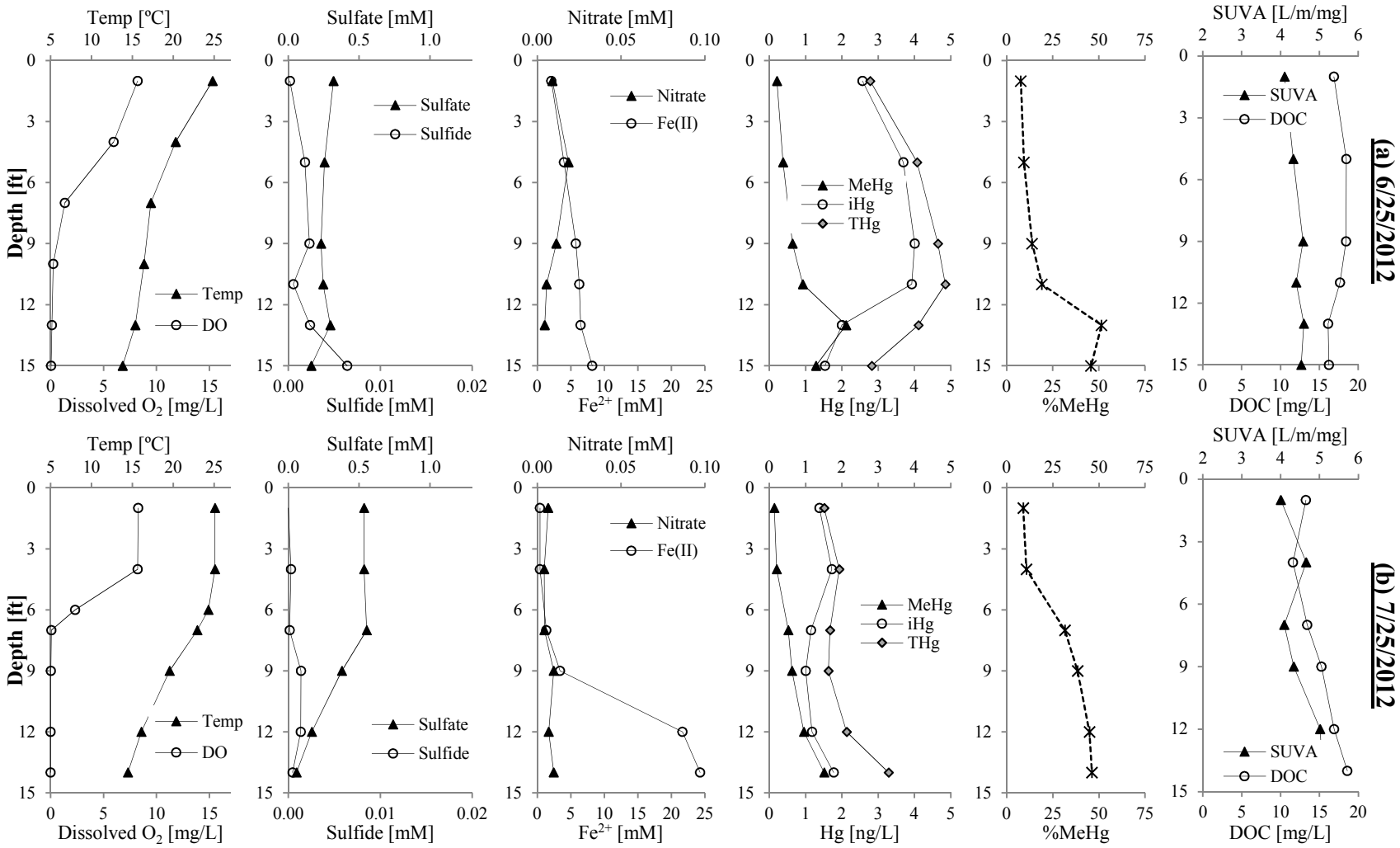

Fig 3.5(a-b). Depth profiles of McQ1 water column, collected on dates (a) 6/25/2012 (top row), and (b) 7/25/2012 (bottom row)

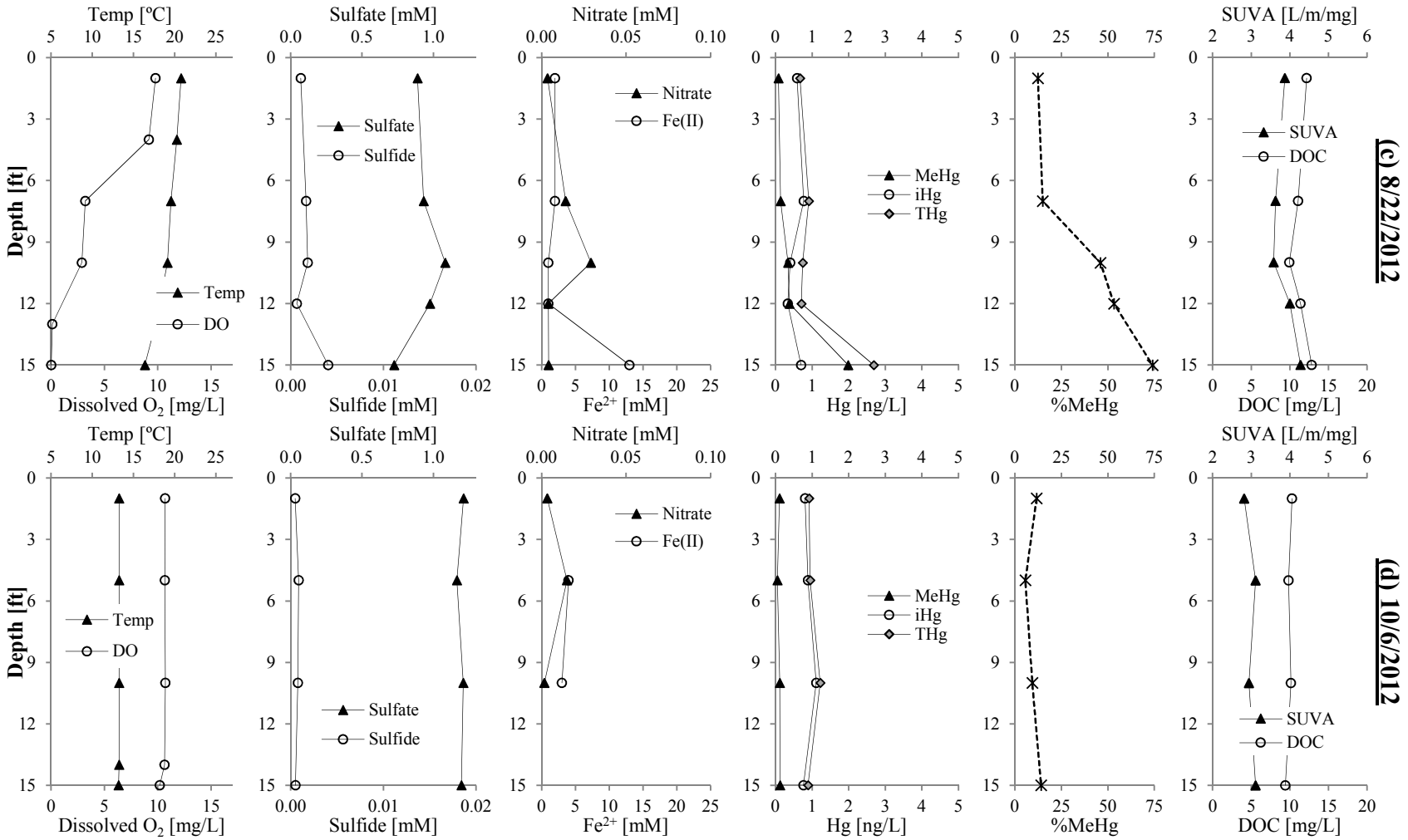

Fig 3.5(c-d). Depth profiles of McQ1 water column, collected on dates (c) 8/22/2012 (top row), and (d) 10/6/2012 (bottom row)

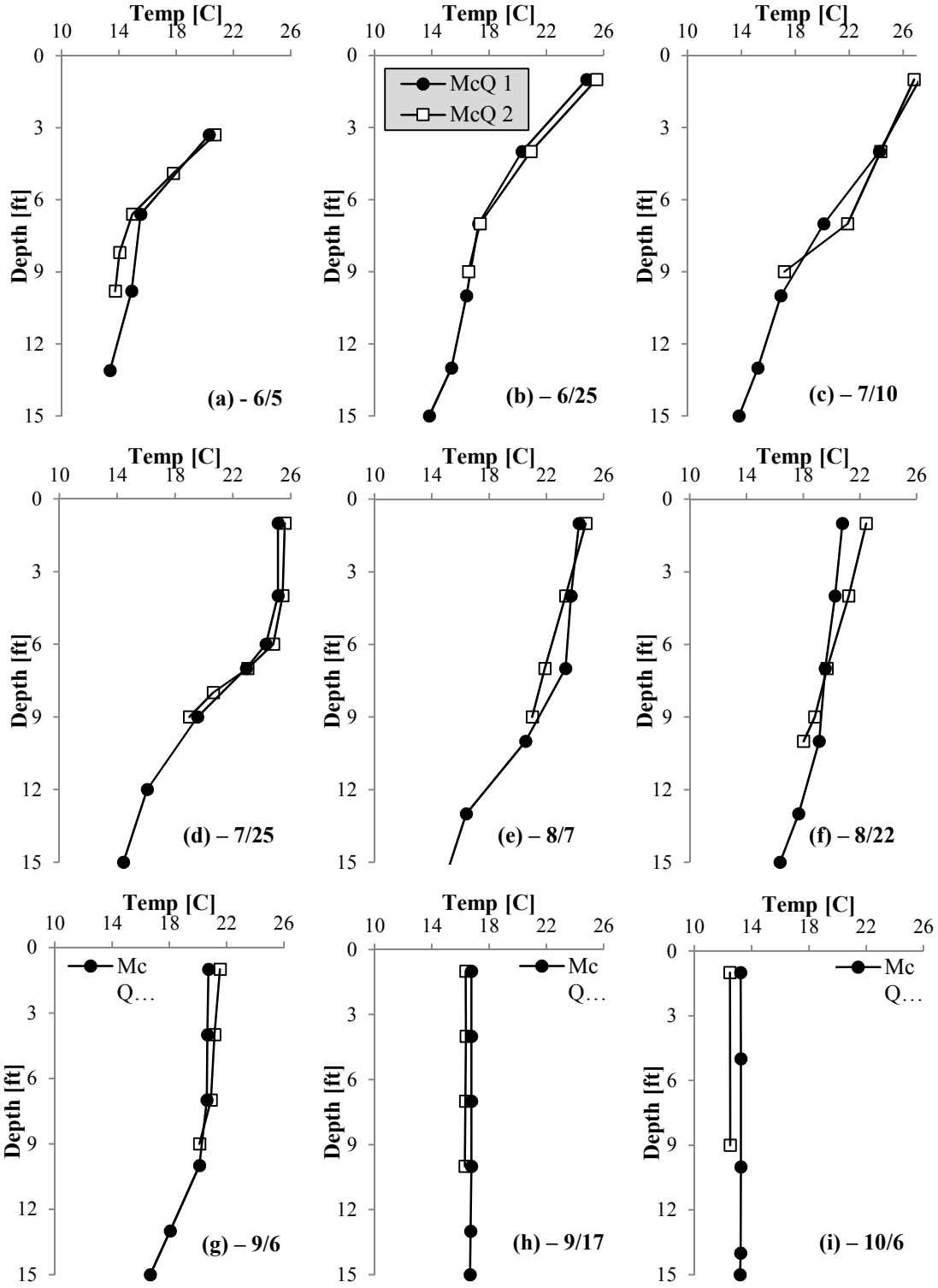

Fig 3.6(a-i). Temperature profiles at both sampling locations in Lake McQuade, measured biweekly from June to October 2012.

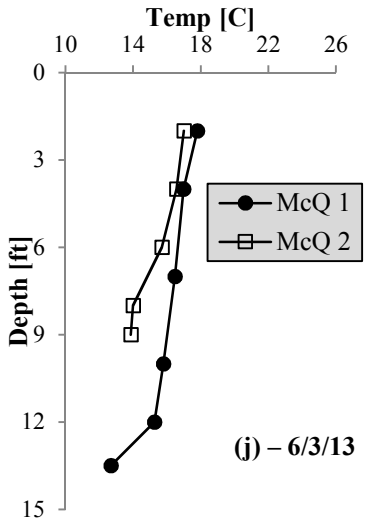

Fig 3.6(j). Temperature profiles at both sampling locations in Lake McQuade in June 2013.

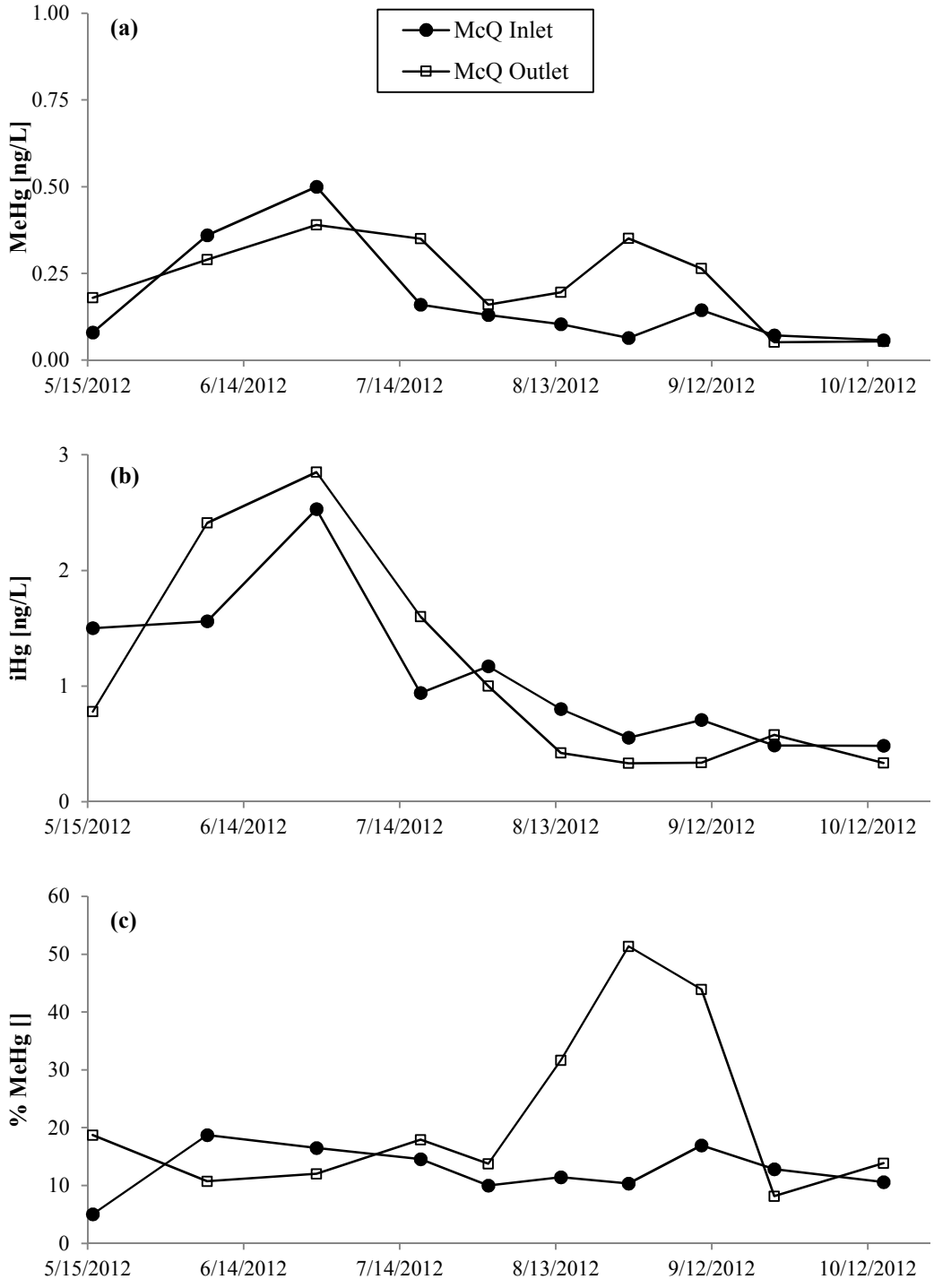

Fig 3.7(a-c). Time-series of Lake McQuade inlet and outlet streams, measured for: (a) MeHg, (b) iHg, (c) %MeHg

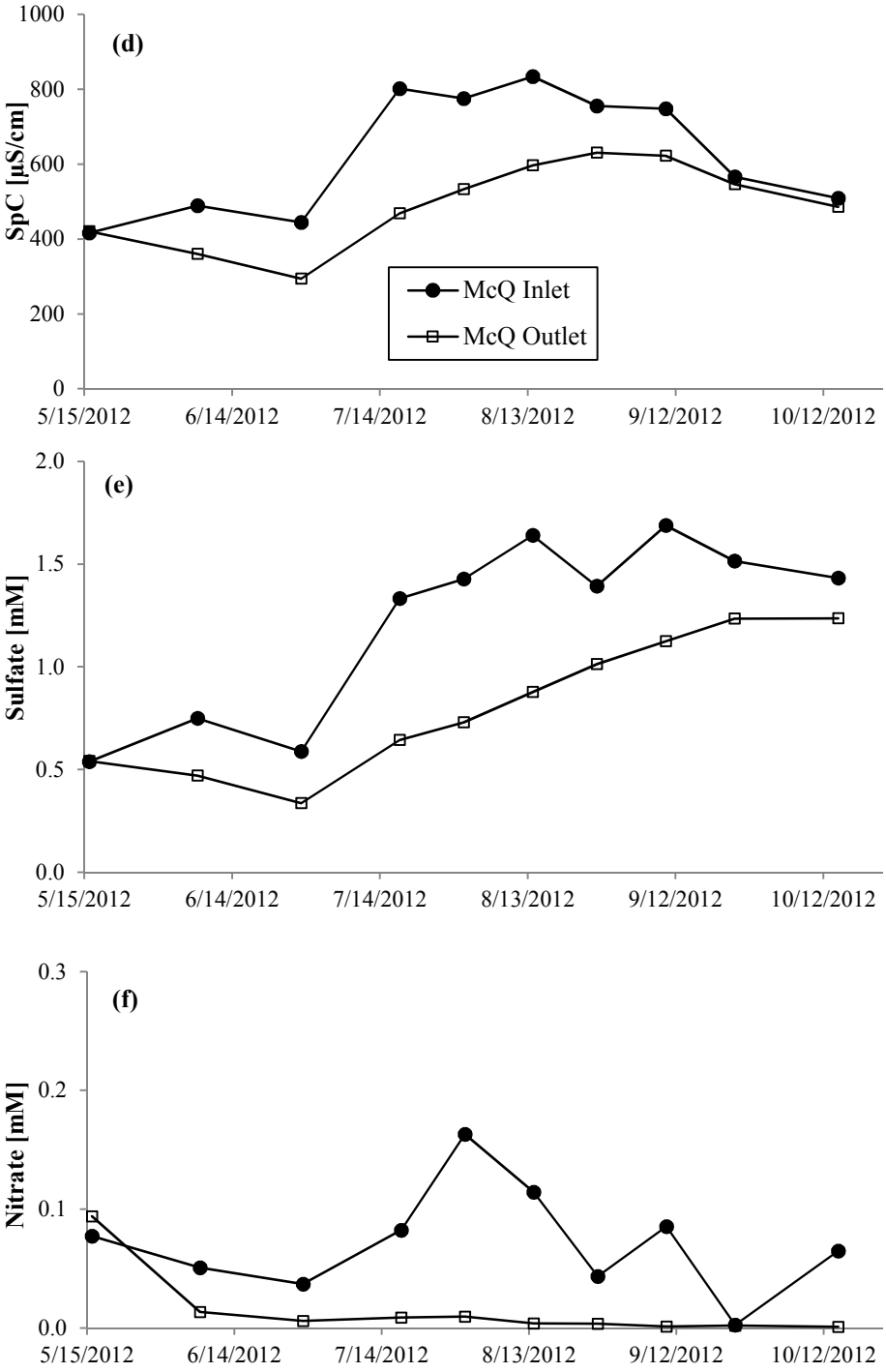

Fig 3.7(d-f). Time-series of Lake McQuade inlet and outlet streams, measured for: (d) specific conductivity, (e) sulfate, (f) nitrate

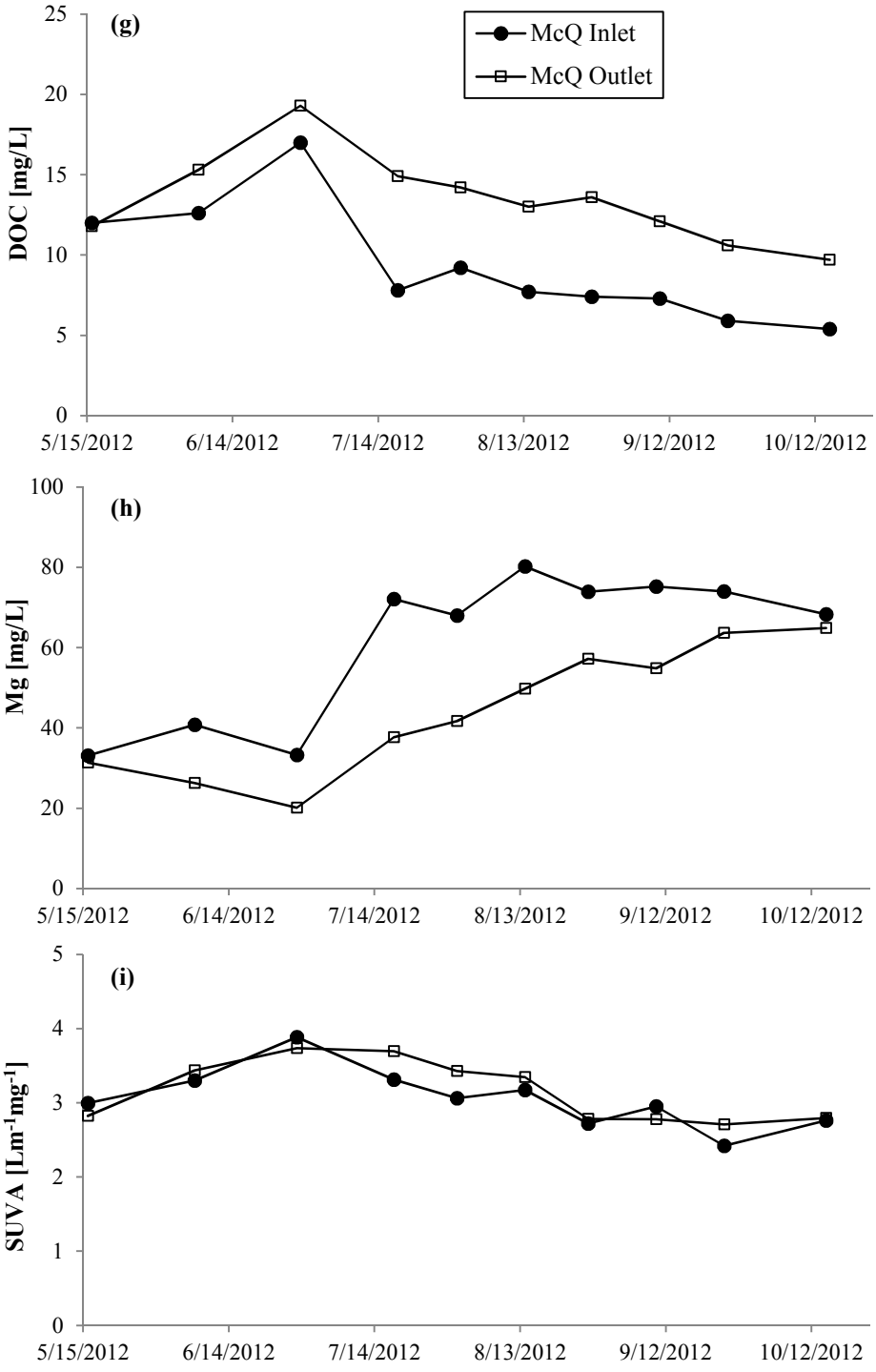

Fig 3.7(g-i). Time-series of Lake McQuade inlet and outlet streams, measured for: (g) DOC, (h) magnesium, (i) SUVA

Depth profiles in July 2012 (Fig 3.5b) and limnetic exchange calculations (Appendix F4) suggest a continued supply of sulfate to the hypolimnion from overlying waters. Reported half-saturation constants for sulfate reduction in lakes were found to range from 5 – 30 μM (~0.5 – 2.9 mg/L) in a review by Holmer & Storkholm (2001). Thus, despite relatively low bottom water sulfate concentrations, sulfate reduction in the hypolimnion may not have been sulfate-limited. However, it is not clear what bottom water sulfide concentrations would have been realized had bottom water sulfate been present at higher levels earlier in the summer.

Profiles of lake temperature and dissolved oxygen in mid-August provide evidence of mixing between the hypolimnion and epilimnion (Figs 3.6e & 3.6f), though anoxic conditions in bottom waters were quickly re-established (Figs 3.3a & 3.5c). This lake mixing event was associated with a rapid increase in bottom water sulfate (Fig 3.3c). However, bottom and surface water sulfate again diverged during late August and early September (Fig 3.3c) at a time when Mg concentrations in the surface and bottom waters were similar (Fig 3.3j). This observation is consistent with Phelps & Zeikus (1985), which found that the mixing of oxic surface waters with reduced bottom waters can result in the re-oxidation of reduced species in bottom waters and sediment (Phelps & Zeikus 1985). This can, in turn, supply favorable electron acceptors (oxidized iron, nitrate, and sulfate) for microbial metabolism if anoxic conditions are re-established in the bottom waters and sediment. This may explain the increase of sulfate observed in McQuade sediment porewater from July to October (Appendix B). Dissolved sulfide concentrations in the bottom water also increased after turnover, after sulfate was re-

supplied to the bottom waters and anoxic conditions were re-established (Fig 3.3e), suggesting sulfate reduction occurred following lake mixing.

Isotope analysis of sulfate molecules consistently showed that both $\delta^{18}O_{SO4}$ and $\delta^{34}S_{SO4}$ increased in the outlet compared to the inlet (Fig 3.8), a pattern consistent with the preferential reduction and removal of lighter sulfate molecules within the lake (Kelly et al. 2014). Isotope analysis of bottom water samples collected in late-August and early-September also suggested that sulfate reduction occurred in the bottom waters following partial lake mixing in mid-August (Kelly et al. 2014).

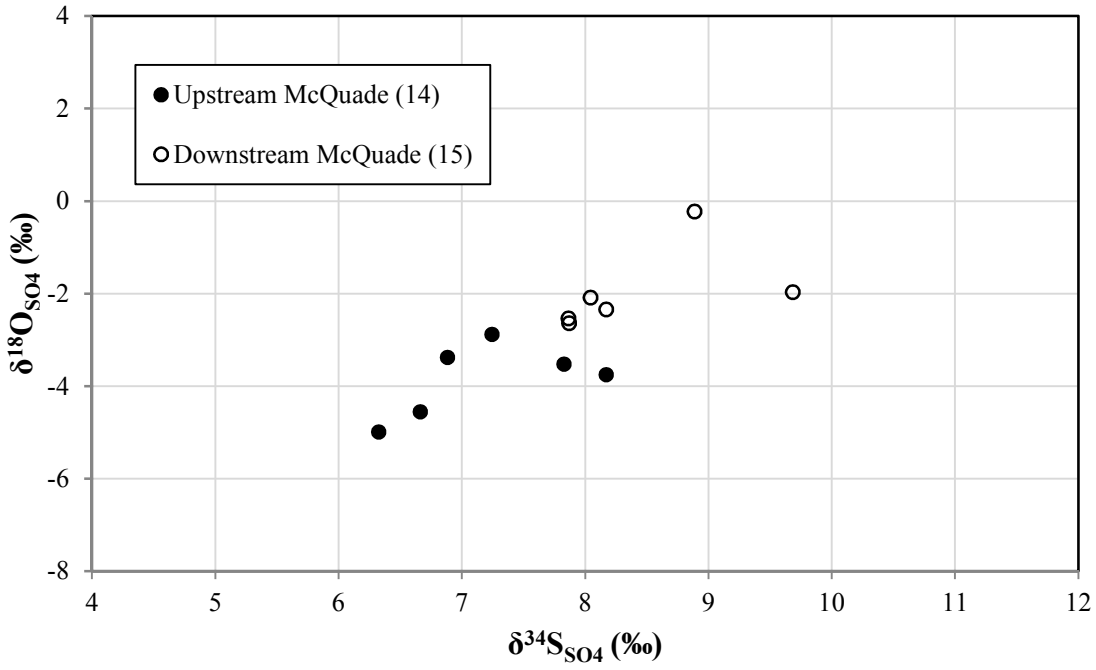

Fig 3.8. Isotope analysis on sulfate molecules in the inlet and outlet streams of Lake McQuade. Reduction preferentially favors lighter molecules, leaving behind a heavier pool of sulfate. Figure modified from data reported in Kelly et al. 2014.

Water Column Mercury

MeHg concentrations and %MeHg in the bottom waters of Lake McQuade increased from late-June to early-August (Figs 3.3g & 3.3f), with MeHg concentrations as high as 6.5 ng/L observed in the bottom water just prior to mid-August lake mixing (Fig 3.3g). A similar temporal trend in bottom water MeHg was observed in 0.7 μm filtered bottom water samples collected by the MnDNR, with bottom water MeHg concentrations peaking in early-August before lake mixing (Appendix C). The accumulation of MeHg in the hypolimnion could have been a result of: (1) production of MeHg in sediment porewater with subsequent flux into the hypolimnion, (2) production of MeHg in the bottom water, and (3) settling of particles carrying MeHg (e.g. algae, detritus) from the epilimnion.

Depth profiles at the deepest portion of Lake McQuade revealed higher %MeHg (25-50%) at depths below the redoxcline in June, July, and August 2012 than at oxygenated shallower depths (< 25%) (Fig 3.5a-c). This could be the result of both MeHg production in anoxic zones (porewater and/or anoxic water column) and demethylation in the epilimnion. A period of increased MeHg and %MeHg in bottom waters (Figs 3.3f & 3.3g) corresponded with an observed period of decreased bottom water sulfate (Fig 3.3c). Thus it is possible that sulfate reduction and MeHg production within the anoxic water column contributed to the observed accumulation in the hypolimnion. Alternatively, the observed accumulation of MeHg in the hypolimnion could have been a result of preferential MeHg (as opposed to iHg) flux out of sediment porewaters.

From early-July to mid-August, dissolved iHg in the bottom water declined from 2.2 to 1.6 ng/L (Fig 3.3h), while a far larger increase was observed in bottom water MeHg (1.5 to 6.5 ng/L, Fig 3.3g). Thus, if water column methylation was the primary driver of MeHg accumulation in the hypolimnion, an additional source of iHg to the hypolimnion would be required. Inlet and surface water concentrations of iHg were not significantly different from bottom water concentrations (Figs 3.3h & 3.7b), and measurements of iHg in unfiltered surface water samples were not excessively higher than filtered samples (Appendix D), suggesting a low potential for the epilimnion to be a source of iHg to bottom waters either by flux across the limnetic surface or settling algal detritus. Sediment porewater iHg concentrations were also not excessively higher than bottom water concentrations (Table 3.1), however an advective transport mechanism of particulate-bound iHg in sediments to bottom waters cannot be ruled out as a source of iHg.

Bottom water MeHg concentrations increased at a similar time to an increase in bottom water DOC concentrations (Fig 3.3k). A supply of fresh DOC to the hypolimnion (e.g. settling algal detritus) under conditions favorable for sulfate reduction could have facilitated net mercury methylation. However, evidence of sulfate reduction in the bottom waters after partial lake mixing in mid-August, a time when bottom water DOC had decreased (Figs 3.3c & 3.3k), suggests that variations in DOC concentration did not govern the activity of SRB in the bottom waters.

Estimated Sediment Flux of Methyl- and Inorganic- Mercury

Flux of MeHg and iHg mass from sediment porewater was estimated for three sampling trips: July 2012, representing summer conditions with lake stratification, October 2012, representing fall season conditions with a well-mixed lake, and June 2013, representing late spring conditions. Though these three sampling times may not have captured the effects of all factors that influence MeHg in bottom waters over the course of a season, they are likely to reflect some general characteristic seasonal variations. It should be noted that although estimates were made assuming diffusive flux, molecular diffusion may not be the only process responsible for transport across the sediment-water interface (SWI). Methane was quantified in the bottom waters of Lake McQuade during summer 2012 by the MnDNR (unpublished data), raising the possibility that methane ebullition from sediment could provide an additional transport pathway for exchange between sediment and the water column.

Diffusive flux estimates of MeHg from Lake McQuade sediment porewater were positive during all three sampling events, ranging from 8.5 – 38.3 pmol/m^2/d at McQ1 and 5.0 – 11.6 pmol/m^2/d at McQ2 (Table 3.1). Diffusive MeHg flux estimates at both sampling locations displayed similar seasonal trends, with the lowest flux estimate occurring in July 2012, the median in October 2012, and the highest in June 2013 (Fig 3.9). During late spring conditions in June 2013 methylation rate potentials in the bottom water were not measured above the detection limit (Appendix B), likely because the lake had not yet established strong stratification (Fig 3.6j) and bottom water conditions in late spring may have been favorable to sulfate reduction for only a short period of time. The resulting

low amount of MeHg in the bottom water created a concentration gradient between surficial sediment porewater and the lake bottom water which drove higher diffusive flux across the SWI. In July 2012, anoxic conditions after lake stratification led to MeHg accumulation in the bottom waters, such that bottom water concentrations were 80-90% that of surficial sediment porewater concentrations (Fig 3.3g, Table 3.1, Appendix B). This yielded lower, but still positive, sediment to water flux estimates for mid-summer conditions. In October 2012, well-mixed lake conditions and decreased biological activity at lower temperatures likely limited net MeHg production in both the bottom waters and sediment porewater.

Table 3.1. Estimated sediment flux of methylmercury (MeHg) and inorganic mercury (iHg) from sediment porewater to lake bottom waters in Lake McQuade

Sampling Location & Date	BW MeHg [ng/L]	PW MeHg (0-2cm) [ng/L]	**MeHg Flux [pmol/m^2/d]**	BW iHg [ng/L]	PW iHg (0-2cm) [ng/L]	**iHg Flux [pmol/m^2/d]**
McQ 1						
July '12	1.52	1.80	**8.5**	1.77	2.02	**2.3**
October '12	0.12	0.68	**15.9**	0.76	2.80	**18.7**
June '13	0.21	1.57	**38.3**	2.37	10.42	**72.9**
McQ 2						
July '12	0.39	0.54	**5.0**	1.35	2.81	**12.9**
October '12	0.07	0.33	**6.7**	0.92	1.80	**7.4**
June '13	0.21	0.65	**11.6**	4.02	8.51	**37.6**

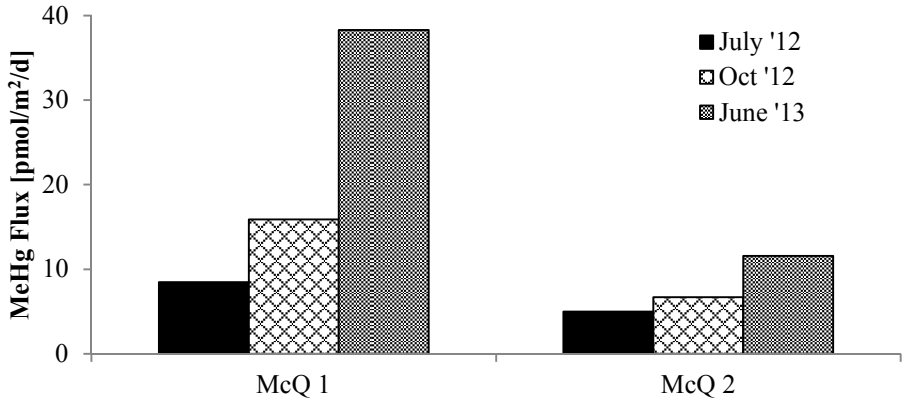

Fig. 3.9. Estimated flux of MeHg from Lake McQuade sediment to water column

Inlet & Outlet Methylmercury and Dissolved Organic Carbon

Outlet DOC concentrations were consistently higher than inlet DOC throughout the summer and fall, implying that Lake McQuade is a net source of DOC to the downstream system (Fig 3.7g). Outlet concentrations of MeHg were also slightly higher on average than inlet concentrations over the course of the sampling period (Fig 3.7a). MeHg was positively correlated with DOC in both inlet ($R^2 = 0.74$) and outlet ($R^2 = 0.66$) streams. While linear trendlines of inlet and outlet data had nearly identical slopes, the outlet trendline was shifted towards higher DOC concentrations, implying that the outlet stream carried less MeHg per mass of DOC than the inlet stream (Fig 3.10). The similarity between inlet and outlet SUVA measurements (Fig 3.7i) suggests that this difference in carrying capacity was not related to a change in the aromaticity of the DOC pool (Fig 3.7i). Alternatively, a previous study of DOC and MeHg in the watershed proposed that DOC pools composed of heavier molecules had a reduced capacity to carry MeHg (Berndt & Bavin 2012a). Thus, one possible explanation for the shift in the MeHg:DOC trendlines could be that the DOC added in Lake McQuade was of higher molecular

weight than the existing DOC pool, causing a change in the DOC-MeHg binding capacity.

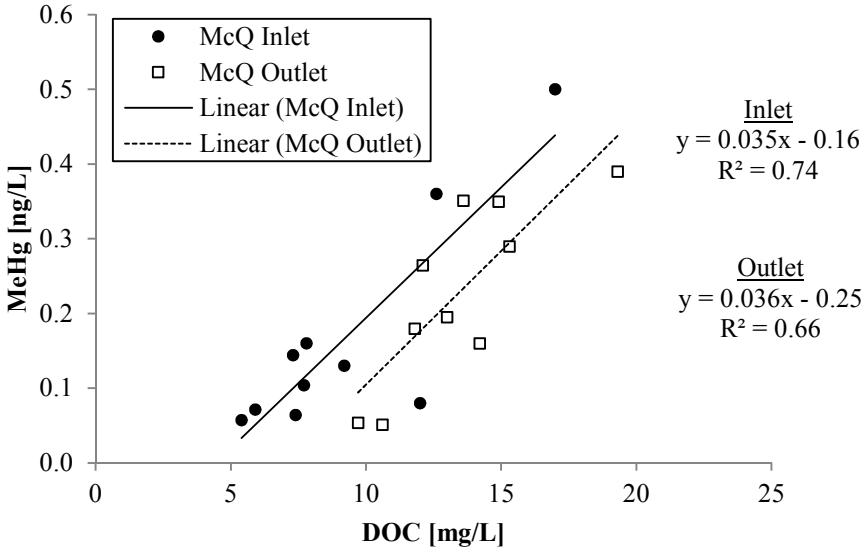

Fig. 3.10. Relationship between MeHg and DOC in Lake McQuade inlet and outlet streams. Samples collected during summer and fall 2012.

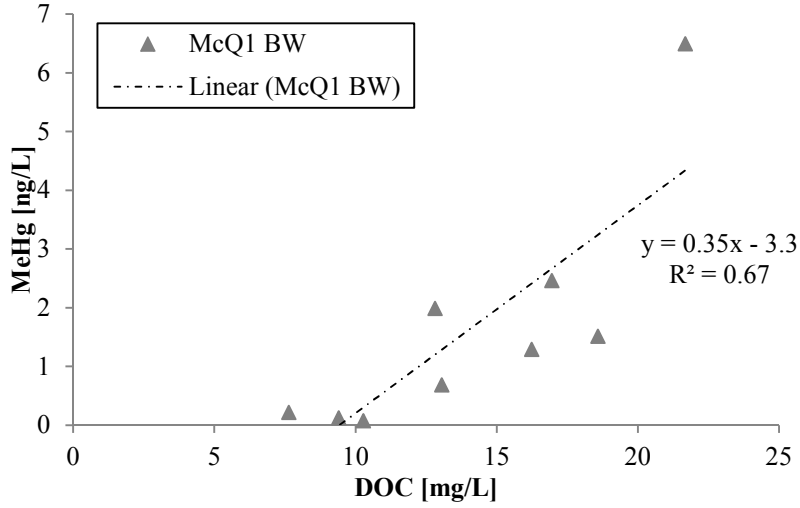

Fig. 3.11. Relationship between MeHg and DOC concentrations in the bottom waters of Lake McQuade. Samples collected during summer and fall 2012. Note difference in y-axis scale with Fig 3.10.

Bottom water concentrations of DOC and MeHg were also correlated (Fig 3.11), however the MeHg:DOC relationship in the bottom water was much different than that observed in the inlet and outlet (10x higher slope). Transport of MeHg in oxic waters, such as streams, typically occurs through binding with DOC. Thus, DOC is important in determining MeHg concentrations in areas where production is unlikely and transport is the primary source of MeHg. This may explain why the inlet and outlet streams contained 4 – 10 times less MeHg for a given DOC concentration than the bottom waters.

Modeling Results

Magnesium and Lake Residence Time

Specific conductivity, magnesium (Mg), and sulfate increased in the surface waters of Lake McQuade over the course of the summer (Figs 3.3c, 3.3j, 3.3l, 3.4c, 3.4j) in response to an abrupt increase in inlet concentrations occurring between 6/28 and 7/18 (Figs 3.7d, 3.7e, 3.7h). The summer of 2012 was characterized by a multiple large regional hydrologic events in May and June, followed by extremely dry months of July, August, and September (Fig 3.12). Previous research in the watershed observed steadily increasing concentrations of dissolved sulfate, Mg, and Ca over the course of a dry summer as mine-influenced water comprised a larger portion of the river flow (Berndt & Bavin 2012b). It is likely that the abrupt increase in inlet concentrations of Mg, sulfate, and conductivity reflect the change between wet spring conditions (with high flows) and dry summer conditions (with low flows), though changes in the inlet stream composition could have also been affected by a mid-summer change in mine water management.

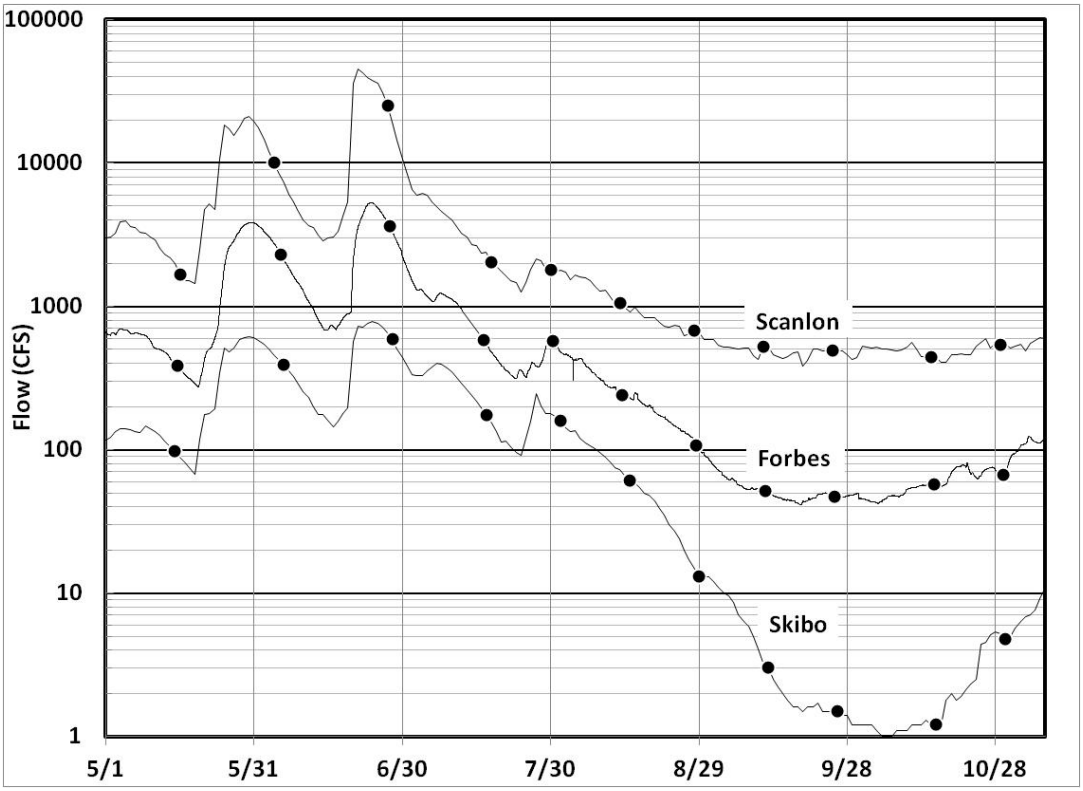

Fig 3.12. Stream flow data recorded at three different gauges along the St. Louis River from May to October 2012. Lake McQuade lies on a tributary to the St. Louis River between Forbes and Scanlon. Figure reproduced from Berndt et al. 2014.

Inlet Mg increased from 29 mg/L in late June to between 68 – 75 mg/L from early-July through mid-October (Fig 3.7h). By modeling Mg as a conservative tracer (i.e. assuming Mg is non-reactive in the water column), the response of Mg in the outlet stream to this rapid increase in inlet Mg can be used to estimate the mean lake residence time (τ) during the lower flow period of July through October.

Despite the close proximity of inlet and outlet streams, little difference was observed in surface water Mg, Ca, and conductivity between the two lake sampling sites (Figs 3.3j, 3.3l, 3.4j, Appendix B), supporting the assumption of a well-mixed epilimnion. Since little difference was also observed among surface water observations at McQ1 and McQ2

and observations in the outlet, the epilimnetic Mg concentrations calculated in the model were fit to data observations in the outlet and both surface water locations in the lake. The start date (t_0) of the Mg model was set to the date 7/10 so that measured field data could be used for initial values. A constant inlet concentration (C_{in}) of 78 mg/L (average inlet concentration during low flow conditions) was applied to the model (Fig 3.13).

Mean whole-lake residence time was estimated to be in the range of 45–65 days (Fig 3.14), with the model optimized at a residence time of 55.4 days. This suggests an average flow rate of approximately 36,000 m^3/d into and out of Lake McQuade during dry, low flow conditions. Though some variation in flow likely occurred over this time period, this average flow rate is used in describing mass loads from streams into and out of Lake McQuade as a means of comparing to internal loading/cycling.

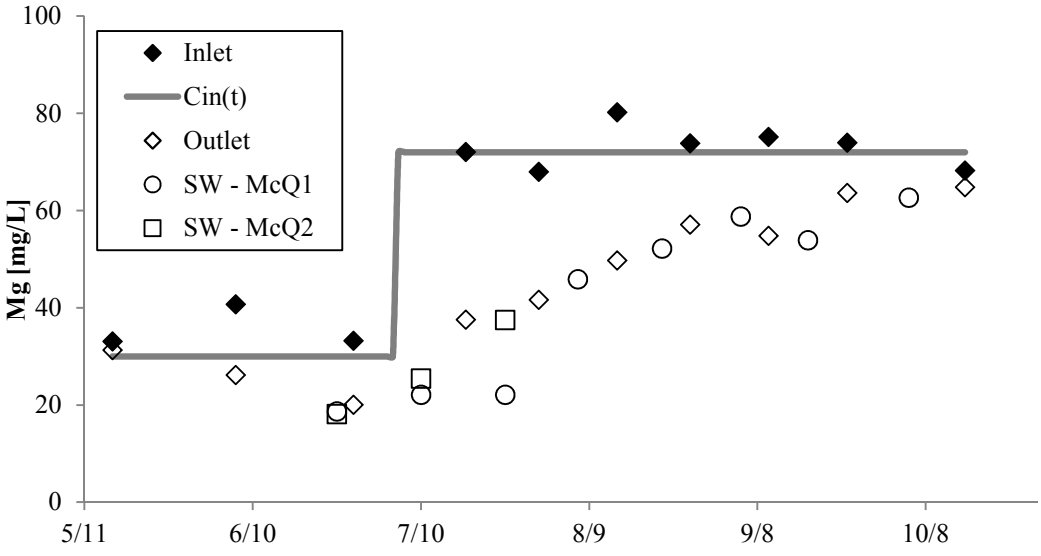

Fig 3.13. Concentrations of magnesium in the inlet, outlet, and surface waters of Lake McQuade over the summer and early fall. Dotted line represents the modeled inlet concentration during wet, high flow conditions (May to early July 2012) and during dry, summer conditions (mid-July to September 2012)

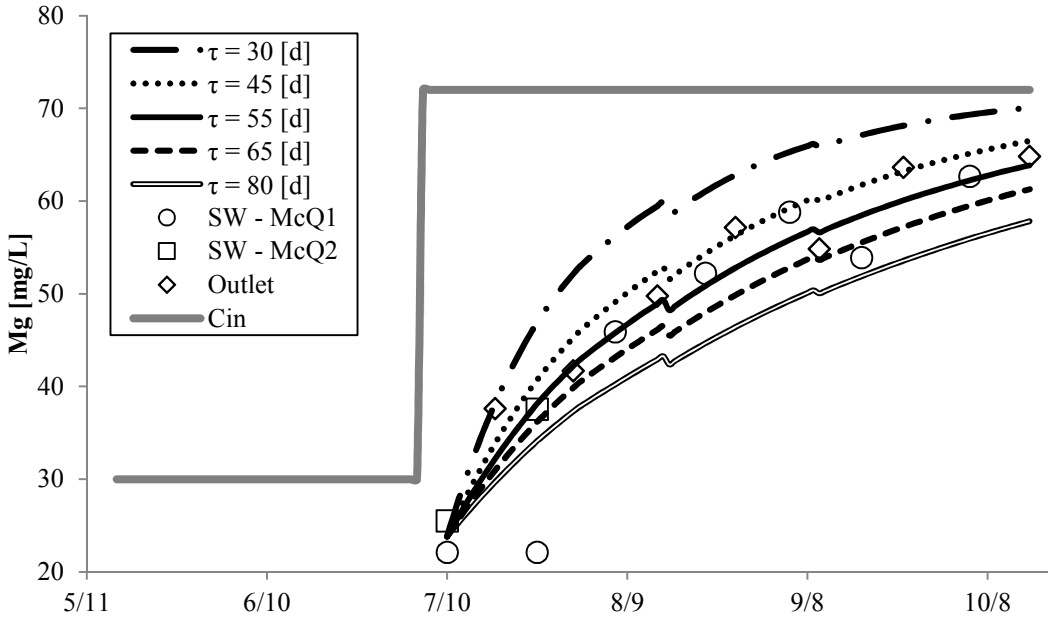

Fig 3.14. Measured concentrations of Mg in Lake McQuade surface water and outlet samples, overlain with modeled epilimnetic magnesium concentrations at varying residence times.

Since flux across the limnetic surface is likely to be the sole source of high-Mg water to the hypolimnion, the vertical diffusivity coefficients (K_z) estimated from thermal-density gradients can be validated through a comparison of modeled and observed bottom water Mg concentrations (Fig 3.15). The large increase in hypolimnion Mg between 8/7 & 8/22 is described by a mixing event which occurred in mid-August (Fig 3.6e & 3.6f). In the absence of other information, this mixing event was included in the model on 8/15 (halfway between sampling dates 8/7 & 8/22). A comparison of modeled and observed bottom water Mg (Fig 3.15) shows that the modeled exchange between layers does a reasonable job in describing hypolimnion Mg concentrations.

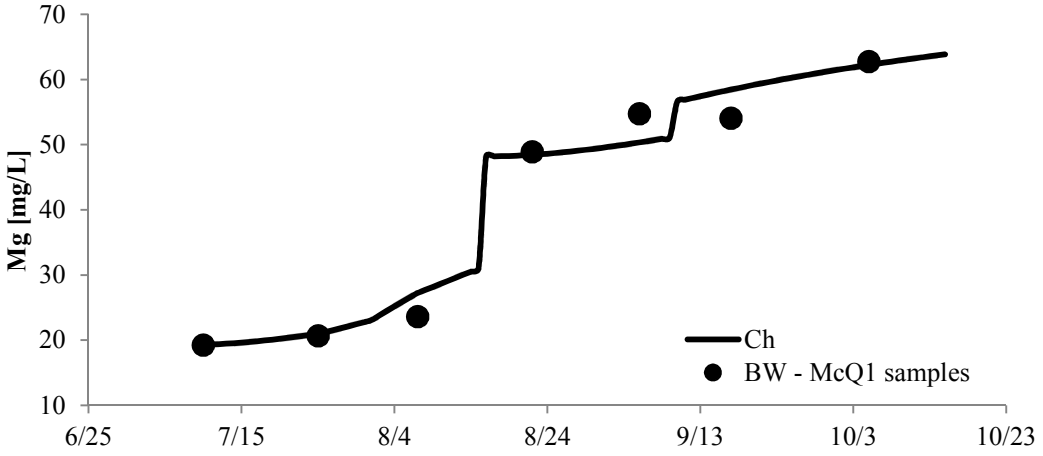

Fig 3.15. Observed and modeled hypolimnetic Mg concentrations, using a lake residence time of 55 days.

Sulfate Loss Estimates

An increase in sulfate concentration occurred in the inlet stream concurrently with the increase in Mg (Fig 3.7e). Sulfate concentrations in the outlet stream did not rise to match inlet concentrations as quickly or completely as Mg concentrations, implying loss of sulfate from within the lake (Figs 3.13 & 3.16). While sulfate reduction is typical in the anoxic upper layers of freshwater sediment underlying water containing sulfate, net sulfate reduction within the water column is less common. However, the absence of more favorable electron acceptors in the bottom waters of Lake McQuade suggests that conditions were sufficiently reduced to support sulfate reduction in the hypolimnion. Additionally, the low amount of sulfate present in sediment porewater (<0.01 mM in July at McQ1; Appendix B) compared to bottom water concentrations prior to lake mixing (0.04 – 0.16 mM, Fig 3.3c) would have driven diffusive flux from epilimnetic and hypolimnetic overlying waters into sediment porewaters, creating a sink for water column

sulfate. Thus, the observed loss of sulfate from the lake during stratified conditions was likely due to a combination of sulfate reduction in the hypolimnion and sulfate flux into sediment porewater.

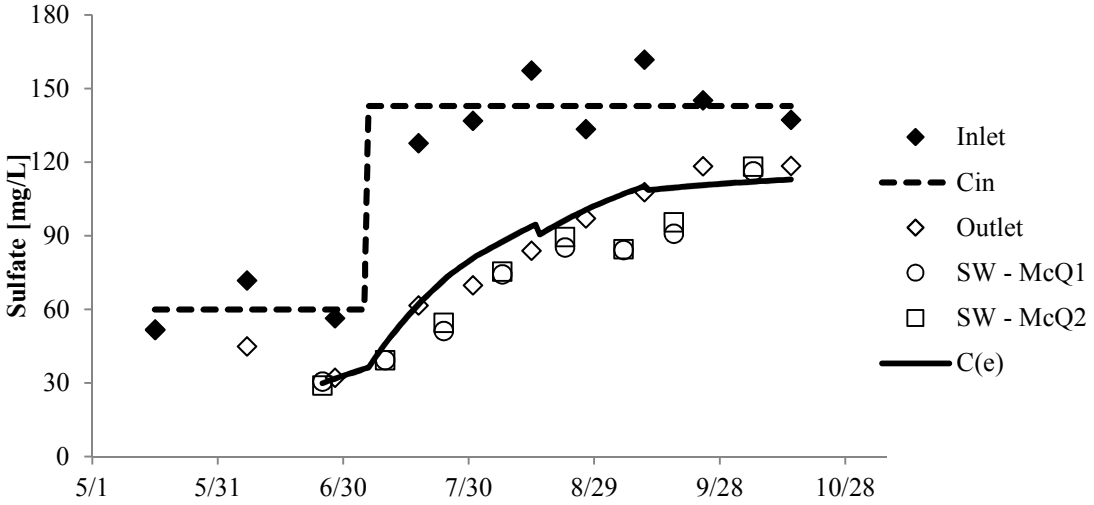

Fig 3.16. Observed and modeled sulfate concentrations in the epilimnion and inlet and outlet streams of Lake McQuade.

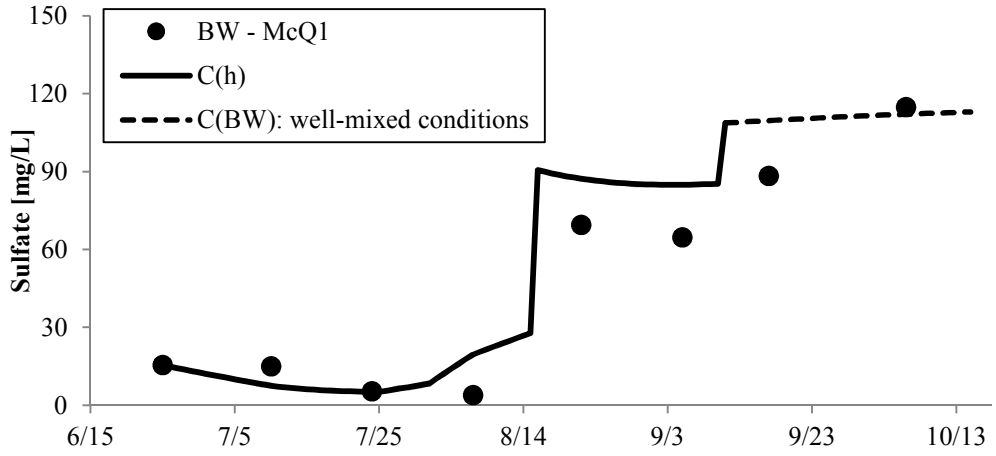

Fig 3.17. Observed and modeled sulfate concentrations in the bottom waters of Lake McQuade (hypolimnion disappears after lake turnover in mid-September).

A sulfate reaction term was included in the sulfate model to estimate the rate of sulfate loss in Lake McQuade. The term was applied in the hypolimnion volume only and represents a lumped, summer averaged, zero-order rate variable. As such, the sulfate reaction term was not intended to fully capture the complexity of transient sulfur dynamics or parse out the difference among sulfate reduction within the hypolimnion water column, flux to sediment in the hypolimnion, or flux to sediment in contact with the epilimnion. Instead, the sulfate loss term represents the average net sulfate loss from the entire lake over the course of the modeled time period. Fitting of modeled epilimnion and hypolimnion concentrations with observed surface and bottom water concentrations resulted in an estimated average sulfate loss term of ~200 kg/d (Fig 3.17) from 6/25 until the disappearance of hypolimnion in early-September.

Methylmercury Mass Flows

Consistent with previous research in stratified lakes (Eckley et al. 2005), dissolved MeHg accumulated in the hypolimnion from late June through mid-August. The estimated mass of dissolved MeHg present in the hypolimnion increased from ~480 mg to ~1000 mg between 6/25 and 8/7 – an average accumulation rate of 12.1 mg/d (Fig 3.18). Though bottom water MeHg concentrations peaked on the 8/7 sampling date (Fig 3.3g), total mass estimates of hypolimnetic MeHg peaked in early-July. This discrepancy is due to changes in the hypolimnion volume, which was largest in July and then decreased through August as the thermocline deepened (Fig 3.6b-f, Appendix F5).

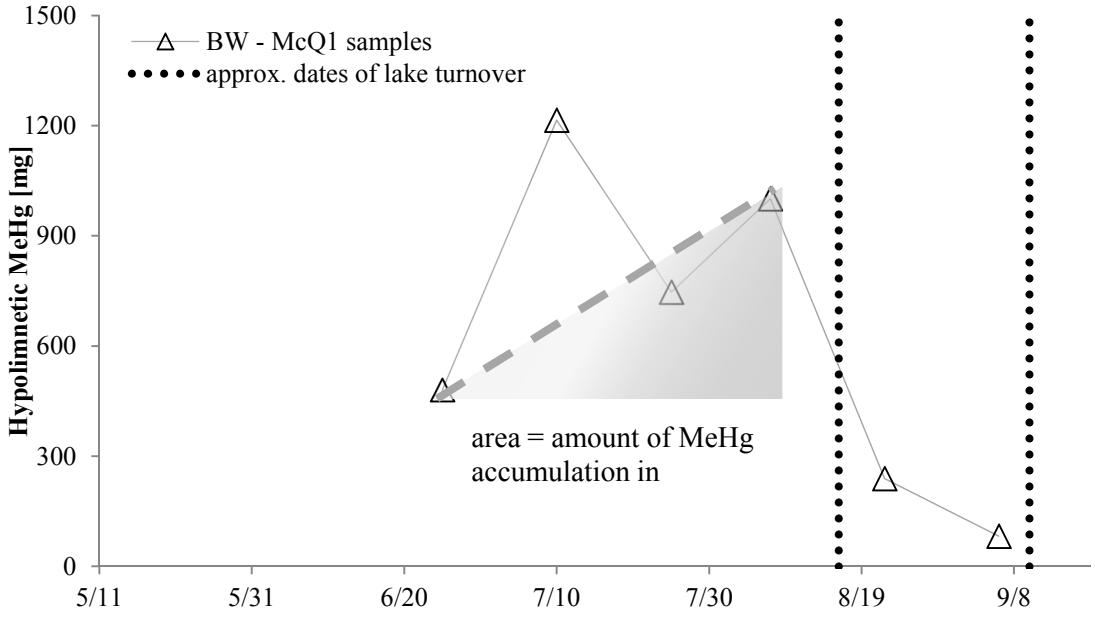

Fig 3.18. Estimates of total mass of MeHg in the hypolimnion over the summer. The dotted triangle represents the MeHg accumulation used in estimates of MeHg sinks and sources.

Since MeHg concentrations in the hypolimnion were consistently higher than in the epilimnion (Figs 3.3g, 3.5a, 3.5b), mixing across the limnetic surface resulted in a net movement of MeHg out of the hypolimnion and into the epilimnion. Based on limnetic transport coefficients estimated from temperature profiles (Appendix F4), loss of mass due to flux across the limnetic surface occurred at an average rate of 12.3 mg/d from 6/25 – 8/7 (Table 3.2). Sensitivity analysis on the estimated limnetic diffusion coefficients showed that even if the estimates were reduced by half, the resulting mass flux estimate would still represent the largest input of MeHg to the epilimnion (6.2 mg/d) during this time period.

Table 3.2. MeHg mass balances on the hypolimnion and epilimnion of Lake McQuade from 6/25/12 – 8/7/12

Hypolimnion mass balance		
m(SWI-hypolimnion)	[mg/d]	+0.8
m(limnetic surface)	[mg/d]	-12.3
net MeHg production	[mg/d]	+23.6
accumulation rate	**[mg/d]**	**+12.1**
Epilimnion mass balance		
m(inlet)	[mg/d]	+3.0
m(outlet)	[mg/d]	-4.4
m(limnetic surface)	[mg/d]	+12.3
m(SWI-epilimnion)	[mg/d]	+0.5
net MeHg destruction	[mg/d]	-16.8
accumulation rate	**[mg/d]**	**-5.4**

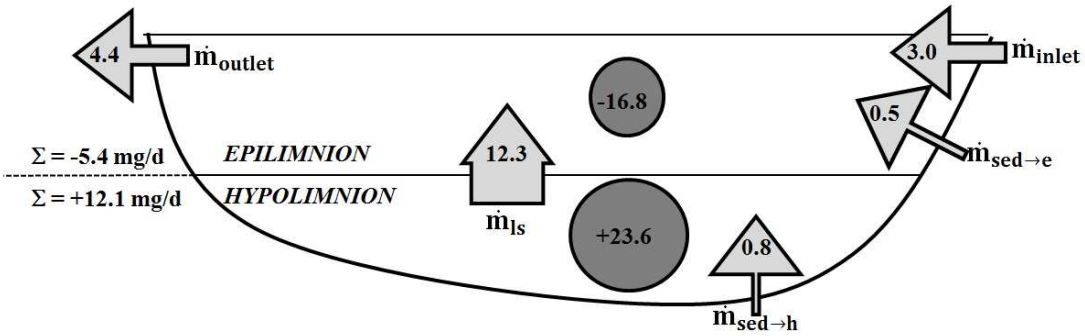

Fig 3.19. Schematic displaying estimated dissolved MeHg mass flows rates (arrows) into and out of both the epilimnion and hypolimnion, and estimated MeHg production and destruction in the water column. All values are in units of mg/d, and represent average of estimates made between 6/25/12 and 8/7/12. Net rates of accumulation and/or loss of MeHg are displayed to the left of the figure.

In order to account for the observed accumulation in the hypolimnion and the estimated loss across the limnetic surface, approximately 24.4 mg/d of MeHg must have contributed to the hypolimnion from various source pathways (Table 3.2, Fig 3.19). Estimations of MeHg flux from sediment porewater were in the range of 5 – 8.5 pmol/m^2/d during summer conditions (Table 3.1). This equates to an estimated loading rate of ~0.8 mg/d to the hypolimnion, which is more than an order of magnitude smaller than the total source loading required from the mass balance. Loading of MeHg sorbed to settling particles in the water column was not accounted for in the mass balance, however analysis of concurrent filtered and unfiltered water column samples showed that a majority of the MeHg present in surface and bottom waters existed in the dissolved phase (Appendix D), suggesting particle-bound MeHg was not a significant MeHg source to the hypolimnion. Additionally, because mass flow rates were estimated over a time period characterized by dry, low flow conditions (Fig 3.12), the contributions of MeHg from near shore surface runoff and wet precipitation were believed to be negligible. In the absence of another known source of MeHg, it can be inferred that net production of MeHg in the anoxic water column was the primary source of MeHg to the hypolimnion during summer 2012.

With other terms constrained by empirical observations, the mass balance analysis suggests that water column production of MeHg contributed 23.6 mg/d MeHg to the hypolimnion during the low flow, stratified period (Table 3.2, Fig 3.19). Based on the average of iHg mass in the hypolimnion over this time period, this rate of production corresponds to a bulk net methylation rate of 0.034 d^{-1}, which falls within the range of

reported methylation rates in hypolimnia (Eckley et al. 2005; Eckley & Hintelmann 2006). It should be noted that this average rate of net methylation represents a time period during which sulfate was depleted in the bottom waters, and that methylation rates could have increased later in the summer due to a re-supply of sulfate following partial lake mixing and re-establishment of anoxic conditions in the bottom waters (Figs 3.3c & 3.3a).

Estimates of total MeHg mass in the epilimnion fluctuated during the summer (100 to 500 mg), however the mass inventory was consistently smaller than in the hypolimnion during stable stratified conditions (Fig 3.20). The decline in total epilimnetic MeHg mass beginning in July corresponded with the onset of low flow conditions, when inlet concentrations of MeHg declined to <0.2 ng/L (Fig 3.7a), and epilimnetic MeHg did not increase again until after lake mixing in mid-August. Consistent with rainfall driven export observed in wetlands from other regions of the watershed (Johnson et al. 2014), inlet MeHg concentrations peaked in late-June/early-July (Fig 3.7a), likely causing the relatively high epilimnetic MeHg mass in early July. Stream gauging stations in other areas of the watershed showed that stream flows on 6/24/12 were 4-10 times higher than on 8/7/12 (Fig 3.12). This suggests that the inlet stream was likely the dominant MeHg source to the epilimnion under high flow conditions.

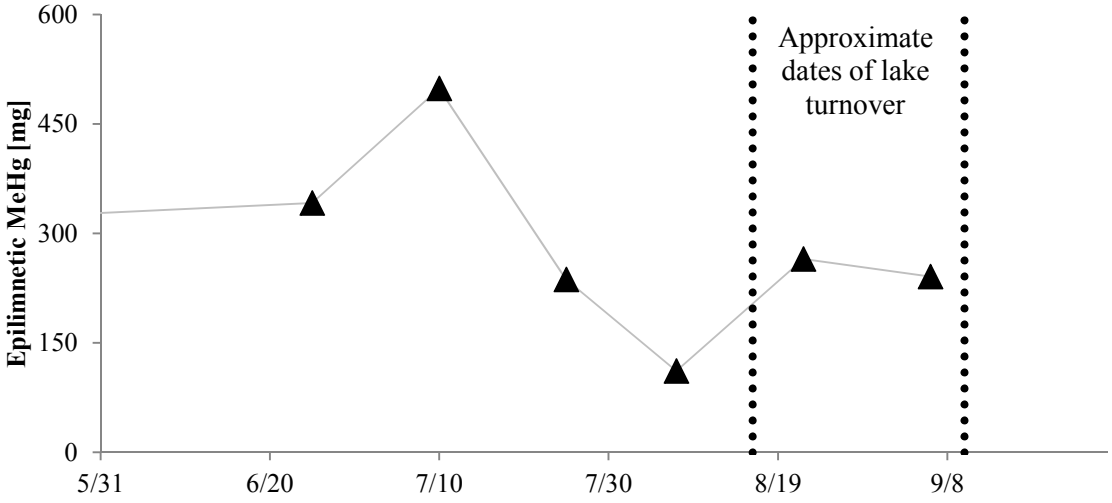

Fig 3.20. Estimated total mass of MeHg in the epilimnion of Lake McQuade from June to early-September 2012.

Inputs of MeHg to the epilimnion totaled ~16 mg/d from 6/25 – 8/7, while only ~4 mg/d was exported from the epilimnion via the outlet stream (Table 3.2, Fig 3.19). Thus, it appears that the epilimnion acted as a net sink for MeHg during this low-flow, stratified period. Mass balance analysis on the epilimnion suggests that net degradation of MeHg in the epilimnion occurred at a rate of 16.8 mg/d (Table 3.2). Thus, of the total MeHg mass input into the epilimnion during dry summer conditions, it is likely that most was degraded within the epilimnion prior to being exported downstream.

During June, MeHg concentrations in the outlet exceeded those in the inlet (Fig 3.7a), suggesting that Lake McQuade was a net sink for MeHg under high flow. However, from July to early-September 2012, outlet MeHg exceeded inlet MeHg (Fig 3.7a), suggesting that under low-flow stratified conditions Lake McQuade acted as a small net source of MeHg to downstream waters (Table 3.2). The difference in inlet and outlet

MeHg was especially pronounced during the time between initial lake turnover in mid-August to complete mixing in mid-September (i.e. dates 8/16 thru 9/10), during which MeHg was exported to the outlet stream at a rate of 4.3 mg/d despite a loading of only 1.5 mg/d from the inlet. Additionally, %MeHg was elevated in the outlet stream over this time period relative to the rest of the year (Fig 3.7c). Since the rise in outlet MeHg and %MeHg occurred in the weeks following at least partial mixing of the epilimnion with the MeHg-rich hypolimnetic waters, it is possible that mixing brought MeHg from the hypolimnion into surface waters, rendering it available for downstream export. A similar pattern in surface water MeHg concentrations was observed following lake turnover in Watras et al. (2005).

Although the volume of the hypolimnion was estimated to be about 1/10th that of the epilimnion at the time of lake turnover (Appendix F5), the amount of MeHg mass in the hypolimnion was estimated to be more than three times that of the epilimnion (Figs 3.18 & 3.20). Observations just prior to mid-August lake turnover showed MeHg present at 0.06 ng/L in the surface water and 6.50 ng/L in the bottom water (Fig 3.3g). Using these measurements to represent epilimnion and hypolimnion concentrations at the time of turnover, basic mixing calculations (assuming complete mixing) suggest that a whole-lake concentration of MeHg could have exceeded 0.56 ng/L immediately following lake turnover. Though epilimnetic demethylation rates are not known with certainty, the total mass of MeHg in the hypolimnion was more than sufficient to be the source of the measureable increase in MeHg export from Lake McQuade in the outlet stream.

Discussion & Conclusions

Evidence of sulfate loss and MeHg accumulation in the hydrologically isolated, anoxic bottom waters of Lake McQuade during the summer of 2012 suggests concurrent sulfate reduction and net MeHg production in the anoxic zones of the lake. Both geochemical and isotopic data provide evidence of sulfate reduction in the hypolimnion of Lake McQuade. However, due to limitations in sampling resolution, the analysis performed in this chapter is not able to quantitatively identify the precise locations where process such as Hg-methylation and sulfate reduction occurred.

A mass balance on MeHg in the hypolimnion identified production in the anoxic water column as the primary contributor of MeHg to the hypolimnion during the stratified, low-flow summer period. This is consistent with a study evaluating the MeHg budget of Devil's Lake in Wisconsin, where water column MeHg production was an order of magnitude larger than loading from external sources (Watras et al. 2005). However, the observed increase in bottom water MeHg concentrations was not coupled with a corresponding decrease in bottom water iHg. This can be interpreted in two different ways:

(1) The observed accumulation of MeHg in the hypolimnion was primarily a result of sediment flux of MeHg. This case does not require methylation in the anoxic water column to occur at a rate significant enough to diminish iHg concentrations in the bottom water, though it does require flux from sediment to be significantly larger than the flux estimated using July data. It is possible that

estimates derived from discrete time points underestimated the contribution of sediment flux to the hypolimnion at different points in the summer. However, it remains unlikely that sediment flux driven by diffusion alone would reach the levels required to account for the rate of MeHg accumulation in the hypolimnion, as sediment flux estimates were more than an order of magnitude smaller than what was required, despite falling within range of other reported values of diffusive MeHg flux from sediment.

(2) Production of MeHg in the water column was a substantial source of MeHg to the hypolimnion. In this case, bottom waters needed to be replenished with iHg from an external source or sources at a rate similar to the rate of MeHg production. This possibility of rapid iHg cycling could explain the relatively consistent concentrations of bottom water iHg during the summer, as well as the robust rate of net MeHg production in the water column suggested by the mass balance analysis. However, a source with the potential to supply iHg to the bottom waters at a rate consistent with MeHg accumulation in bottom waters has not been identified with certainty since: (a) epilimnion concentrations of dissolved iHg were too low to drive substantial iHg transport across the limnetic surface, (b) only a small fraction of total epilimnetic iHg was present on the particulate phase, ruling out settling particles as a possible significant iHg source, and (c) diffusion-driven flux of iHg from sediment porewater is far lower than the rate of MeHg accumulation in the hypolimnion.

Although bottom water concentrations of sulfate in June and July were low, water column depth profiles suggest continued re-supply of sulfate from the epilimnion. At times when the surface water was elevated with sulfate, %MeHg was in excess of 30% immediately below the oxic-anoxic boundary. Thus, although stratification appeared to limit the supply of sulfate to the hypolimnion and anoxic sediments, sulfate reduction may have been more active in areas of the hypolimnion closer to the oxic-anoxic boundary.

Since bottom water and surface water measurements were used to define the entire hypolimnion and epilimnion, the estimated MeHg mass flow rates used in the mass balance analysis do not fully account for variations with depth in the water column. Future work to observe and quantify possible depth trends of sulfate reduction and MeHg production and investigate sulfur- and mercury- related processes at varying flow regimes will improve our understanding of MeHg production and transport within stratified lakes.

A comparison of inlet and outlet MeHg suggests that Lake McQuade was small net exporter of MeHg during stable lake stratification. The estimated rate of net export, as compared to estimated rates of production and accumulation in the hypolimnion, suggests that very little of the MeHg produced in anoxic zones was exported downstream. Since MeHg in the hypolimnion was elevated at levels more than 50 times that of surface water, it appears lake stratification slowed export of hypolimnetic MeHg to surface waters. Nevertheless, modeling of the limnetic exchange in Lake McQuade suggests that MeHg was transported across the limnetic surface at a rate larger than estimated rates of MeHg mass inflow and outflow from streams during dry, low flow conditions. Thus,

degradation of MeHg in the epilimnion – by either photodegradation or microbial demethylation – also appears to be an important process limiting MeHg export from the production zones in the hypolimnetic waters and sediment.

A brief period of increased MeHg export appears to have occurred during the weeks immediately following lake mixing in August 2012. After the relatively large mass of hypolimnetic MeHg mixed quickly with surface waters, an abrupt increase in outlet MeHg concentration occurred. This period of partial mixing also re-supplied sulfate to the hypolimnion which, after anoxic conditions in the bottom waters were re-established, accelerated the production of sulfide in the hypolimnion. However, this did not result in significant MeHg accumulation in bottom waters, possibly due to weaker stratification and shorter time of exposure to bottom water anoxia prior to the establishment of well-mixed conditions in mid-September.

To conclude, sulfate loading to Lake McQuade resulted in production of MeHg in the anoxic zones of the lake, causing MeHg accumulation in the hypolimnion during the summer months. However, very little of the MeHg produced in the anoxic zones appeared to be exported from the lake over the course of the summer due to limited exchange across the limnetic surface and degradation reactions in the epilimnion. Evidence suggests that production in the anoxic water column was a significant contributor of MeHg, though production in anoxic sediments cannot be ruled out as a source of MeHg. The presence of dissolved Fe(II) in excess of dissolved sulfide in the bottom waters and anoxic porewaters for most of the stratified season may have provided a mechanism for limiting accumulation of dissolved sulfide in the anoxic regions of Lake

McQuade, which likely explains why sulfate reduction did not lead to stoichiometric increases in dissolved sulfide. Because dissolved sulfide does not appear to inhibit methylation below 10 μM (Chapter 2), sulfate reduction by SRB could lead to continuous and robust MeHg production in the anoxic zones of Lake McQuade.

Bibliography

Achá, D., Hintelmann, H., & Pabón, C. A. (2012). Sulfate-reducing bacteria and mercury methylation in the water column of the lake 658 of the experimental lake area. *Geomicrobiology Journal*, *29*(7), 667-674.

ASTM D2216-10 (2010). Standard test methods for laboratory determination of water (moisture) content of soil and rock by mass. ASTM International, West Conshohocken, PA. doi: 10.1520/D2216-10.

ASTM D7348 (2008). Standard test methods for loss on ignition (LOI) of soil combustion residues. ASTM International, West Conshohocken, PA.

Balogh, S. J., Swain, E. B., & Nollet, Y. H. (2006). Elevated methylmercury concentrations and loadings during flooding in Minnesota rivers. *Science of the Total Environment*, *368*(1), 138-148.

Barkay, T., Gillman, M., & Turner, R. R. (1997). Effects of dissolved organic carbon and salinity on bioavailability of mercury. *Applied and environmental microbiology*, *63*(11), 4267-4271.

Benoit, J. M., Gilmour, C. C., Heyes, A., Mason, R. P., & Miller, C. L. (2003). Geochemical and biological controls over methylmercury production and degradation in aquatic ecosystems. In *ACS symposium series* (Vol. 835, pp. 262-297). Washington, DC; American Chemical Society; 1999.

Benoit, J. M., Gilmour, C. C., Mason, R. P., & Heyes, A. (1999). Sulfide controls on mercury speciation and bioavailability to methylating bacteria in sediment pore waters. *Environmental Science & Technology*, *33*(6), 951-957.

Benoit, J. M., Gilmour, C. C., & Mason, R. P. (2001a). Aspects of bioavailability of mercury for methylation in pure cultures of Desulfobulbus propionicus (1pr3).*Applied and environmental microbiology*, *67*(1), 51-58.

Benoit, J. M., Gilmour, C. C., & Mason, R. P. (2001b). The influence of sulfide on solid-phase mercury bioavailability for methylation by pure cultures of Desulfobulbus propionicus (1pr3). *Environmental Science & Technology*, *35*(1), 127-132.

Benoit, J. M., Mason, R. P., Gilmour, C. C., & Aiken, G. R. (2001c). Constants for mercury binding by dissolved organic matter isolates from the Florida Everglades. *Geochimica et cosmochimica acta*, *65*(24), 4445-4451.

Berndt, M. E., & Bavin, T. K. (2009). Sulfate and mercury chemistry of the St. Louis River in Northeastern Minnesota: A Report to the Minerals Coordinating Committee. *Minnesota Department of Natural Resources, Division of Lands and Minerals. St. Paul, MN*.

Berndt, M. E., & Bavin, T. K. (2011). Sulfate and Mercury Cycling in Five Wetlands and a Lake Receiving Sulfate from Taconite Mines in Northeastern Minnesota. *Minnesota Department of Natural Resources, Division of Lands and Minerals. St. Paul, MN*.

Berndt, M. E., & Bavin, T. K. (2012a). Methylmercury and dissolved organic carbon relationships in a wetland-rich watershed impacted by elevated sulfate from mining. *Environmental Pollution*, *161*, 321-327.

Berndt, M. E., & Bavin, T. K. (2012b). On the cycling of sulfur and mercury in the St. Louis River Watershed, Northeastern Minnesota: An Environmental and Natural Resources Trust Fund final report. *Minnesota Department of Natural Resources, Division of Lands and Minerals. St. Paul, MN*.

Berndt, M., Jeremiason, J., Von Korff, B. (2014). Hydrologic and Geochemical Controls on St. Louis River Chemistry with Implications for Regulating Sulfate to Control Methylmercury Concentrations. *Minnesota Department of Natural Resources, Division of Lands and Minerals. St. Paul, MN*.

Bloom, N. S., Gill, G. A., Cappellino, S., Dobbs, C., McShea, L., Driscoll, C., ... & Rudd, J. (1999). Speciation and cycling of mercury in Lavaca Bay, Texas, sediments. *Environmental Science & Technology*, *33*(1), 7-13.

Blum, J. D., Popp, B. N., Drazen, J. C., Choy, C. A., & Johnson, M. W. (2013). Methylmercury production below the mixed layer in the North Pacific Ocean. *Nature Geoscience*, *6*(10), 879-884.

Bothner, M. H., Jahnke, R. A., Peterson, M. L., & Carpenter, R. (1980). Rate of mercury loss from contaminated estuarine sediments. *Geochimica et Cosmochimica Acta*, *44*(2), 273-285.

Boudreau, B. P. (1996). The diffusive tortuosity of fine-grained unlithified sediments. *Geochimica et Cosmochimica Acta*, *60*(16), 3139-3142.

Boudreau, B. P. (1997). *Diagenetic models and their implementation* (Vol. 505). Berlin: Springer.

Branfireun, B. A., Heyes, A., & Roulet, N. T. (1996). The hydrology and methylmercury dynamics of a Precambrian Shield headwater peatland. *Water Resources Research*, *32*(6), 1785-1794.

Branfireun, B. A., Roulet, N. T., Kelly, C., & Rudd, J. W. (1999). In situ sulphate stimulation of mercury methylation in a boreal peatland: Toward a link between acid rain and methylmercury contamination in remote environments.*Global Biogeochemical Cycles*, *13*(3), 743-750.

Bridou, R., Monperrus, M., Gonzalez, P. R., Guyoneaud, R., & Amouroux, D. (2011). Simultaneous determination of mercury methylation and demethylation capacities of various sulfate-reducing bacteria using species-specific isotopic tracers. *Environmental Toxicology and Chemistry*, *30*(2), 337-344.

Choi, S. C., Chase, T., & Bartha, R. (1994). Metabolic pathways leading to mercury methylation in Desulfovibrio desulfuricans LS. *Applied and environmental microbiology*, *60*(11), 4072-4077.

Clarkson, T. W. (1997). The toxicology of mercury. Critical reviews in clinical laboratory sciences, 34(4), 369-403.

Coleman Wasik, J. K., Mitchell, C. P., Engstrom, D. R., Swain, E. B., Monson, B. A., Balogh, S. J., ... & Almendinger, J. E. (2012). Methylmercury declines in a boreal peatland when experimental sulfate deposition decreases. *Environmental science & technology*, *46*(12), 6663-6671.

Compeau, G. C., & Bartha, R. (1984). Methylation and demethylation of mercury under controlled redox, pH and salinity conditions. *Applied and Environmental Microbiology*, *48*(6), 1203-1207.

Compeau, G. C., & Bartha, R. (1985). Sulfate-reducing bacteria: principal methylators of mercury in anoxic estuarine sediment. *Applied and environmental microbiology*, *50*(2), 498-502.

Correia, R. R., Miranda, M. R., & Guimarães, J. R. (2012). Mercury methylation and the microbial consortium in periphyton of tropical macrophytes: effect of different inhibitors. *Environmental research*, *112*, 86-91.

Cossa, D., Averty, B., & Pirrone, N. (2009). The origin of methylmercury in open Mediterranean waters. *Limnol. Oceanogr*, *54*(3), 837-844.

Covelli, S., Faganeli, J., Horvat, M., & Brambati, A. (1999). Porewater distribution and benthic flux measurements of mercury and methylmercury in the Gulf of Trieste (Northern Adriatic Sea). *Estuarine, Coastal and Shelf Science*, *48*(4), 415-428.

Devereux, R., Winfrey, M. R., Winfrey, J., & Stahl, D. A. (1996). Depth profile of sulfate-reducing bacterial ribosomal RNA and mercury methylation in an estuarine sediment. *FEMS microbiology ecology*, *20*(1), 23-31.

Drott, A., Lambertsson, L., Björn, E., & Skyllberg, U. (2007). Importance of dissolved neutral mercury sulfides for methyl mercury production in contaminated sediments. *Environmental science & technology*, *41*(7), 2270-2276.

Drott, A., Lambertsson, L., Björn, E., & Skyllberg, U. (2008). Do potential methylation rates reflect accumulated methyl mercury in contaminated sediments?. *Environmental science & technology*, *42*(1), 153-158.

Dyrssen, D., & Wedborg, M. (1991). The sulphur-mercury (II) system in natural waters. *Water Air & Soil Pollution*, *56*(1), 507-519.

Eaton, A. D., Clesceri, L. S., Rice, E. W., Greenberg, A. E., & Franson, M. A. H. (2005). APHA: Standard Methods for the Examination of Water and Wastewater. *Centennial Edition., APHA, AWWA, WEF, Washington, DC*.

Eckley, C. S., & Hintelmann, H. (2006). Determination of mercury methylation potentials in the water column of lakes across Canada. *Science of the Total Environment*, *368*(1), 111-125.

Eckley, C. S., Watras, C. J., Hintelmann, H., Morrison, K., Kent, A. D., & Regnell, O. (2005). Mercury methylation in the hypolimnetic waters of lakes with and without connection to wetlands in northern Wisconsin. *Canadian Journal of Fisheries and Aquatic Sciences*, *62*(2), 400-411.

Emerson, S., & Hedges, J. (2008). *Chemical oceanography and the marine carbon cycle*. Cambridge University Press.

Fleming, E. J., Mack, E. E., Green, P. G., & Nelson, D. C. (2006). Mercury methylation from unexpected sources: molybdate-inhibited freshwater sediments and an iron-reducing bacterium. *Applied and environmental microbiology*, *72*(1), 457-464.

Friedli, H. R., Radke, L. F., Lu, J. Y., Banic, C. M., Leaitch, W. R., & MacPherson, J. I. (2003). Mercury emissions from burning of biomass from temperate North American forests: laboratory and airborne measurements.*Atmospheric Environment*, *37*(2), 253-267.

Furutani, A., & Rudd, J. W. (1980). Measurement of mercury methylation in lake water and sediment samples. *Applied and environmental microbiology*, *40*(4), 770-776.

Gerbig, C. A., Kim, C. S., Stegemeier, J. P., Ryan, J. N., & Aiken, G. R. (2011). Formation of nanocolloidal metacinnabar in mercury-DOM-sulfide systems. *Environmental science & technology*, *45*(21), 9180-9187.

Gill, G. A., Bloom, N. S., Cappellino, S., Driscoll, C. T., Dobbs, C., McShea, L., Mason, R. P., & Rudd, J. W. (1999). Sediment-water fluxes of mercury in Lavaca Bay, Texas. *Environmental science & technology*, *33*(5), 663-669.

Gill, G. A., & Bruland, K. W. (1990). Mercury speciation in surface freshwater systems in California and other areas. *Environmental Science & Technology*, *24*(9), 1392-1400.

Gilmour, C. C., Henry, E. A., & Mitchell, R. (1992). Sulfate stimulation of mercury methylation in freshwater sediments. *Environmental Science & Technology*, *26*(11), 2281-2287.

Gilmour, C. C., Riedel, G. S., Ederington, M. C., Bell, J. T., Gill, G. A., & Stordal, M. C. (1998). Methylmercury concentrations and production rates across a trophic gradient in the northern Everglades. *Biogeochemistry*, *40*(2-3), 327-345.

Gobeil, C., & Cossa, D. (1993). Mercury in sediments and sediment pore water in the Laurentian Trough. *Canadian Journal of Fisheries and Aquatic Sciences*, *50*(8), 1794-1800.

Gorski, P. R., Armstrong, D. E., Hurley, J. P., & Krabbenhoft, D. P. (2008). Influence of natural dissolved organic carbon on the bioavailability of mercury to a freshwater alga. *Environmental pollution*, *154*(1), 116-123.

Goyer, R. A., Vasken Aposhian, H., Arab, L., Bellinger, D. C., Burbacher, T. M., Burke, T. M., Burke, T. A., Jacobson, J. L., Knobloch, L. M., Ryan, L. M. and Stern, A.: 2000, Toxicological Effects of Methylmercury, National Academy Press, Washington, DC, 290 pp.

Graham, A. M., Aiken, G. R., & Gilmour, C. C. (2012a). Dissolved organic matter enhances microbial mercury methylation under sulfidic conditions.*Environmental science & technology*, *46*(5), 2715-2723.

Gray, J. E., & Hines, M. E. (2009). Biogeochemical mercury methylation influenced by reservoir eutrophication, Salmon Falls Creek Reservoir, Idaho, USA. *Chemical Geology*, *258*(3), 157-167.

Guimarães, J. R. D., Meili, M., Hylander, L. D., Roulet, M., Mauro, J. B. N., & de Lemos, R. A. (2000). Mercury net methylation in five tropical flood plain regions of Brazil: high in the root zone of floating macrophyte mats but low in surface sediments and flooded soils. *Science of the Total Environment*, *261*(1), 99-107.

Gustin, M. S., Lindberg, S. E., Austin, K., Coolbaugh, M., Vette, A., & Zhang, H. (2000). Assessing the contribution of natural sources to regional atmospheric mercury budgets. *Science of the Total Environment*, *259*(1), 61-71.

Hamelin, S., Amyot, M., Barkay, T., Wang, Y., & Planas, D. (2011). Methanogens: principal methylators of mercury in lake periphyton.*Environmental science & technology*, *45*(18), 7693-7700.

Hammerschmidt, C. R., & Fitzgerald, W. F. (2006). Photodecomposition of methylmercury in an arctic Alaskan lake. *Environmental science & technology*, *40*(4), 1212-1216.

Hammerschmidt, C. R., Fitzgerald, W. F., Balcom, P. H., & Visscher, P. T. (2008). Organic matter and sulfide inhibit methylmercury production in sediments of New York/New Jersey Harbor. *Marine Chemistry*, *109*(1), 165-182.

Hammerschmidt, C. R., Fitzgerald, W. F., Lamborg, C. H., Balcom, P. H., & Visscher, P. T. (2004). Biogeochemistry of methylmercury in sediments of Long Island Sound. *Marine Chemistry*, *90*(1), 31-52.

Harmon, S. M., King, J. K., Gladden, J. B., Chandler, G. T., & Newman, L. A. (2004). Methylmercury formation in a wetland mesocosm amended with sulfate.*Environmental science & technology*, *38*(2), 650-656.

Hayduk, W., & Laudie, H. (1974). Prediction of diffusion coefficients for nonelectrolytes in dilute aqueous solutions. *AIChE Journal*, *20*(3), 611-615.

Helms, J. R., Stubbins, A., Ritchie, J. D., Minor, E. C., Kieber, D. J., & Mopper, K. (2008). Absorption spectral slopes and slope ratios as indicators of molecular weight, source, and photobleaching of chromophoric dissolved organic matter. *Limnology and Oceanography*, *53*(3), 955.

Hildebrand, S. G., Strand, R. H., & Huckabee, J. W. (1980). Mercury accumulation in fish and invertebrates of the North Fork Holston River, Virginia and Tennessee. *Journal of Environmental Quality*, *9*(3), 393-400.

Hines, N. A., & Brezonik, P. L. (2007). Mercury inputs and outputs at a small lake in northern Minnesota. *Biogeochemistry*, *84*(3), 265-284.

Hines, N. A., Brezonik, P. L., & Engstrom, D. R. (2004). Sediment and porewater profiles and fluxes of mercury and methylmercury in a small seepage lake in northern Minnesota. *Environmental science & technology*, *38*(24), 6610-6617.

Hintelmann, H., & Evans, R. D. (1997). Application of stable isotopes in environmental tracer studies–Measurement of monomethylmercury (CH3Hg+) by isotope dilution ICP-MS and detection of species transformation. *Fresenius' journal of analytical chemistry*, *358*(3), 378-385.

Hintelmann, H., Keppel-Jones, K., & Evans, R. D. (2000). Constants of mercury methylation and demethylation rates in sediments and comparison of tracer and ambient mercury availability. *Environmental toxicology and chemistry*, *19*(9), 2204-2211.

Hintelmann, H., Ogrinc, N., (2003). Determination of stable mercury isotopes by ICP/MS and their application in environmental studies. In Cai, Y., & Braids, O. C. (Eds.), *Biogeochemistry of environmentally important trace elements: ACS Symposium Series Vol. 835* (p. 321-338). Washington, DC.

Holmer, M., & Storkholm, P. (2001). Sulphate reduction and sulphur cycling in lake sediments: a review. *Freshwater Biology*, *46*(4), 431-451.

Horvat, M., Liang, L., & Bloom, N. S. (1993). Comparison of distillation with other current isolation methods for the determination of methyl mercury compounds in low level environmental samples: Part II. Water. *Analytica Chimica Acta*, *282*(1), 153-168.

Hsu-Kim, H., Kucharzyk, K. H., Zhang, T., & Deshusses, M. A. (2013). Mechanisms regulating mercury bioavailability for methylating microorganisms in the aquatic environment: A critical review. *Environmental science & technology*, *47*(6), 2441-2456.

Hurley, J. P., Benoit, J. M., Babiarz, C. L., Shafer, M. M., Andren, A. W., Sullivan, J. R., Hammond, R., & Webb, D. A. (1995). Influences of watershed characteristics on mercury levels in Wisconsin rivers. *Environmental Science & Technology*, *29*(7), 1867-1875.

Jassby, A., & Powell, T. (1975). Vertical patterns of eddy diffusion during stratification in Castle Lake, California. *Limnol Oceanogr*, *20*, 530-543.

Jay, J. A., Murray, K. J., Gilmour, C. C., Mason, R. P., Morel, F. M., Roberts, A. L., & Hemond, H. F. (2002). Mercury methylation by Desulfovibrio desulfuricans ND132 in the presence of polysulfides. *Applied and environmental microbiology*, *68*(11), 5741-5745.

Jeremiason, J. D., Engstrom, D. R., Swain, E. B., Nater, E. A., Johnson, B. M., Almendinger, J. E., ... & Kolka, R. K. (2006). Sulfate addition increases methylmercury production in an experimental wetland. *Environmental science & technology*, *40*(12), 3800-3806.

Johnson, N. W., Mitchell, C. P., Engstrom, D. E., Bailey, L. T., Kelly, M. J., Coleman-Wasik, J. K., Berndt, M. E. (2014). Methylmercury production and transport in a sulfate-impacted sub-boreal wetland. Project Report. *Minnesota Department of Natural Resources, Division of Lands and Minerals. St. Paul, MN*.

Kelly, M. J., Berndt, M. E., Bavin, T. K. (2014). Use of sulfate and water isotopes to improve water and chemical balance estimates for water seeping from tailings basins (focus on US Steel's Minntac Basin). *Minnesota Department of Natural Resources, Division of Lands and Minerals. St. Paul, MN*.

Kerin, E. J., Gilmour, C. C., Roden, E., Suzuki, M. T., Coates, J. D., & Mason, R. P. (2006). Mercury methylation by dissimilatory iron-reducing bacteria.*Applied and environmental microbiology*, *72*(12), 7919-7921.

King, J. K., Kostka, J. E., Frischer, M. E., & Saunders, F. M. (2000). Sulfate-reducing bacteria methylate mercury at variable rates in pure culture and in marine sediments. *Applied and Environmental Microbiology*, *66*(6), 2430-2437.

King, J. K., Saunders, F. M., Lee, R. F., & Jahnke, R. A. (1999). Coupling mercury methylation rates to sulfate reduction rates in marine sediments.*Environmental Toxicology and Chemistry*, *18*(7), 1362-1369.

Korthals, E. T., & Winfrey, M. R. (1987). Seasonal and spatial variations in mercury methylation and demethylation in an oligotrophic lake. *Applied and environmental microbiology*, *53*(10), 2397-2404.

Langer, C. S., Fitzgerald, W. F., Visscher, P. T., & Vandal, G. M. (2001). Biogeochemical cycling of methylmercury at Barn Island salt marsh, Stonington, CT, USA. *Wetlands Ecology and Management*, *9*(4), 295-310.

Lehnherr, I., St. Louis, V. L., Emmerton, C. A., Barker, J. D., & Kirk, J. L. (2012). Methylmercury cycling in high arctic wetland ponds: sources and sinks. *Environmental science & technology*, *46*(19), 10514-10522.

Li, Y.-H., & Gregory, S. (1974). Diffusion of ions in sea water and in deep-sea sediments. *Geochimica et cosmochimica acta*, *38*(5), 703-714.

Maillacheruvu, K. Y., Parkin, G. F., Peng, C. Y., Kuo, W. C., Oonge, Z. I., & Lebduschka, V. (1993). Sulfide toxicity in anaerobic systems fed sulfate and various organics. *Water environment research*, 100-109.

Mason, R. P., Fitzgerald, W. F., & Morel, F. M. (1994). The biogeochemical cycling of elemental mercury: anthropogenic influences. *Geochimica et Cosmochimica Acta*, *58*(15), 3191-3198.

Matilainen, T., & Verta, M. (1995). Mercury methylation and demethylation in aerobic surface waters. *Canadian Journal of Fisheries and Aquatic Sciences*, *52*(8), 1597-1608.

Matthews, D. A., Effler, S. W., Driscoll, C. T., O'Donnell, S. M., & Matthews, C. M. (2008). Electron budgets for the hypolimnion of a recovering urban lake, 1989-2004: Response to changes in organic carbon deposition and availability of electron acceptors. *Limnology and Oceanography*, *53*(2), 743.

Mauro, J., Guimaraes, J., Hintelmann, H., Watras, C., Haack, E., & Coelho-Souza, S. (2002). Mercury methylation in macrophytes, periphyton, and water–comparative studies with stable and radio-mercury additions. *Analytical and bioanalytical chemistry*, *374*(6), 983-989.

Mergler, D., Anderson, H. A., Chan, L. H. M., Mahaffey, K. R., Murray, M., Sakamoto, M., & Stern, A. H. (2007). Methylmercury exposure and health effects in humans: a worldwide concern. *AMBIO: A Journal of the Human Environment*, *36*(1), 3-11.

Merritt, K. A., & Amirbahman, A. (2007). Mercury dynamics in sulfide-rich sediments: Geochemical influence on contaminant mobilization within the Penobscot River estuary, Maine, USA. *Geochimica et cosmochimica acta*,*71*(4), 929-941.

Merritt, K. A., & Amirbahman, A. (2008). Methylmercury cycling in estuarine sediment pore waters (Penobscot River estuary, Maine, USA). *Limnology and Oceanography*, *53*(3), 1064.

Miller, C. L. (2006). The role of organic matter in the dissolved phase speciation and solid phase partitioning of mercury. Univ. of Maryland. Ph.D. Dissertation.

Miller, C. L., Mason, R. P., Gilmour, C. C., & Heyes, A. (2007). Influence of dissolved organic matter on the complexation of mercury under sulfidic conditions. *Environmental Toxicology and Chemistry*, *26*(4), 624-633.

Miller, C. L., Southworth, G., Brooks, S., Liang, L., & Gu, B. (2009). Kinetic controls on the complexation between mercury and dissolved organic matter in a contaminated environment. *Environmental science & technology*, *43*(22), 8548-8553.

Mitchell, C. P., Branfireun, B. A., & Kolka, R. K. (2008). Assessing sulfate and carbon controls on net methylmercury production in peatlands: An in situ mesocosm approach. *Applied Geochemistry*, *23*(3), 503-518.

Mitchell, C. P., & Gilmour, C. C. (2008). Methylmercury production in a Chesapeake Bay salt marsh. *Journal of Geophysical Research: Biogeosciences (2005–2012)*, *113*(G2).

Monperrus, M., Tessier, E., Amouroux, D., Leynaert, A., Huonnic, P., & Donard, O. F. X. (2007). Mercury methylation, demethylation and reduction rates in coastal and marine surface waters of the Mediterranean Sea. *Marine Chemistry*, *107*(1), 49-63.

Morel, F. M., Kraepiel, A. M., & Amyot, M. (1998). The chemical cycle and bioaccumulation of mercury. *Annual review of ecology and systematics*, 543-566.

Oremland, R. S., Culbertson, C. W., & Winfrey, M. R. (1991). Methylmercury decomposition in sediments and bacterial cultures: involvement of methanogens and sulfate reducers in oxidative demethylation. *Applied and environmental microbiology*, *57*(1), 130-137.

Pacyna, E. G., Pacyna, J. M., Steenhuisen, F., & Wilson, S. (2006). Global anthropogenic mercury emission inventory for 2000. *Atmospheric environment*,*40*(22), 4048-4063.

Parks, J. M., Johs, A., Podar, M., Bridou, R., Hurt, R. A., Smith, S. D., Tomanicek, S. J., Qian, Y., Brown, S. D., Brandt, C. C., Palumbo, A. V., Smith, J. C., Wall, J. D., Elias, D. A., & Liang, L. (2013). The genetic basis for bacterial mercury methylation. *Science*,*339*(6125), 1332-1335.

Phelps, T. J., & Zeikus, J. G. (1985). Effect of fall turnover on terminal carbon metabolism in Lake Mendota sediments. *Applied and environmental microbiology*, *50*(5), 1285-1291.

Poulin, B.A., Ryan, J.N., & Aiken, G.R., (2014). Effects of iron on optical properties of dissolved organic matter. *Environmental science & technology*, *48*, 10098-10106.

Powell, T., & Jassby, A. (1974). The estimation of vertical eddy diffusivities below the thermocline in lakes. *Water Resources Research*, *10*(2), 191-198.

Pyle, D. M., & Mather, T. A. (2003). The importance of volcanic emissions for the global atmospheric mercury cycle. *Atmospheric Environment*, *37*(36), 5115-5124.

Ravichandran, M. (2004). Interactions between mercury and dissolved organic matter—a review. *Chemosphere*, *55*(3), 319-331.

Regnell, O., Ewald, G., & Lord, E. (1997). Factors controlling temporal variation in methyl mercury levels in sediment and water in a seasonally stratified lake. *Limnology and oceanography*, *42*(8), 1784-1795.

Rudd, J. W. (1995). Sources of methyl mercury to freshwater ecosystems: a review. *Water, Air, and Soil Pollution*, *80*(1-4), 697-713.

Schaefer, J. K., & Morel, F. M. (2009). High methylation rates of mercury bound to cysteine by Geobacter sulfurreducens. *Nature geoscience*, *2*(2), 123-126.

Schaefer, J. K., Rocks, S. S., Zheng, W., Liang, L., Gu, B., & Morel, F. M. (2011). Active transport, substrate specificity, and methylation of Hg (II) in anaerobic bacteria. *Proceedings of the National Academy of Sciences*, *108*(21), 8714-8719.

Schaefer, J. K., Yagi, J., Reinfelder, J. R., Cardona, T., Ellickson, K. M., Tel-Or, S., & Barkay, T. (2004). Role of the bacterial organomercury lyase (MerB) in controlling methylmercury accumulation in mercury-contaminated natural waters. *Environmental science & technology*, *38*(16), 4304-4311.

Schwarzenbach, R. P., Gschwend, P. M., & Imboden, D. M. (1993). Environmental Organic Chemistry. John Wiley & Sons.

Seeberg-Elverfeld, J., & Schlueter, M. (2005). *U.S. Patent Application 11/262,034*.

Seller, P., Kelly, C. A., Rudd, J. W. M., & MacHutchon, A. R. (1996). Photodegradation of methylmercury in lakes.

Sellers, P., Kelly, C. A., & Rudd, J. W. (2001). Fluxes of methylmercury to the water column of a drainage lake: the relative importance of internal and external sources. *Limnology and Oceanography*, *46*(3), 623-631.

St. Louis, V. L., Rudd, J. W., Kelly, C. A., Beaty, K. G., Bloom, N. S., & Flett, R. J. (1994). Importance of wetlands as sources of methyl mercury to boreal forest ecosystems. *Canadian Journal of fisheries and aquatic sciences*, *51*(5), 1065-1076.

Stoor, R. W., Hurley, J. P., Babiarz, C. L., & Armstrong, D. E. (2006). Subsurface sources of methyl mercury to Lake Superior from a wetland–forested watershed. *Science of the total environment*, *368*(1), 99-110.

Stumm, W., & Morgan, J. J. (1996). Aquatic chemistry: Chemical Equilibria and Rates in Natural Waters. Wiley and Sons.

Sunderland, E. M., Gobas, F. A., Branfireun, B. A., & Heyes, A. (2006). Environmental controls on the speciation and distribution of mercury in coastal sediments. *Marine chemistry*, *102*(1), 111-123.

Sunderland, E. M., Krabbenhoft, D. P., Moreau, J. W., Strode, S. A., & Landing, W. M. (2009). Mercury sources, distribution, and bioavailability in the North Pacific Ocean: Insights from data and models. *Global Biogeochemical Cycles*, *23*(2).

US EPA (1997). Method 300.1, Determination of Inorganic Anions in Drinking Water by Ion Chromatography. Office of Water, Washington, DC.

US EPA (2002). Method 1631, Revision E: Mercury in Water by Oxidation, Purge and Trap, and Cold Vapor Atomic Fluorescence Spectrometry. Office of Water, Washington, DC.

Watras, C. J., Bloom, N. S., Claas, S. A., Morrison, K. A., Gilmour, C. C., & Craig, S. R. (1995a). Methylmercury production in the anoxic hypolimnion of a dimictic seepage lake. *Water, Air, and Soil Pollution*, *80*(1-4), 735-745.

Watras, C. J., Morrison, K. A., Host, J. S., & Bloom, N. S. (1995b). Concentration of mercury species in relationship to other site-specific factors in the surface waters of northern Wisconsin lakes. *Limnology and Oceanography*,*40*(3), 556-565.

Watras, C. J., Morrison, K. A., Kent, A., Price, N., Regnell, O., Eckley, C., ... & Hubacher, T. (2005). Sources of methylmercury to a wetland-dominated lake in northern Wisconsin. *Environmental science & technology*, *39*(13), 4747-4758.

Weishaar, J. L., Aiken, G. R., Bergamaschi, B. A., Fram, M. S., Fujii, R., & Mopper, K. (2003). Evaluation of specific ultraviolet absorbance as an indicator of the chemical composition and reactivity of dissolved organic carbon. *Environmental Science & Technology*, *37*(20), 4702-4708.

Wiener, J. G., Knights, B. C., Sandheinrich, M. B., Jeremiason, J. D., Brigham, M. E., Engstrom, D. R., Woodruff, L. G., Cannon, W. F., & Balogh, S. J. (2006). Mercury in soils, lakes, and fish in Voyageurs National Park (Minnesota): importance of atmospheric deposition and ecosystem factors. *Environmental science & technology*,*40*(20), 6261-6268.

Winfrey, M. R., & Rudd, J. W. (1990). Environmental factors affecting the formation of methylmercury in low pH lakes. *Environmental Toxicology and Chemistry*, *9*(7), 853-869.

Zanko, L. M., Niles, H. B., & Oreskovich, J. A. (2008). Mineralogical and microscopic evaluation of coarse taconite tailings from Minnesota taconite operations. *Regulatory Toxicology and Pharmacology*, *52*(1), S51-S65.

Zhang, T., Kim, B., Levard, C., Reinsch, B. C., Lowry, G. V., Deshusses, M. A., & Hsu-Kim, H. (2012). Methylation of mercury by bacteria exposed to dissolved, nanoparticulate, and microparticulate mercuric sulfides. *Environmental science & technology*, *46*(13), 6950-6958.

Appendix A: Summary of Analytes Collected and Reported

Table A.1. List of analytes quantified and reported for each sample type

Parameter	Sediment - Solid Phase	Sediment - Porewater	Lake Water Column*	Inlet & Outlet Stream**
In-Situ Measurements				
pH			X	X
Temperature			X	X
Dissolved Oxygen			X	X
Conductivity			X	X
ORP			X	X
Mercury Analysis				
Methylmercury (MeHg)	X	X	X	X
Total Mercury (THg)	X	X	X	X
K_{meth}	X		(6/2013)	
K_{demeth}	X		(6/2013)	
Chemical Analytes				
Sulfate		X	X	X
Nitrate		X	X	X
Phosphate		X	X	X
Chloride (Cl^-)		X	X	
Ferrous Iron (Fe^{2+})		X	X	X
Sulfide		X	X	
Ammonium		X	X	
Mg			X	X
DIC		X	X	
DOC		X	X	X
SUVA		X	X	X
AVS	X			
WEM-Iron	X			
Physical Characteristics				
%C-Organic	X			
%C-Calcite	X			
%C-Inorganic	X			
Dry density	X			
dry/wet	X			

*Samples taken at the surface water and bottom water biweekly; intermediate water column depths sampled monthly

**Collected and measured by Minnesota DNR

Appendix B: Raw Data Tables

Table B.1(a). Long Lake Creek Wetland Pond (LLC) Sediment Porewater Raw Data (1 of 2)

		5/15/2012						7/24/2012					
Sample Label & Depth Interval	[cm]	A 0-2	A 2-4	A 4-8	B 0-4	C 0-4	**Average 0-4**	A 4-8	A 4-8	A 4-8	B 4-8	C 4-8	**Average 0-4**
Analytes													
Sulfate	[mg/L]	50.2	9.2	5.0	9.2	26.5	**21.8**	22.0	10.6	7.6	22.9	22.4	**20.5**
Nitrate	[mg/L]	0.7	0.2	0.3	0.0	0.0	**0.1**	0.3	0.2	0.2	0.3	0.1	**0.2**
Phosphate	[mg/L]	0.0	0.0	0.0	0.0	0.0	**0.0**	0.0	0.0	0.0	0.1	0.3	**0.1**
Chloride	[mg/L]												
Ferrous Iron	[mmol/L]	0.007	0.005	0.011	0.023	0.040	**0.023**	0.009	0.007	0.012	0.008	0.013	**0.010**
Sulfide	[µmol/L]	8	362	425	70	339	**198**	754	806	779	506	422	**569**
Ammonium	[mg/L]												
DIC	[mg/L]	97.9	112.1	124.7	117.7	103.2	**108.6**	120.8	117.8	124.7	112.7	124.1	**118.7**
DOC	[mg/L]	27.9	22.7	17.7	25.3	21.9	**24.2**	30.9	26.6	26.6	29.7	29.3	**29.2**
SUVA	[$Lm^{-1}mg^{-1}$]	5.0	5.3	6.1	5.6	5.9	**5.5**	4.4	4.2	3.6	4.2		**4.3**
Mercury Analysis													
MeHg	[ng/L]	0.28	0.12	0.02	0.67	0.19	**0.36**	1.64	0.23	0.19	0.13	0.37	**0.48**
THg	[ng/L]	1.56	1.41	1.28	1.95	1.47	**1.63**		4.05	2.82	3.77	3.75	**3.76**
iHg	[ng/L]	1.3	1.28	1.26	1.28	1.27	**1.28**		3.81	2.63	3.64	3.38	**3.51**
% MeHg	[]	17.7	8.8	1.5	34.5	13.3	**21.8**	n/a	5.8	6.8	3.6	10.0	**12.8**

Table B.1(b). Long Lake Creek Wetland Pond (LLC) Sediment Porewater Raw Data (2 of 2)

Sample Label & Depth Interval	[cm]	10/6/2012						6/3/2013					
		A	A	A	B	C	**Average**	A	A	A	B	C	**Average**
		4-8	4-8	4-8	4-8	4-8	**0-4**	4-8	4-8	4-8	4-8	4-8	**0-4**
Analytes													
Sulfate	[mg/L]	521.5		397.5		482.3	**482.3**	15.8	14.7	36.9	22.0	25.8	**21.0**
Nitrate	[mg/L]	0.9		1.2		1.2	**1.2**	4.3	0.7	2.2	0.9	0.5	**1.3**
Phosphate	[mg/L]	0.0		0.0		0.0	**0.0**	0.0	0.0	0.0	0.0	0.0	**0.0**
Chloride	[mg/L]		33.7		32.4		**32.4**		10.7	12.7	10.9	8.8	**9.9**
Ferrous Iron	[mmol/L]	0.005	0.004	0.005	0.004	0.003	**0.004**	0.000	0.000	0.021	0.000	0.000	**0.000**
Sulfide	[µmol/L]	11	104	701	113	16	**62**			1197	422	365	**393**
Ammonium	[mg/L]							2.0	2.7	3.2		1.1	**1.7**
DIC	[mg/L]		114.5					82.1	94.8	111.4	66.7	68.8	**74.7**
DOC	[mg/L]		8.1					27.9	20.2	15.1	29.2	27.9	**27.1**
SUVA	[$Lm^{-1}mg^{-1}$]		3.2					3.1	3.2	4.0	3.3	3.1	**3.2**
Mercury Analysis													
MeHg	[ng/L]	0.22	0.16	0.11	0.06	0.11	**0.12**	0.22	0.14	0.14	1.06	0.55	**0.60**
THg	[ng/L]	1.59	1.30	1.22	1.31	1.34	**1.36**	6.27	3.00	9.95	7.19	16.82	**9.55**
iHg	[ng/L]	1.37	1.14	1.11	1.25	1.23	**1.24**	6.05	2.86	9.81	6.13	16.27	**8.95**
% MeHg	[]	14.0	12.6	9.1	4.7	8.5	**9.0**	3.4	4.8	1.4	14.7	3.3	**6.2**

Table B.2(a). Long Lake Creek Wetland Pond (LLC) Sediment Solid Phase Raw Data, Collected: 5/15/2012

Mercury Analysis

Sample Label & Depth Interval	[cm]	A 0-2	A 2-4	A 4-8	B 0-4	C 0-4	**Average 0-4**
MeHg	[ng/g]	0.3	0.0	0.1	0.6	0.1	**0.3**
THg	[ng/g]	50.4	53.5	30.9	61.7	37.0	**50.2**
iHg	[ng/g]	50.1	53.5	30.8	61.1	37.0	**49.9**
% MeHg	[]	0.69	0.09	0.26	0.99	0.16	**0.58**
log K_D^* (iHg)	[]						**4.59**
log K_D^* (MeHg)	[]						**2.91**
K_{meth}	[d^{-1}]	0.014	0.007	0.007	0.010	0.016	**0.012**
K_{demeth}	[hr^{-1}]	0.032	0.037	0.033	0.051	0.044	**0.043**
K_m/K_d	[]	0.43	0.20	0.21	0.21	0.37	**0.30**

Sediment Composition

Sample Label & Depth Interval	[cm]	A 0-2	A 2-4	A 4-8	B 0-4	C 0-4	**Average 0-4**
WEM - Iron	[g/kg]						
AVS	[µmol/g]	76.4	65.7	107.1	100.0	100.5	**90.5**
%C-Organic	[]	38.8	30.6	34.2	37.6	39.3	**37.2**
%C-Calcite	[]	33.3	42.3	39.8	36.3	33.7	**35.9**
%C-Inorganic	[]	27.9	27.0	26.1	26.1	27.0	**26.9**
Dry density	[g/cc]	0.06	0.09	0.08	0.07	0.06	**0.07**
dry/wet	[]	0.06	0.09	0.08	0.06	0.06	**0.07**

Table B.2(b). Long Lake Creek Wetland Pond (LLC) Sediment Solid Phase Raw Data, Collected: 7/24/2012

Mercury Analysis

Sample Label & Depth Interval	[cm]	A 0-2	A 2-4	A 4-8	B 0-2	B 2-4	B 4-8	C 0-2	C 2-4	C 4-8	**Average 0-4**
MeHg	[ng/g]	1.6	0.1	0.0	0.3	0.2	0.1	0.1	0.1	0.2	**0.4**
THg	[ng/g]	65.8	54.2	53.3	96.8	87.6	87.9	67.1	64.9	65.3	**72.7**
iHg	[ng/g]	64.3	54.1	53.3	96.4	87.4	87.8	66.9	64.8	65.1	**72.3**
% MeHg	[]	2.36	0.23	0.01	0.33	0.21	0.08	0.18	0.17	0.34	**0.55**
log K_D^* (iHg)	[]										**4.31**
log K_D^* (MeHg)	[]										**2.92**
K_{meth}	[d^{-1}]	0.008	0.006	0.006	0.011	0.006	0.003	0.007	0.003	0.004	**0.007**
K_{demeth}	[hr^{-1}]	0.038	0.036	0.045	0.057	0.042	0.042	0.072	0.050	0.044	**0.049**
K_m/K_d	[]	0.21	0.18	0.13	0.19	0.14	0.08	0.09	0.07	0.10	**0.15**

Sediment Composition

Sample Label & Depth Interval	[cm]	A 0-2	A 2-4	A 4-8	B 0-4	C 0-4	**Average 0-4**
WEM - Iron	[g/kg]	13.4	10.5	8.9	9.9	11.6	**11.2**
AVS	[µmol/g]	208.3	197.2	120.6	202.5	207.4	**204.2**
%C-Organic	[]	55.3	47.0	27.1	37.7	41.8	**43.6**
%C-Calcite	[]	13.0	22.1	47.0	36.3	30.3	**28.1**
%C-Inorganic	[]	31.7	30.8	25.9	26.0	27.8	**28.4**
Dry density	[g/cc]	0.06	0.06	0.11	0.06	0.05	**0.06**
dry/wet	[]	0.06	0.06	0.10	0.05	0.05	**0.05**

Table B.2(c). Long Lake Creek Wetland Pond (LLC) Sediment Solid Phase Raw Data, Collected: 10/6/2012

Mercury Analysis

Sample Label & Depth Interval	[cm]	A 0-2	A 2-4	A 4-8	B 0-2	B 2-4	B 4-8	C 0-2	C 2-4	C 4-8	**Average 0-4**
MeHg	[ng/g]	0.0	0.0	0.0		0.2	0.1	0.0	0.0	0.0	**0.1**
THg	[ng/g]	61.4	61.0	59.7	49.0	57.8	104.0	52.4	36.7	23.0	**53.0**
iHg	[ng/g]	61.4	61.0	59.7		57.6	103.9	52.4	36.7	23.0	**53.8**
% MeHg	[]	0.06	0.07	0.05		0.35	0.09	0.03	0.08	0.01	**0.12**
log K_D^* (iHg)	[]										**4.64**
log K_D^* (MeHg)	[]										**2.73**
K_{meth}	[d^{-1}]	0.016	0.011	0.012	0.011	0.012	0.010	0.015	0.010	0.011	**0.013**
K_{demeth}	[hr^{-1}]	0.093	0.105	0.098	0.098	0.104	0.099	0.095	0.113	0.104	**0.101**
K_m/K_d	[]	0.17	0.11	0.12	0.11	0.12	0.10	0.16	0.09	0.10	**0.13**

Sediment Composition

Sample Label & Depth Interval	[cm]	A 0-2	A 2-4	A 4-8	B 0-4	C 0-4	**Average 0-4**
WEM - Iron	[g/kg]						
AVS	[µmol/g]	136.2	129.6	125.6	70.0	53.1	**85.4**
%C-Organic	[]	48.9	46.0	35.5	30.7	25.5	**34.6**
%C-Calcite	[]	21.3	23.7	35.0	40.5	51.6	**38.2**
%C-Inorganic	[]	29.8	30.3	29.5	28.7	22.9	**27.2**
Dry density	[g/cc]	0.05	0.06	0.07	0.10	0.12	**0.09**
dry/wet	[]	0.05	0.06	0.07	0.10	0.12	**0.09**

Table B.2(d). Long Lake Creek Wetland Pond (LLC) Sediment Solid Phase Raw Data, Collected: 6/3/2013

Mercury Analysis

Sample Label & Depth Interval	[cm]	A 0-2	A 2-4	A 4-8	B 0-2	B 2-4	B 4-8	C 0-2	C 2-4	C 4-8	**Average 0-4**
MeHg	[ng/g]		0.3	0.1	1.4	0.2	0.1	1.5	0.5	0.1	**0.9**
THg	[ng/g]		70.7	55.9	69.9	59.3	60.3	55.7	59.5	81.1	**63.0**
iHg	[ng/g]		70.3	55.8	68.4	59.1	60.2	54.1	59.0	80.9	**62.2**
% MeHg	[]		0.47	0.25	2.06	0.41	0.18	2.73	0.76	0.15	**1.45**
log K_D^* (iHg)	[]										**3.84**
log K_D^* (MeHg)	[]										**3.18**
K_{meth}	[d^{-1}]		0.021	0.013	0.079	0.026	0.012	0.118	0.051	0.017	**0.066**
K_{demeth}	[hr^{-1}]		0.023		0.034					0.051	**0.028**
K_m/K_d	[]		0.91		2.34					0.33	**1.63**

Sediment Composition

Sample Label & Depth Interval	[cm]	A 0-2	A 2-4	A 4-8	B 0-4	C 0-4	**Average 0-4**
WEM - Iron	[g/kg]						
AVS	[µmol/g]	132.5	103.9	88.3	64.1	140.5	**107.6**
%C-Organic	[]	39.9	33.9	29.6	28.6	34.9	**33.5**
%C-Calcite	[]	32.1	39.6	46.9	47.7	41.8	**41.8**
%C-Inorganic	[]	28.0	26.5	23.5	23.7	23.3	**24.7**
Dry density	[g/cc]	0.05	0.09	0.11	0.11	0.07	**0.08**
dry/wet	[]	0.05	0.08	0.10	0.11	0.07	**0.08**

Table B.3(a). Lake Manganika - Plot 1 (Mng1) Sediment Porewater Raw Data (1 of 2)

		5/15/2012						7/24/2012					
Sample Label & Depth Interval	[cm]	A 0-2	A 2-4	A 4-8	B 0-4	C 0-4	**Average 0-4**	A 4-8	A 4-8	A 4-8	B 4-8	C 4-8	**Average 0-4**
Analytes													
Sulfate	[mg/L]	2.5	3.7	10.9	8.3	2.5	**4.6**	2.6	2.3	3.6	2.8	6.4	**3.9**
Nitrate	[mg/L]	0.0	0.0	0.0	0.0	0.0	**0.0**	0.1	0.2	1.1	0.7	0.5	**0.4**
Phosphate	[mg/L]	5.9	12.6	22.1	8.8	8.8	**9.0**	13.6	3.0	32.9	16.4	12.6	**12.4**
Chloride	[mg/L]			116.2						692.4			
Ferrous Iron	[mmol/L]	0.011	0.005	0.004	0.004	0.007	**0.006**	0.004	0.002	0.006	0.003	0.004	**0.003**
Sulfide	[µmol/L]	1152	1720	1648	898	1542	**1292**	1631	1301	882	906	1656	**1342**
Ammonium	[mg/L]			42.5									
DIC	[mg/L]	202.0	226.9	231.7	220.9	207.1	**214.2**	211.3	234.4	273.0	216.8	206.7	**215.5**
DOC	[mg/L]	78.1	10.5	10.3	19.9	26.1	**30.1**	42.5	15.4	17.2	18.3	23.3	**23.5**
SUVA	[$Lm^{-1}mg^{-1}$]	1.0	6.4	7.8	3.7	3.8	**3.7**	1.1	2.6		2.3		**2.1**
Mercury Analysis													
MeHg	[ng/L]	2.51	0.52	0.01	2.78	1.16	**1.82**	0.69	0.19	0.19	0.80	0.87	**0.71**
THg	[ng/L]	5.38	2.31	1.22	2.86	3.14	**3.28**	3.88	1.72	1.63	2.28	2.57	**2.55**
iHg	[ng/L]	2.9	1.78	1.21	0.08	1.98	**1.46**	3.18	1.53	1.44	1.48	1.70	**1.85**
% MeHg	[]	46.8	22.6	0.8	97.2	36.9	**55.5**	17.9	10.9	11.9	35.1	33.9	**27.6**

Table B.3(b). Lake Manganika - Plot 1 (Mng1) Sediment Porewater Raw Data (2 of 2)

		10/6/2012						6/3/2013					
Sample Label & Depth Interval	[cm]	A 4-8	A 4-8	A 4-8	B 4-8	C 4-8	**Average 0-4**	A 4-8	A 4-8	A 4-8	B 4-8	C 4-8	**Average 0-4**
Analytes													
Sulfate	[mg/L]	52.7	25.1	10.8	48.8	51.3	**46.3**	25.2	13.2	16.7	32.5	124.5	**58.7**
Nitrate	[mg/L]	0.7	0.3	1.4	0.0	2.6	**1.5**	1.6	0.3	2.7	2.6	2.2	**1.9**
Phosphate	[mg/L]	12.2	18.2	26.9	15.2	16.0	**15.5**	11.7	26.3	29.6	10.8	10.7	**13.5**
Chloride	[mg/L]								149.1	149.6		135.7	**135.7**
Ferrous Iron	[mmol/L]	0.004	0.005	0.006	0.007	0.007	**0.006**	0.008	0.006	0.009	0.004	0.007	**0.006**
Sulfide	[µmol/L]	1678	1661	716	829	1954	**1484**	2112	1815	1503	2442	1644	**2017**
Ammonium	[mg/L]			57.7					38.0	47.6			
DIC	[mg/L]	191.8						220.2	236.4	250.2	223.0	234.0	**228.4**
DOC	[mg/L]	13.9						14.1	12.5	14.2	13.4	13.3	**13.3**
SUVA	[$Lm^{-1}mg^{-1}$]	3.1							3.6	3.3	2.5	2.9	**2.7**
Mercury Analysis													
MeHg	[ng/L]	2.91	0.32	0.23	0.73	0.56	**0.97**	1.32	0.29	0.30	1.48	0.51	**0.93**
THg	[ng/L]	8.83	3.06	1.78	24.18	3.88	**11.33**	43.16	1.95	51.36	17.47	2.93	**14.32**
iHg	[ng/L]	5.92	2.73	1.56	23.45	3.32	**10.37**	41.85	1.66	51.06	15.99	2.42	**13.39**
% MeHg	[]	32.9	10.5	12.7	3.0	14.4	**8.5**	3.1	15.0	0.6	8.5	17.3	**6.5**

Table B.4(a). Lake Manganika - Plot 1 (Mng1) Sediment Solid Phase Raw Data, Collected: 5/15/2012

Mercury Analysis

Sample Label & Depth Interval	[cm]	A 0-2	A 2-4	A 4-8	B 0-2	B 2-4	B 4-8	C 0-2	C 2-4	C 4-8	**Average 0-4**
MeHg	[ng/g]	1.2	1.1	1.1	1.2	0.9	0.9	1.4	1.2	0.8	**1.2**
THg	[ng/g]	355.3	260.5	397.8	246.2	402.3	412.3	302.7	323.2	392.8	**315.0**
iHg	[ng/g]	354.2	259.4	396.7	245.0	401.4	411.4	301.3	322.0	392.0	**313.9**
% MeHg	[]	0.32	0.44	0.26	0.50	0.24	0.23	0.47	0.37	0.20	**0.38**
log K_D^* (iHg)	[]										**5.33**
log K_D^* (MeHg)	[]										**2.81**
K_{meth}	[d^{-1}]	0.006	0.010	0.003	0.007	0.004	0.002	0.006	0.003	0.002	**0.006**
K_{demeth}	[hr^{-1}]	0.088	0.071	0.073	0.086	0.077	0.105	0.104	0.105	0.104	**0.089**
K_m/K_d	[]	0.07	0.14	0.04	0.08	0.05	0.02	0.05	0.02	0.02	**0.07**

Sediment Composition

Sample Label & Depth Interval	[cm]	A 0-2	A 2-4	A 4-8	B 0-4	C 0-4	**Average 0-4**
WEM - Iron	[g/kg]						
AVS	[µmol/g]	139.3	166.0	252.8	161.6	191.6	**168.6**
%C-Organic	[]	23.4	22.3	21.9	22.5	22.0	**22.5**
%C-Calcite	[]	37.0	31.6	29.9	35.8	37.6	**35.9**
%C-Inorganic	[]	39.6	46.1	48.2	41.6	40.5	**41.7**
Dry density	[g/cc]	0.06	0.07	0.07	0.08	0.08	**0.07**
dry/wet	[]	0.06	0.07	0.07	0.07	0.07	**0.07**

Table B.4(b). Lake Manganika - Plot 1 (Mng1) Sediment Solid Phase Raw Data, Collected: 7/24/2012

Mercury Analysis

Sample Label & Depth Interval	[cm]	A 0-2	A 2-4	A 4-8	B 0-2	B 2-4	B 4-8	C 0-2	C 2-4	C 4-8	**Average 0-4**
MeHg	[ng/g]	1.3	0.9	0.7	1.1	1.1	0.7	1.6	1.2	0.8	**1.2**
THg	[ng/g]	320.9	361.8	386.9	286.0	373.3	474.4	256.6	355.5	451.2	**325.7**
iHg	[ng/g]	319.5	360.8	386.2	284.9	372.2	473.7	255.0	354.3	450.5	**324.5**
% MeHg	[]	0.42	0.26	0.18	0.40	0.30	0.15	0.61	0.32	0.17	**0.37**
log K_D^* (iHg)	[]										**5.24**
log K_D^* (MeHg)	[]										**3.23**
K_{meth}	[d^{-1}]	0.024	0.012	0.011	0.013	0.008	0.006	0.010	0.006	0.005	**0.012**
K_{demeth}	[hr^{-1}]	0.084	0.086	0.065	0.087	0.096	0.097	0.110	0.110	0.126	**0.095**
K_m/K_d	[]	0.28	0.14	0.17	0.15	0.08	0.07	0.09	0.06	0.04	**0.13**

Sediment Composition

Sample Label & Depth Interval	[cm]	A 0-2	A 2-4	A 4-8	B 0-4	C 0-4	**Average 0-4**
WEM - Iron	[g/kg]	17.4	16.8	18.3	16.8	19.9	**17.9**
AVS	[µmol/g]	307.9	284.9	383.5	248.3	358.7	**301.1**
%C-Organic	[]	24.9	21.0	21.1	24.0	23.1	**23.4**
%C-Calcite	[]	31.7	32.8	32.2	32.6	30.4	**31.7**
%C-Inorganic	[]	43.5	46.1	46.7	43.4	46.5	**44.9**
Dry density	[g/cc]	0.06	0.07	0.07	0.05	0.06	**0.06**
dry/wet	[]	0.05	0.07	0.07	0.05	0.06	**0.06**

Table B.4(c). Lake Manganika - Plot 1 (Mng1) Sediment Solid Phase Raw Data, Collected: 10/6/2012

Mercury Analysis

Sample Label & Depth Interval	[cm]	A 0-2	A 2-4	A 4-8	B 0-2	B 2-4	B 4-8	C 0-2	C 2-4	C 4-8	**Average 0-4**
MeHg	[ng/g]	1.8	1.0	1.0	1.8	1.0	0.8	1.8	0.8	0.6	**1.4**
THg	[ng/g]	276.3	326.2	447.1	277.8	355.1	455.1	273.9	345.0	393.1	**309.0**
iHg	[ng/g]	274.5	325.2	446.2	276.0	354.1	454.4	272.1	344.2	392.5	**307.7**
% MeHg	[]	0.64	0.32	0.21	0.65	0.27	0.17	0.65	0.24	0.15	**0.44**
log K_D^* (iHg)	[]										**4.47**
log K_D^* (MeHg)	[]										**3.15**
K_{meth}	[d^{-1}]	0.045	0.017	0.013	0.042	0.014	0.011	0.026	0.010	0.010	**0.026**
K_{demeth}	[hr^{-1}]	0.054	0.074	0.063	0.071	0.047	0.063	0.081	0.072	0.085	**0.066**
K_m/K_d	[]	0.84	0.23	0.21	0.59	0.31	0.18	0.32	0.14	0.12	**0.41**

Sediment Composition

Sample Label & Depth Interval	[cm]	A 0-2	A 2-4	A 4-8	B 0-4	C 0-4	**Average 0-4**
WEM - Iron	[g/kg]						
AVS	[µmol/g]	366.6	308.9	349.8	136.2	287.8	**253.9**
%C-Organic	[]	22.6	21.1	21.1	21.4	21.9	**21.7**
%C-Calcite	[]	36.7	31.8	30.3	35.2	35.7	**35.0**
%C-Inorganic	[]	40.7	47.1	48.6	43.4	42.4	**43.2**
Dry density	[g/cc]	0.05	0.07	0.08	0.08	0.07	**0.07**
dry/wet	[]	0.05	0.07	0.07	0.07	0.07	**0.07**

Table B.4(d). Lake Manganika - Plot 1 (Mng1) Sediment Solid Phase Raw Data, Collected: 6/3/2013

Mercury Analysis

Sample Label & Depth Interval	[cm]	A 0-2	A 2-4	A 4-8	B 0-2	B 2-4	B 4-8	C 0-2	C 2-4	C 4-8	**Average 0-4**
MeHg	[ng/g]	1.4	1.0	0.6	1.2	1.0	0.6	1.5	1.1	0.7	**1.2**
THg	[ng/g]	226.9	278.6	433.1	229.8	256.2	394.6	246.9	266.4	419.4	**250.8**
iHg	[ng/g]	225.6	277.7	432.5	228.6	255.2	394.0	245.4	265.2	418.7	**249.6**
% MeHg	[]	0.60	0.35	0.14	0.53	0.37	0.15	0.62	0.42	0.17	**0.48**
log K_D^* (iHg)	[]										**4.27**
log K_D^* (MeHg)	[]										**3.11**
K_{meth}	[d^{-1}]	0.028	0.014	0.003	0.022	0.010	0.004	0.023	0.018	0.004	**0.019**
K_{demeth}	[hr^{-1}]	0.059	0.052	0.019	0.042	0.050	0.023	0.056	0.080	0.030	**0.057**
K_m/K_d	[]	0.47	0.26	0.16	0.53	0.20	0.19	0.41	0.23	0.15	**0.35**

Sediment Composition

Sample Label & Depth Interval	[cm]	A 0-2	A 2-4	A 4-8	B 0-4	C 0-4	**Average 0-4**
WEM - Iron	[g/kg]						
AVS	[µmol/g]	293.0	243.7	356.6	269.6	396.8	**311.6**
%C-Organic	[]	26.7	19.7	19.3	20.7	22.5	**22.1**
%C-Calcite	[]	36.1	41.1	35.4	41.7	37.6	**39.3**
%C-Inorganic	[]	37.2	39.2	45.2	37.5	39.9	**38.5**
Dry density	[g/cc]	0.04	0.08	0.08	0.06	0.05	**0.06**
dry/wet	[]	0.04	0.07	0.08	0.06	0.05	**0.05**

Table B.5(a). Lake Manganika - Plot 2 (Mng2) Sediment Porewater Raw Data (1 of 2)

		5/15/2012						7/24/2012					
Sample Label & Depth Interval	[cm]	A 0-2	A 2-4	A 4-8	B 0-4	C 0-4	**Average 0-4**	A 4-8	A 4-8	A 4-8	B 4-8	C 4-8	**Average 0-4**
Analytes													
Sulfate	[mg/L]	68.3	80.3	200.3	92.6	51.3	**72.7**	42.3	10.7	14.9	31.6	34.8	**31.0**
Nitrate	[mg/L]	0.0	0.9	0.0	0.0	0.7	**0.4**	0.0	0.2	0.0	0.5	0.3	**0.3**
Phosphate	[mg/L]	0.0	2.1	0.0	0.0	0.0	**0.4**	3.8	5.6	6.1	6.6	8.0	**6.5**
Chloride	[mg/L]												
Ferrous Iron	[mmol/L]	0.009	0.011	0.007	0.007	0.007	**0.008**	0.013	0.005	0.004	0.002	0.001	**0.004**
Sulfide	[µmol/L]	1405	1563	1453	1340	1555	**1460**	2292	981	1519	1379	1504	**1507**
Ammonium	[mg/L]		6.6	3.7									
DIC	[mg/L]	140.5	150.3	109.0	155.2	154.2	**151.6**	171.8	190.5	169.0	174.6	171.8	**175.8**
DOC	[mg/L]	10.9	6.6	5.9	6.9	9.0	**8.2**	11.2	9.2	10.0	10.0	10.7	**10.3**
SUVA	[$Lm^{-1}mg^{-1}$]	6.6	10.1	9.9	9.5	7.7	**8.5**		4.0	3.9	3.4	3.2	**3.3**
Mercury Analysis													
MeHg	[ng/L]	9.42	5.69	0.42	8.21	7.61	**7.79**	0.38	0.08	0.18	0.27	0.63	**0.38**
THg	[ng/L]	14.61	9.96	2.39	10.86	11.75	**11.63**	4.17	2.06	2.37	2.87	3.06	**3.02**
iHg	[ng/L]	5.2	4.27	1.96	2.65	4.15	**3.84**	3.79	1.98	2.19	2.60	2.43	**2.64**
% MeHg	[]	64.5	57.2	17.6	75.6	64.7	**67.0**	9.1	3.9	7.7	9.5	20.7	**12.6**

Table B.5(b). Lake Manganika - Plot 2 (Mng2) Sediment Porewater Raw Data (2 of 2)

Sample Label & Depth Interval	[cm]	10/6/2012 A 4-8	A 4-8	A 4-8	B 4-8	C 4-8	**Average 0-4**	6/3/2013 A 4-8	A 4-8	A 4-8	B 4-8	C 4-8	**Average 0-4**
Analytes													
Sulfate	[mg/L]	168.2	83.4	50.5	208.4	167.3	**167.2**	69.1	77.1		24.5	38.2	**45.3**
Nitrate	[mg/L]	0.0	0.0	0.3	0.0	0.0	**0.0**	1.1	0.2		0.4	2.3	**1.1**
Phosphate	[mg/L]	4.4	6.0	7.1	4.1	3.9	**4.4**	6.4	6.7		6.9	5.9	**6.5**
Chloride	[mg/L]								84.6	81.4	82.7	84.8	**83.8**
Ferrous Iron	[mmol/L]	0.003	0.002	0.009	0.003	0.004	**0.003**	0.005	0.002	0.003	0.004	0.003	**0.004**
Sulfide	[µmol/L]	35	524	288	109	32	**140**	2321	939	1154	2121	1902	**1884**
Ammonium	[mg/L]									11.2			
DIC	[mg/L]		184.1	191.4	157.7	169.4	**163.5**	139.8	147.0	158.7	163.2	157.3	**154.6**
DOC	[mg/L]		11.4	11.1	9.8	5.6	**7.7**	9.9	6.4	7.4	9.4	9.4	**9.0**
SUVA	[$Lm^{-1}mg^{-1}$]		4.4	4.9	4.5	8.4	**6.4**	3.6	5.2	5.4	4.5	3.5	**4.1**
Mercury Analysis													
MeHg	[ng/L]	0.15	0.09	0.06	0.08	0.11	**0.10**	6.59	0.27		2.09	1.10	**2.21**
THg	[ng/L]	3.58	4.88	1.53	9.09	2.09	**5.14**	10.18	35.21	43.65	6.40	4.42	**11.17**
iHg	[ng/L]	3.43	4.80	1.47	9.02	1.97	**5.04**	3.59	34.95		4.30	3.32	**8.96**
% MeHg	[]	4.2	1.8	3.9	0.8	5.4	**2.0**	64.8	0.8		32.7	24.9	**19.8**

Table B.6(a). Lake Manganika - Plot 2 (Mng2) Sediment Solid Phase Raw Data, Collected: 5/15/2012

Mercury Analysis

Sample Label & Depth Interval	[cm]	A 0-2	A 2-4	A 4-8	B 0-2	B 2-4	B 4-8	C 0-2	C 2-4	C 4-8	**Average 0-4**
MeHg	[ng/g]	3.6	3.1	1.1	3.7	2.3	1.2	3.0	2.7	1.0	**3.1**
THg	[ng/g]	824.9	831.0	964.1	772.2	840.9	971.9	802.3	823.4	1022.1	**815.8**
iHg	[ng/g]	821.4	827.9	963.0	768.5	838.6	970.7	799.3	820.7	1021.1	**812.7**
% MeHg	[]	0.43	0.38	0.11	0.48	0.27	0.12	0.37	0.33	0.10	**0.38**
log K_D^* (iHg)	[]										**5.33**
log K_D^* (MeHg)	[]										**2.60**
K_{meth}	[d^{-1}]	0.017	0.014	0.010	0.016	0.011	0.009	0.015	0.014	0.010	**0.014**
K_{demeth}	[hr^{-1}]	0.103	0.072	0.124	0.100	0.118	0.120	0.118	0.101	0.067	**0.102**
K_m/K_d	[]	0.16	0.19	0.08	0.16	0.09	0.08	0.13	0.14	0.15	**0.15**

Sediment Composition

Sample Label & Depth Interval	[cm]	A 0-2	A 2-4	A 4-8	B 0-4	C 0-4	**Average 0-4**
WEM - Iron	[g/kg]						
AVS	[µmol/g]	182.2	160.8	159.6	242.8	227.6	**214.0**
%C-Organic	[]	19.9	20.0	19.2	19.9	20.0	**19.9**
%C-Calcite	[]	31.8	30.7	27.3	28.8	31.0	**30.4**
%C-Inorganic	[]	48.3	49.3	53.5	51.3	49.0	**49.7**
Dry density	[g/cc]	0.10	0.11	0.14	0.11	0.11	**0.11**
dry/wet	[]	0.09	0.11	0.13	0.11	0.10	**0.10**

Table B.6(b). Lake Manganika - Plot 2 (Mng2) Sediment Solid Phase Raw Data, Collected: 7/24/2012

Mercury Analysis

Sample Label & Depth Interval	[cm]	A 0-2	A 2-4	A 4-8	B 0-2	B 2-4	B 4-8	C 0-2	C 2-4	C 4-8	**Average 0-4**
MeHg	[ng/g]	1.8	1.2	1.3	1.8	1.7	1.1	1.9	1.4	1.1	**1.6**
THg	[ng/g]	706.2	805.9	842.9	772.0	830.6	859.5	764.5	809.5	877.0	**781.5**
iHg	[ng/g]	704.4	804.7	841.6	770.3	828.9	858.4	762.6	808.1	875.9	**779.8**
% MeHg	[]	0.25	0.15	0.15	0.23	0.20	0.13	0.25	0.17	0.12	**0.21**
log K_D^* (iHg)	[]										**5.47**
log K_D^* (MeHg)	[]										**3.63**
K_{meth}	[d^{-1}]	0.037	0.012	0.021	0.026	0.013	0.007	0.025	0.007	0.013	**0.020**
K_{demeth}	[hr^{-1}]	0.006		0.038	0.056		0.022	0.060	0.123	0.067	**0.061**
K_m/K_d	[]	6.01		0.54	0.47		0.32	0.42	0.05	0.19	**1.74**

Sediment Composition

Sample Label & Depth Interval	[cm]	A 0-2	A 2-4	A 4-8	B 0-4	C 0-4	**Average 0-4**
WEM - Iron	[g/kg]	22.0	22.4	26.9	23.0	22.7	**22.6**
AVS	[µmol/g]	488.7	441.2	515.8	627.7	470.8	**521.1**
%C-Organic	[]	24.9	21.0	21.1	24.0	23.1	**23.4**
%C-Calcite	[]	31.7	32.8	32.2	32.6	30.4	**31.7**
%C-Inorganic	[]	43.5	46.1	46.7	43.4	46.5	**44.9**
Dry density	[g/cc]	0.06	0.07	0.07	0.05	0.06	**0.06**
dry/wet	[]	0.05	0.07	0.07	0.05	0.06	**0.06**

Table B.6(c). Lake Manganika - Plot 2 (Mng2) Sediment Solid Phase Raw Data, Collected: 10/6/2012

Mercury Analysis

Sample Label & Depth Interval	[cm]	A 0-2	A 2-4	A 4-8	B 0-2	B 2-4	B 4-8	C 0-2	C 2-4	C 4-8	**Average 0-4**
MeHg	[ng/g]	1.5	1.5	1.1	1.4	1.2	1.5	1.4	1.1	0.9	**1.4**
THg	[ng/g]	809.1	810.0	871.2	789.4	717.1	848.1	772.8	834.0	880.1	**788.7**
iHg	[ng/g]	807.6	808.6	870.0	788.0	715.9	846.6	771.4	832.8	879.2	**787.4**
% MeHg	[]	0.19	0.18	0.13	0.18	0.17	0.18	0.18	0.14	0.11	**0.17**
log K_D^* (iHg)	[]										**5.19**
log K_D^* (MeHg)	[]										**4.12**
K_{meth}	[d^{-1}]	0.018	0.016	0.012	0.022	0.014	0.015	0.020	0.015	0.014	**0.018**
K_{demeth}	[hr^{-1}]	0.050	0.047	0.086	0.040	0.053	0.020	0.036	0.104	0.124	**0.055**
K_m/K_d	[]	0.37	0.34	0.13	0.55	0.27	0.73	0.55	0.14	0.12	**0.37**

Sediment Composition

Sample Label & Depth Interval	[cm]	A 0-2	A 2-4	A 4-8	B 0-4	C 0-4	**Average 0-4**
WEM - Iron	[g/kg]						
AVS	[µmol/g]	216.7	287.7	164.5	276.2		**264.2**
%C-Organic	[]	20.2	19.4	19.3	19.3		**19.5**
%C-Calcite	[]	29.4	30.4	28.8	31.2		**30.6**
%C-Inorganic	[]	50.4	50.1	52.0	49.5		**49.9**
Dry density	[g/cc]	0.10	0.09	0.11	0.09		**0.10**
dry/wet	[]	0.10	0.09	0.11	0.09		**0.09**

Table B.6(d). Lake Manganika - Plot 2 (Mng2) Sediment Solid Phase Raw Data, Collected: 6/3/2013

Mercury Analysis

Sample Label & Depth Interval	[cm]	A 0-2	A 2-4	A 4-8	B 0-2	B 2-4	B 4-8	C 0-2	C 2-4	C 4-8	**Average 0-4**
MeHg	[ng/g]	2.2	1.1	0.9	2.7	1.5	1.0	2.6	1.2	1.0	**1.9**
THg	[ng/g]	680.5	709.8	885.1	670.2	840.0	874.5	585.2	750.3	889.7	**706.0**
iHg	[ng/g]	678.3	708.7	884.2	667.5	838.5	873.5	582.6	749.0	888.7	**704.1**
% MeHg	[]	0.33	0.15	0.10	0.40	0.18	0.12	0.44	0.16	0.11	**0.27**
log K_D^* (iHg)	[]										**4.90**
log K_D^* (MeHg)	[]										**2.93**
K_{meth}	[d^{-1}]	0.085	0.012	0.005	0.084	0.013	0.006	0.116	0.012	0.008	**0.054**
K_{demeth}	[hr^{-1}]	0.146	0.160	0.165	0.156	0.176	0.172	0.154	0.185	0.195	**0.163**
K_m/K_d	[]	0.58	0.07	0.03	0.54	0.08	0.04	0.75	0.07	0.04	**0.35**

Sediment Composition

Sample Label & Depth Interval	[cm]	A 0-2	A 2-4	A 4-8	B 0-4	C 0-4	**Average 0-4**
WEM - Iron	[g/kg]						
AVS	[µmol/g]	258.7	249.3	324.9	259.2	299.1	**270.8**
%C-Organic	[]	19.9	19.5	18.8	19.4	19.1	**19.4**
%C-Calcite	[]	31.9	29.9	25.9	32.8	33.0	**32.2**
%C-Inorganic	[]	48.2	50.6	55.3	47.8	48.0	**48.4**
Dry density	[g/cc]	0.10	0.11	0.13	0.11	0.11	**0.11**
dry/wet	[]	0.09	0.10	0.12	0.10	0.10	**0.10**

Table B.7(a). Lake McQuade - Plot 1 (McQ1) Sediment Porewater Raw Data (1 of 2)

Sample Label & Depth Interval	[cm]	7/25/2012						10/6/2012					
		A	A	A	B	C	**Average**	A	A	A	B	C	**Average**
		0-2	2-4	4-8	0-4	0-4	**0-4**	4-8	4-8	4-8	4-8	4-8	**0-4**
Analytes													
Sulfate	[mg/L]	0.3	0.2	0.2	0.3	0.5	**0.4**	2.5	4.1	3.3	5.6	7.4	**5.5**
Nitrate	[mg/L]	0.4	0.4	0.3	0.2	0.4	**0.3**	0.7	0.2	1.0	0.2	0.3	**0.3**
Phosphate	[mg/L]	10.3	13.0	14.0	10.2	11.2	**11.0**	8.7	8.4	9.2	7.0	5.8	**7.2**
Chloride	[mg/L]		11.3	11.7	10.8		**10.8**	7.4			7.5	7.2	**7.3**
Ferrous Iron	[mmol/L]	0.069	0.093	0.118	0.036	0.062	**0.060**	0.055	0.054	0.083	0.031	0.046	**0.044**
Sulfide	[µmol/L]	7	11		8	8	**8**	5	7	3	3	2	**4**
Ammonium	[mg/L]	4.4	8.1	9.6	5.8	5.9	**6.0**	8.5	5.5	11.4	7.1	5.6	**6.5**
DIC	[mg/L]	50.5	61.9	81.5	49.9	48.5	**51.5**	89.5	102.7	88.7	87.0	97.4	**93.5**
DOC	[mg/L]	27.6	25.8	24.4	25.1	26.1	**26.0**	25.8	28.0	25.5	25.6	23.4	**25.3**
SUVA	[$Lm^{-1}mg^{-1}$]	6.2	5.8	4.5	5.0	5.6	**5.5**	5.6	5.8	7.4	5.2	6.0	**5.6**
Mercury Analysis													
MeHg	[ng/L]	1.80	0.67	0.33	1.22	0.64	**1.03**	0.68	0.39	0.29	1.20	0.62	**0.78**
THg	[ng/L]	3.82	2.21	1.91	3.38	2.31	**2.90**	3.48	1.88	1.84	2.39	2.16	**2.41**
iHg	[ng/L]	2.0	1.55	1.58	2.17	1.67	**1.87**	2.80	1.49	1.55	1.19	1.55	**1.63**
% MeHg	[]	47.1	30.1	17.2	36.0	27.7	**35.5**	19.5	20.5	15.7	50.4	28.5	**32.5**

Table B.7(b). Lake McQuade - Plot 1 (McQ1) Sediment Porewater Raw Data (2 of 2)

Sample Label & Depth Interval	[cm]	6/3/2013 A 4-8	A 4-8	A 4-8	B 4-8	C 4-8	**Average 0-4**
Analytes							
Sulfate	[mg/L]	2.2	2.0	1.5	4.1	2.6	**2.9**
Nitrate	[mg/L]	0.4	0.3	0.2	0.2	0.3	**0.3**
Phosphate	[mg/L]	5.8	6.7	12.4	7.8	7.3	**7.1**
Chloride	[mg/L]	10.214	10.179	9.952	9.201		**9.699**
Ferrous Iron	[mmol/L]	0.010	0.058	0.083	0.065	0.020	**0.040**
Sulfide	[µmol/L]	32	26	5	14	23	**22**
Ammonium	[mg/L]	4.5	5.6	7.0	5.4		**5.2**
DIC	[mg/L]	34.2	68.7	76.9	79.8	70.6	**67.3**
DOC	[mg/L]	8.3	20.0	21.8	19.4	20.2	**17.9**
SUVA	[$Lm^{-1}mg^{-1}$]	13.0	5.9	5.9	5.7	5.1	**6.8**
Mercury Analysis							
MeHg	[ng/L]	1.57	0.42	0.04	0.84	0.76	**0.86**
THg	[ng/L]	12.00	2.32	1.51	11.26	14.15	**10.86**
iHg	[ng/L]	10.42	1.91	1.47	10.42	13.39	**9.99**
% MeHg	[]	13.1	18.0	2.4	7.4	5.4	**8.0**

Table B.8(a). Lake McQuade - Plot 1 (McQ1) Sediment Solid Phase Raw Data, Collected: 7/25/2012

Mercury Analysis

Sample Label & Depth Interval	[cm]	A 0-2	A 2-4	A 4-8	B 0-2	B 2-4	B 4-8	C 0-2	C 2-4	C 4-8	**Average 0-4**
MeHg	[ng/g]	3.4	2.0	1.1	4.9	2.2	1.3	5.1	1.9	1.4	**3.2**
THg	[ng/g]	191.6	191.8	185.6	177.9	190.8	196.1	183.9	185.7	195.4	**187.0**
iHg	[ng/g]	188.3	189.9	184.5	173.0	188.5	194.8	178.8	183.8	194.0	**183.7**
% MeHg	[]	1.76	1.02	0.60	2.76	1.16	0.69	2.77	1.03	0.72	**1.74**
log K_D^* (iHg)	[]										**4.99**
log K_D^* (MeHg)	[]										**3.50**
K_{meth}	[d^{-1}]	0.067	0.059	0.028	0.089	0.061	0.040	0.095	0.060	0.031	**0.072**
K_{demeth}	[hr^{-1}]	0.043	0.059	0.060	0.029	0.042	0.038	0.044	0.050	0.057	**0.044**
K_m/K_d	[]	1.54	1.00	0.46	3.10	1.43	1.06	2.18	1.20	0.55	**1.74**

Sediment Composition

Sample Label & Depth Interval	[cm]	A 0-2	A 2-4	A 4-8	B 0-4	C 0-4	**Average 0-4**
WEM - Iron	[g/kg]	28.1	29.6	24.8	27.7	26.7	**27.8**
AVS	[µmol/g]	350.0	379.2	224.2	135.6	173.1	**224.4**
%C-Organic	[]	25.4	24.8	23.5	24.1	24.4	**24.5**
%C-Calcite	[]	7.1	7.9	7.9	8.1	7.6	**7.7**
%C-Inorganic	[]	67.6	67.3	68.6	67.8	68.0	**67.7**
Dry density	[g/cc]	0.05	0.07	0.08	0.15	0.09	**0.10**
dry/wet	[]	0.05	0.07	0.08	0.14	0.08	**0.09**

Table B.8(b). Lake McQuade - Plot 1 (McQ1) Sediment Solid Phase Raw Data, Collected: 10/6/2012

Mercury Analysis

Sample Label & Depth Interval	[cm]	A 0-2	A 2-4	A 4-8	B 0-2	B 2-4	B 4-8	C 0-2	C 2-4	C 4-8	**Average 0-4**
MeHg	[ng/g]	4.9	3.4	1.5	3.4	1.8	1.1	3.9	2.4	1.2	**3.3**
THg	[ng/g]	187.7	187.5	197.1	189.2	197.1	196.1	191.9	189.8	199.1	**190.5**
iHg	[ng/g]	182.8	184.2	195.6	185.8	195.2	195.0	188.0	187.4	197.8	**187.2**
% MeHg	[]	2.63	1.79	0.76	1.79	0.93	0.57	2.02	1.29	0.62	**1.74**
log K_D^* (iHg)	[]										**5.06**
log K_D^* (MeHg)	[]										**3.63**
K_{meth}	[d^{-1}]	0.108	0.061	0.039	0.100	0.059	0.031	0.114	0.049	0.035	**0.082**
K_{demeth}	[hr^{-1}]	0.038	0.043	0.039	0.049	0.041	0.056	0.037	0.030	0.033	**0.040**
K_m/K_d	[]	2.80	1.42	1.02	2.02	1.43	0.56	3.06	1.64	1.07	**2.06**

Sediment Composition

Sample Label & Depth Interval	[cm]	A 0-2	A 2-4	A 4-8	B 0-4	C 0-4	**Average 0-4**
WEM - Iron	[g/kg]						
AVS	[µmol/g]	324.9	326.5	296.4	293.3	417.0	**345.3**
%C-Organic	[]	25.9	24.5	24.4	24.8	25.4	**25.1**
%C-Calcite	[]	8.8	8.6	8.3	7.9	8.0	**8.2**
%C-Inorganic	[]	65.3	66.9	67.3	67.3	66.6	**66.7**
Dry density	[g/cc]	0.06	0.08	0.08	0.08	0.06	**0.07**
dry/wet	[]	0.05	0.08	0.07	0.07	0.06	**0.07**

Table B.8(c). Lake McQuade - Plot 1 (McQ1) Sediment Solid Phase Raw Data, Collected: 6/3/3013

Mercury Analysis

Sample Label & Depth Interval	[cm]	A 0-2	A 2-4	A 4-8	B 0-2	B 2-4	B 4-8	C 0-2	C 2-4	C 4-8	**Average 0-4**
MeHg	[ng/g]	2.1	1.6	1.1	2.6	1.5	1.0	1.4	1.2	0.9	**1.7**
THg	[ng/g]	209.7	207.0	210.0	198.5	201.4	198.6	191.5	191.8	200.8	**200.0**
iHg	[ng/g]	207.6	205.3	208.9	195.9	199.9	197.6	190.1	190.6	199.9	**198.2**
% MeHg	[]	1.00	0.79	0.51	1.32	0.73	0.51	0.74	0.63	0.46	**0.87**
log K_D^* (iHg)	[]										**4.30**
log K_D^* (MeHg)	[]										**3.30**
K_{meth}	[d^{-1}]	0.045	0.044	0.024	0.040	0.034	0.023	0.041	0.026	0.024	**0.039**
K_{demeth}	[hr^{-1}]	0.074	0.057	0.044	0.062	0.055	0.052	0.070	0.011	0.067	**0.055**
K_m/K_d	[]	0.61	0.76	0.54	0.65	0.62	0.45	0.59	2.49	0.35	**0.95**

Sediment Composition

Sample Label & Depth Interval	[cm]	A 0-2	A 2-4	A 4-8	B 0-4	C 0-4	**Average 0-4**
WEM - Iron	[g/kg]						
AVS	[µmol/g]	533.7	438.1	361.4	402.2	367.3	**418.5**
%C-Organic	[]	24.5	23.6	23.0	23.4	22.6	**23.3**
%C-Calcite	[]	12.8	12.2	11.0	11.1	11.4	**11.7**
%C-Inorganic	[]	62.7	64.2	66.0	65.5	66.0	**65.0**
Dry density	[g/cc]	0.07	0.09	0.09	0.07	0.07	**0.07**
dry/wet	[]	0.06	0.09	0.08	0.07	0.07	**0.07**

Table B.9. Lake McQuade - Plot 1 (McQ1) Surface Water Raw Data

Sampling Date		6/25/2012	7/10/2012	7/25/2012	8/7/2012	8/22/2012	9/5/2012	9/17/2012	10/6/2012	6/3/2013
In-situ measurements										
pH	[]	7.8	8.6	8.5	8.4	8.5	8.4	8.4	8.3	
Temp	[^{o}C]	24.8	27.2	25.1	24.3	20.8	20.7	16.8	13.2	
DO	[mg/L]	8.2	10.5	8.3	9.8	9.8	5.7	9.9	10.7	
Conductivity	[µS/cm]	300	276	441	539	623	648	732	737	
ORP	[mV]	72	33	117		140	115	44	133	
Analytes										
Sulfate	[mM]	0.32	0.41	0.53	0.77	0.89	0.88	0.95	1.21	3.27
Nitrate	[mM]	0.01	0.01	0.01	0.01	0.00	0.05	0.05	0.00	0.01
Phosphate	[mM]								0.005	
Chloride	[mM]								0.21	0.29
Ferrous Iron	[mM]	0.008	0.009	0.024	0.025	0.013	0.008	0.001		0.004
Sulfide	[mM]	0.000	0.001	0.000	0.000	0.001	0.004	0.001	0.000	0.001
Ammonium	[mM]		0.001						0.002	0.001
Mg*	[mg/L]	18.7	22.1	22.1	45.9	52.2	58.8	53.9	62.7	
DIC	[mg/L]	25.7	25.8	36.5	47.6	56.9	62.6	66.5	67.8	34.2
DOC	[mg/L]	16.9	16.6	13.3	12.1	12.2	12.3	10.4	10.3	8.3
SUVA	[$Lm^{-1}mg^{-1}$]	4.1		4.0	3.9	3.9	3.3	1.5	2.8	3.5
Mercury Analysis										
MeHg	[ng/L]	0.21	0.43	0.13	0.10	0.08	0.06	0.05	0.11	0.14
THg	[ng/L]	2.78	2.87	1.52	0.84	0.67	1.24	1.20	0.91	2.74
iHg	[ng/L]	2.57	2.45	1.38	0.74	0.59	1.18	1.15	0.81	2.60
% MeHg	[]	7.6	14.8	8.8	12.0	12.3	5.0	4.4	11.5	5.1

*Data provided by MnDNR

Table B.10. Lake McQuade - Plot 1 (McQ1) Bottom Water Raw Data

Sampling Date		6/25/2012	7/10/2012	7/25/2012	8/7/2012	8/22/2012	9/5/2012	9/17/2012	10/6/2012	6/3/2013
In-situ measurements										
pH	[]	7.1	6.8	6.8	6.8	7.3	7.2	8.4	8.3	
Temp	[^{o}C]	13.8	13.8	14.4	15.0	16.4	16.7	16.7	13.2	
DO	[mg/L]	0.1	0.0		0.1	0.0	0.0	8.5	10.2	
Conductivity	[µS/cm]	256	207	302	387	628	594	734	738	
ORP	[mV]	-184	-173	-221	-206	-242	-277			
Analytes										
Sulfate	[mM]	0.16	0.16	0.06	0.04	0.72	0.67	0.92	1.20	3.28
Nitrate	[mM]		0.00	0.01	0.00	0.00	0.05	0.04		0.01
Phosphate	[mM]	0.012	0.000	0.027	0.042	0.015	0.019	0.000	0.004	
Chloride	[mM]								0.21	0.29
Ferrous Iron	[mM]	0.008	0.009	0.024	0.025	0.013	0.008	0.001		0.004
Sulfide	[mM]	0.006	0.000	0.000	0.003	0.004	0.019	0.001	0.001	0.001
Ammonium	[mM]								0.002	0.006
Mg*	[mg/L]	19.0	19.3	20.7	23.7	48.9	54.8	54.1	62.8	
DIC	[mg/L]	31.5	31.9	35.7	45.0	62.0	73.1	65.4	70.1	35.4
DOC	[mg/L]	16.2	17.0	18.6	21.7	12.8	13.1	10.3	9.4	7.6
SUVA	[$Lm^{-1}mg^{-1}$]	4.5		5.1	4.7	4.3	2.3	1.4	3.1	3.5
Mercury Analysis										
MeHg	[ng/L]	1.29	2.46	1.52	6.50	1.99	0.68	0.08	0.12	0.21
THg	[ng/L]	2.82	4.63	3.29	8.08	2.68	2.39	1.48	0.89	2.58
iHg	[ng/L]	1.53	2.17	1.77	1.58	0.70	1.71	1.41	0.76	2.37
% MeHg	[]	45.7	53.2	46.1	80.4	74.0	28.6	5.1	14.0	8.3

*Data provided by MnDNR

Table B.11(a). Lake McQuade - Plot 1 (McQ1) Water Column Depth Profiles (1 of 3)

		6/25/2012								
Water Depth	[ft]	1	4	5	7	9	10	11	13	15
In-situ measurements										
pH	[]	7.8	7.4		7.0		7.0		7.1	7.1
Temp	[^{o}C]	24.8	20.3		17.3		16.4		15.4	13.8
DO	[mg/L]	8.2	6.0		1.3		0.3		0.1	0.1
Conductivity	[µS/cm]	300	266		199		213		268	256
ORP	[mV]	72	85		90		84		-103	-184
Analytes										
Sulfate	[mM]	0.32		0.26		0.23		0.25	0.30	0.16
Nitrate	[mM]	0.01		0.02		0.01		0.01	0.00	
Phosphate	[mM]								0.00	0.01
Chloride	[mM]									
Ferrous Iron	[mM]	0.002		0.004		0.006		0.006	0.006	0.008
Sulfide	[mM]	0.000		0.002		0.002		0.001	0.002	0.006
Ammonium	[mM]									
Mg*	[mM]									
DIC	[mg/L]	25.7		22.6		21.9		24.2	30.5	31.5
DOC	[mg/L]	16.9		18.5		18.4		17.6	16.1	16.2
SUVA	[$Lm^{-1}mg^{-1}$]	4.1		4.3		4.6		4.4	4.6	4.5
Mercury Analysis										
MeHg	[ng/L]	0.21		0.38		0.64		0.92	2.11	1.29
THg	[ng/L]	2.78		4.07		4.65		4.85	4.11	2.82
iHg	[ng/L]	2.57		3.69		4.01		3.93	2.00	1.53
% MeHg	[]	7.6		9.3		13.8		19.1	51.4	45.7

*Data provided by MnDNR

Table B.11(b). Lake McQuade - Plot 1 (McQ1) Water Column Depth Profiles (2 of 3)

		7/25/2012						
Water Depth	[ft]	1	4	6	7	9	12	14
In-situ measurements								
pH	[]	8.5	7.5	7.7	7.5	7.2	7.0	6.8
Temp	[^{o}C]	25.1	25.1	24.3	22.9	19.6	16.1	14.4
DO	[mg/L]	8.3	8.2	2.3	0.1	0.0	0.0	0.0
Conductivity	[µS/cm]	441	444	453	444	351	264	302
ORP	[mV]	117	89	82	58	-52	-212	-221
Analytes								
Sulfate	[mM]	0.53	0.53		0.55	0.38	0.17	0.06
Nitrate	[mM]	0.01	0.00		0.00	0.01	0.01	0.01
Phosphate	[mM]						0.02	0.03
Chloride	[mM]							
Ferrous Iron	[mM]	0.000	0.000		0.001	0.003	0.022	0.024
Sulfide	[mM]	0.000	0.000		0.000	0.001	0.001	0.000
Ammonium	[mM]							
Mg*	[mM]							
DIC	[mg/L]	36.5	38.6		41.6	35.7	33.2	35.7
DOC	[mg/L]	13.3	11.6		13.4	15.3	16.9	18.6
SUVA	[$Lm^{-1}mg^{-1}$]	4.0	4.7		4.1	4.3	5.0	5.1
Mercury Analysis								
MeHg	[ng/L]	0.13	0.20		0.52	0.63	0.95	1.52
THg	[ng/L]	1.52	1.93		1.67	1.63	2.13	3.29
iHg	[ng/L]	1.38	1.72		1.15	1.00	1.18	1.77
% MeHg	[]	8.8	10.6		31.4	38.4	44.8	46.1

*Data provided by MnDNR

Table B.11(c). Lake McQuade - Plot 1 (McQ1) Water Column Depth Profiles (3 of 3)

		8/22/2012							10/6/2012				
Water Depth	[ft]	1	4	7	10	12	13	15	1	5	10	14	15
In-situ measurements													
pH	[]	8.5	8.4	7.9	8.0		7.5	7.3	8.3	8.3	8.3	8.4	8.3
Temp	[^{o}C]	20.8	20.3	19.6	19.1		17.7	16.4	13.2	13.3	13.3	13.2	13.2
DO	[mg/L]	9.8	9.2	3.2	2.9		0.1	0.0	10.7	10.7	10.7	10.7	10.2
Conductivity	[µS/cm]	623	634	666	706		671	628	737	737	737	738	738
ORP	[mV]	140	129	139	136		-201	-242	133	134	132		
Analytes													
Sulfate	[mM]	0.89		0.93	1.08	0.98		0.72	1.21	1.16	1.21		1.20
Nitrate	[mM]	0.00		0.01	0.03	0.00		0.00	0.00	0.01	0.00		
Phosphate	[mM]					0.01		0.02	0.00	0.00			0.00
Chloride	[mM]					0.24			0.21	0.21	0.21		0.21
Ferrous Iron	[mM]	0.002		0.002	0.001	0.001		0.013		0.004	0.003		
Sulfide	[mM]	0.001		0.002	0.002	0.001		0.004	0.000	0.001	0.001		0.001
Ammonium	[mM]								0.002	0.003	0.003		0.002
Mg*	[mM]												
DIC	[mg/L]	56.9		61.1	64.1	64.8		62.0	67.8	69.7	67.7		70.1
DOC	[mg/L]	12.2		11.1	9.9	11.4		12.8	10.3	9.8	10.1		9.4
SUVA	[$Lm^{-1}mg^{-1}$]	3.9		3.6	3.6	4.0		4.3	2.8	3.1	2.9		3.1
Mercury Analysis													
MeHg	[ng/L]	0.08		0.13	0.34	0.38		1.99	0.11	0.05	0.11		0.12
THg	[ng/L]	0.67		0.90	0.74	0.71		2.68	0.91	0.94	1.22		0.89
iHg	[ng/L]	0.59		0.77	0.40	0.33		0.70	0.81	0.89	1.11		0.76
% MeHg	[]	12.3		14.9	46.0	53.2		74.0	11.5	5.6	9.3		14.0

*Data provided by MnDNR

Table B.12(a). Lake McQuade - Plot 2 (McQ2) Sediment Porewater Raw Data (1 of 2)

Sample Label & Depth Interval	[cm]	5/15/2012						7/25/2012					
		A 0-2	A 2-4	A 4-8	B 0-4	C 0-4	**Average 0-4**	A 4-8	A 4-8	A 4-8	B 4-8	C 4-8	**Average 0-4**
Analytes													
Sulfate	[mg/L]	13.0	8.8	24.5	20.4	22.1	**17.8**	1.6	0.3	0.2	0.4	0.4	**0.6**
Nitrate	[mg/L]	0.0	0.4	0.4	0.3	0.3	**0.3**	20.0	0.9	0.3	0.3	0.4	**3.7**
Phosphate	[mg/L]	1.1	2.1	1.9	1.2	1.2	**1.3**	8.6	8.0	10.5	9.2	9.0	**8.8**
Chloride	[mg/L]								9.1	9.8			**9.067**
Ferrous Iron	[mmol/L]	0.245	0.043	0.073	0.041	0.043	**0.076**	0.141	0.121	0.077	0.106	0.183	**0.140**
Sulfide	[µmol/L]	1	1	1	2	1	**1**	5				3	**3**
Ammonium	[mg/L]			0.9	0.8	0.9	**0.9**		3.7	3.5	2.2	2.8	**2.5**
DIC	[mg/L]	55.6	57.0	57.4	56.3	56.0	**56.2**		63.7	72.7	59.8	63.2	**61.5**
DOC	[mg/L]	21.7	17.1	12.2	15.0	16.1	**16.8**		27.4	23.4	27.7	27.0	**27.4**
SUVA	[$Lm^{-1}mg^{-1}$]	8.0	8.5	8.9	2.4	8.5	**6.4**				5.0	7.3	**6.2**
Mercury Analysis													
MeHg	[ng/L]	0.21	0.06	0.14	0.56	0.17	**0.29**	0.54	0.51	0.47	0.71	0.58	**0.61**
THg	[ng/L]	2.08	1.52	1.13	1.99	2.08	**1.96**	3.35	2.11	1.91	2.82	2.94	**2.83**
iHg	[ng/L]	1.9	1.47	0.99	1.43	1.92	**1.67**	2.81	1.60	1.44	2.11	2.36	**2.23**
% MeHg	[]	10.1	3.8	12.7	28.3	7.9	**14.7**	16.1	24.2	24.6	25.2	19.9	**21.4**

Table B.12(b). Lake McQuade - Plot 2 (McQ2) Sediment Porewater Raw Data (2 of 2)

Sample Label & Depth Interval	[cm]	10/6/2012						6/3/2013					
		A	A	A	B	C	**Average**	A	A	A	B	C	**Average**
		4-8	4-8	4-8	4-8	4-8	**0-4**	4-8	4-8	4-8	4-8	4-8	**0-4**
Analytes													
Sulfate	[mg/L]	62.4	44.3	67.0	58.6		**56.0**	11.3	20.5	25.3	20.2	27.3	**21.1**
Nitrate	[mg/L]	0.9	0.3	0.2	0.0		**0.3**	3.7	0.5	0.3	0.7	0.1	**1.0**
Phosphate	[mg/L]	1.8	4.2	2.8	0.7		**1.9**	4.4	3.8	2.8	3.1	2.9	**3.4**
Chloride	[mg/L]	7.370	7.151	7.432		7.214	**7.237**	10.516	10.6	11.8		12.2	**11.4**
Ferrous Iron	[mmol/L]	0.025	0.024	0.035	0.029	0.032	**0.029**	0.032	0.024	0.030	0.023	0.045	**0.032**
Sulfide	[µmol/L]	5	5	2	3	6	**5**	3	3	3	4	1	**2**
Ammonium	[mg/L]	1.8		2.6		0.0		0.8	0.8	0.8		0.7	**0.7**
DIC	[mg/L]	91.0	79.8	79.0	83.7	85.4	**84.8**	53.3	43.7	45.5	41.1	41.8	**43.8**
DOC	[mg/L]	16.6	15.5	13.1		14.9	**15.5**	22.6	15.9	12.6	17.3	15.3	**17.3**
SUVA	[$Lm^{-1}mg^{-1}$]	5.0	5.8	6.2		6.7	**6.0**	6.8	5.6	5.3	5.8	5.5	**5.8**
Mercury Analysis													
MeHg	[ng/L]	0.33	0.39	0.72	0.40	0.22	**0.33**	0.65	0.33	0.19	0.54	0.31	**0.45**
THg	[ng/L]	2.12	1.34	1.84	1.94	1.77	**1.81**	9.15	6.03	4.45	1.87	2.04	**3.83**
iHg	[ng/L]	1.80	0.95	1.12	1.54	1.55	**1.49**	8.51	5.70	4.26	1.33	1.73	**3.39**
% MeHg	[]	15.4	28.9	39.2	20.7	12.6	**18.0**	7.0	5.5	4.3	28.9	15.2	**11.6**

Table B.13(a). Lake McQuade - Plot 2 (McQ2) Sediment Solid Phase Raw Data, Collected: 5/15/2012

Mercury Analysis

Sample Label & Depth Interval	[cm]	A 0-2	A 2-4	A 4-8	B 0-4	C 0-4	**Average 0-4**
MeHg	[ng/g]	1.1	1.0	1.2	1.6	1.0	**1.2**
THg	[ng/g]	160.8	154.3	168.4	180.8	175.4	**171.3**
iHg	[ng/g]	159.7	153.3	167.2	179.2	174.4	**170.0**
% MeHg	[]	0.68	0.63	0.72	0.91	0.55	**0.71**
log K_D^* (iHg)	[]						**5.01**
log K_D^* (MeHg)	[]						**3.63**
K_{meth}	[d^{-1}]	0.071	0.101	0.081	0.047	0.058	**0.063**
K_{demeth}	[hr^{-1}]	0.058	0.052	0.079	0.080	0.103	**0.079**
K_m/K_d	[]	1.23	1.95	1.02	0.58	0.56	**0.91**

Sediment Composition

Sample Label & Depth Interval	[cm]	A 0-2	A 2-4	A 4-8	B 0-4	C 0-4	**Average 0-4**
WEM - Iron	[g/kg]						
AVS	[µmol/g]	4.7	42.1	121.4	95.8	29.0	**49.4**
%C-Organic	[]	18.5	17.5	16.6	17.8	17.8	**17.8**
%C-Calcite	[]	4.2	4.7	5.3	4.3	4.2	**4.3**
%C-Inorganic	[]	77.4	77.9	78.1	78.0	78.1	**77.9**
Dry density	[g/cc]	0.11	0.13	0.13	0.11	0.12	**0.12**
dry/wet	[]	0.10	0.12	0.12	0.11	0.11	**0.11**

Table B.13(b). Lake McQuade - Plot 2 (McQ2) Sediment Solid Phase Raw Data, Collected: 7/25/2012

Mercury Analysis

Sample Label & Depth Interval	[cm]	A 0-2	A 2-4	A 4-8	B 0-2	B 2-4	B 4-8	C 0-2	C 2-4	C 4-8	**Average 0-4**
MeHg	[ng/g]	2.9	1.1	1.0	1.9	1.0	1.3	1.8	1.3	1.8	**1.7**
THg	[ng/g]	132.2	141.4	147.1	141.9	144.1	145.1	143.2	143.4	152.7	**141.0**
iHg	[ng/g]	129.3	140.3	146.1	140.0	143.1	143.8	141.4	142.1	150.9	**139.4**
% MeHg	[]	2.16	0.79	0.70	1.35	0.70	0.88	1.26	0.89	1.19	**1.18**
log K_D^* (iHg)	[]										**4.80**
log K_D^* (MeHg)	[]										**3.44**
K_{meth}	[d^{-1}]	0.177	0.121	0.091	0.160	0.114	0.072	0.149	0.080	0.063	**0.134**
K_{demeth}	[hr^{-1}]	0.029	0.025	0.040	0.027		0.047	0.038	0.047	0.039	**0.033**
K_m/K_d	[]	6.13	4.78	2.28	5.82		1.54	3.91	1.71	1.60	**4.47**

Sediment Composition

Sample Label & Depth Interval	[cm]	A 0-2	A 2-4	A 4-8	B 0-4	C 0-4	**Average 0-4**
WEM - Iron	[g/kg]	22.5	22.1	23.4	21.9	24.0	**22.7**
AVS	[µmol/g]	141.5	98.9	93.3	63.5	112.1	**98.6**
%C-Organic	[]	18.0	16.3	16.1	17.3	16.3	**16.9**
%C-Calcite	[]	5.0	6.5	4.7	4.3	4.7	**4.9**
%C-Inorganic	[]	77.0	77.3	79.2	78.3	79.0	**78.2**
Dry density	[g/cc]	0.09	0.16	0.15	0.13	0.15	**0.14**
dry/wet	[]	0.09	0.14	0.14	0.12	0.14	**0.13**

Table B.13(c). Lake McQuade - Plot 2 (McQ2) Sediment Solid Phase Raw Data, Collected: 10/6/2012

Mercury Analysis

Sample Label & Depth Interval	[cm]	A 0-2	A 2-4	A 4-8	B 0-2	B 2-4	B 4-8	C 0-2	C 2-4	C 4-8	**Average 0-4**
MeHg	[ng/g]	2.8	1.7	1.1	1.7	1.4	1.0	1.6	1.5	0.9	**1.8**
THg	[ng/g]	161.5	144.0	150.5	143.5	148.4	152.6	148.0	142.6	164.0	**148.0**
iHg	[ng/g]	158.6	142.3	149.4	141.8	147.0	151.6	146.5	141.1	163.1	**146.2**
% MeHg	[]	1.76	1.20	0.70	1.18	0.94	0.63	1.05	1.04	0.57	**1.20**
log K_D^* (iHg)	[]										**4.99**
log K_D^* (MeHg)	[]										**3.74**
K_{meth}	[d^{-1}]	0.082	0.085	0.096	0.082	0.080	0.063	0.103	0.087	0.070	**0.087**
K_{demeth}	[hr^{-1}]	0.040	0.045	0.013	0.046	0.053	0.030	0.046	0.032	0.050	**0.044**
K_m/K_d	[]	2.04	1.89	7.58	1.79	1.52	2.10	2.22	2.75	1.39	**2.04**

Sediment Composition

Sample Label & Depth Interval	[cm]	A 0-2	A 2-4	A 4-8	B 0-4	C 0-4	**Average 0-4**
WEM - Iron	[g/kg]						
AVS	[µmol/g]	59.6	151.0	176.1	149.8	132.0	**129.1**
%C-Organic	[]	17.1	17.0	15.8	16.5	16.9	**16.8**
%C-Calcite	[]	5.3	5.9	5.6	5.4	5.2	**5.4**
%C-Inorganic	[]	77.6	77.1	78.6	78.1	77.9	**77.8**
Dry density	[g/cc]	0.13	0.13	0.13	0.13	0.11	**0.12**
dry/wet	[]	0.12	0.12	0.12	0.12	0.11	**0.11**

Table B.13(d). Lake McQuade - Plot 2 (McQ2) Sediment Solid Phase Raw Data, Collected: 6/3/2013

Mercury Analysis

Sample Label & Depth Interval	[cm]	A 0-2	A 2-4	A 4-8	B 0-2	B 2-4	B 4-8	C 0-2	C 2-4	C 4-8	**Average 0-4**
MeHg	[ng/g]	1.2	1.3	1.2	1.3	1.1	1.0	1.4	1.2	1.0	**1.3**
THg	[ng/g]	173.2	163.4	170.1	166.5	168.4	176.0	171.9	166.2	174.5	**168.3**
iHg	[ng/g]	172.0	162.1	168.9	165.1	167.3	174.9	170.4	164.9	173.5	**167.0**
% MeHg	[]	0.72	0.82	0.71	0.81	0.63	0.59	0.84	0.75	0.57	**0.76**
log K_D^* (iHg)	[]										**4.69**
log K_D^* (MeHg)	[]										**3.46**
K_{meth}	[d^{-1}]	0.088	0.076	0.045	0.074	0.084	0.038	0.085	0.077	0.048	**0.081**
K_{demeth}	[hr^{-1}]	0.028	0.068	0.078	0.062	0.071	0.043	0.067	0.016	0.074	**0.052**
K_m/K_d	[]	3.14	1.12	0.58	1.18	1.19	0.87	1.28	4.89	0.65	**2.13**

Sediment Composition

Sample Label & Depth Interval	[cm]	A 0-2	A 2-4	A 4-8	B 0-4	C 0-4	**Average 0-4**
WEM - Iron	[g/kg]						
AVS	[µmol/g]	71.3	102.8	153.2	74.6	110.3	**90.6**
%C-Organic	[]	16.5	16.4	15.7	16.5	16.4	**16.4**
%C-Calcite	[]	7.0	6.9	6.9	6.7	7.0	**6.8**
%C-Inorganic	[]	76.6	76.7	77.4	76.9	76.7	**76.7**
Dry density	[g/cc]	0.13	0.15	0.16	0.11	0.12	**0.13**
dry/wet	[]	0.12	0.14	0.15	0.11	0.11	**0.12**

Table B.14. Lake McQuade - Plot 2 (McQ2) Surface Water Raw Data

Sampling Date		5/15/2012	6/25/2012	7/10/2012	7/25/2012	8/7/2012	8/22/2012	9/5/2012	9/17/2012	10/6/2012	6/3/2013
In-situ measurements											
pH	[]	8.1	7.9	8.7	8.6	8.6	8.8		8.5	8.5	
Temp	[^{o}C]	17.3	25.5	26.8	25.6	24.8	22.4		16.4	12.5	
DO	[mg/L]	9.4	8.9	11.3	10.0	11.1	14.0		9.9	10.9	
Conductivity	[µS/cm]	501	297	310	470	554	638		757	759	
ORP	[mV]	348	52		22		68		41	57	
Analytes											
Sulfate	[mM]		0.30	0.41	0.57	0.79	0.93	0.88	1.00	1.23	3.28
Nitrate	[mM]		0.02	0.01		0.00	0.01	0.05	0.07		0.01
Phosphate	[mM]		0.000			0.001	0.022	0.010			
Chloride	[mM]				1.54					0.21	
Ferrous Iron	[mM]			0.001	0.000	0.000	0.002	0.002	0.002		0.006
Sulfide	[mM]			0.000	0.000	0.000	0.001	0.005	0.001	0.000	0.001
Ammonium	[mM]	0.001		0.002						0.000	
Mg*	[mg/L]		18.2	25.5	37.6						
DIC	[mg/L]	40.9	24.9	27.7	39.2	53.6	56.3	64.5	70.1	67.3	32.6
DOC	[mg/L]	9.6	15.8	16.5	12.7	14.3	13.3	11.9	10.0	8.9	9.6
SUVA	[$Lm^{-1}mg^{-1}$]	6.9	4.4		3.9	3.1	3.0	3.4	1.3	1.0	3.9
Mercury Analysis											
MeHg	[ng/L]	0.16		0.24	0.18	0.02	0.20	0.19	0.09	0.01	0.41
THg	[ng/L]	0.79		2.43	1.89	0.77	1.19	2.03	0.78	1.07	1.98
iHg	[ng/L]	0.63		2.19	1.71	0.75	0.99	1.84	0.69	1.06	1.57
% MeHg	[]	20.2		9.8	9.6	2.6	16.8	9.6	11.9	0.9	20.6

*Data provided by MnDNR

Table B.15. Lake McQuade - Plot 2 (McQ2) Bottom Water Raw Data

Sampling Date		5/15/2012	6/25/2012	7/10/2012	7/25/2012	8/7/2012	8/22/2012	9/5/2012	9/17/2012	10/6/2012	6/3/2013
In-situ measurements											
pH	[]	8.0	6.9	7.3	7.3	7.8	8.0		8.4	8.4	7.4
Temp	[^{o}C]	15.3	16.6	17.2	19.0	21.0	18.0		16.3	12.5	13.9
DO	[mg/L]	7.2	0.3	0.0	0.0	0.6	3.6		8.9	10.8	6.2
Conductivity	[µS/cm]	499	187	236	427	663	833		760	759	461
ORP	[mV]	333	71	-71	-120	-60	-70		41	67	
Analytes											
Sulfate	[mM]		0.19	0.28	0.57	0.95	1.47			1.24	
Nitrate	[mM]		0.01	0.00	0.01	0.03	0.06			0.00	
Phosphate	[mM]					0.014	0.012			0.006	
Chloride	[mM]				1.49					0.22	
Ferrous Iron	[mM]			0.014	0.006	0.000					0.004
Sulfide	[mM]			0.002	0.001	0.000	0.002			0.000	0.001
Ammonium	[mM]			0.036						0.002	
Mg*	[mg/L]										
DIC	[mg/L]		20.4	31.4	47.6	63.9	72.9			66.2	
DOC	[mg/L]		17.7	18.1	13.4	10.0	6.7			8.9	
SUVA	[$Lm^{-1}mg^{-1}$]		4.6		4.3	3.7	3.6			1.0	
Mercury Analysis											
MeHg	[ng/L]			1.32	0.39	0.09	0.09			0.07	0.21
THg	[ng/L]			3.45	1.74	1.03	0.77			0.99	4.23
iHg	[ng/L]			2.13	1.35	0.95	0.68			0.92	4.02
% MeHg	[]			38.3	22.3	8.2	11.4			7.1	5.0

*Data provided by MnDNR

Table B.16. Lake McQuade Inlet Stream Raw Data (provided by MnDNR)

Sampling Date		5/16/2012	6/7/2012	6/28/2012	7/18/2012	7/31/2012	8/14/2012	8/27/2012	9/10/2012	9/24/2012	10/15/2012
In-situ measurements											
pH	[]	8.0	7.9	8.1	8.2	7.9	8.0	8.1	8.0	8.2	6.8
Temp	[^{o}C]	14.4	18.7	24.3	24.2	21.2	18.2	19.0	13.1	7.2	5.0
DO	[mg/L]	8.7	6.9	8.1	8.7	6.3	6.8	4.9	7.5	9.9	12.9
Conductivity	[µS/cm]	416	489	444	801	775	834	755	748	566	509
ORP	[mV]				79	173	183	154	204	77	180
*Analytes**											
Sulfate	[mM]	0.54	0.75	0.59	1.33	1.43	1.64	1.39	1.69	1.51	1.43
Nitrate	[mM]	0.078	0.051	0.037	0.082	0.163	0.115	0.044	0.085	0.003	0.065
Phosphate	[mM]										
Chloride	[mM]										
Ferrous Iron	[mM]	0.004	0.008	0.019	0.002	0.002	0.001	0.001	0.001	0.001	0.001
Sulfide	[mM]										
Ammonium	[mM]										
Mg	[mg/L]	33.1	40.8	33.3	72.1	68.0	80.3	73.9	75.2	74.0	68.3
DIC	[mg/L]										
DOC	[mg/L]	12.0	12.6	17.0	7.8	9.2	7.7	7.4	7.3	5.9	5.4
SUVA	[$Lm^{-1}mg^{-1}$]	3.0	3.3	3.9	3.3	3.1	3.2	2.7	2.9	2.4	2.8
*Mercury Analysis***											
MeHg	[ng/L]	0.08	0.36	0.50	0.16	0.13	0.10	0.06	0.14	0.07	0.06
THg	[ng/L]	1.58	1.92	3.03	1.10	1.30	0.91	0.62	0.85	0.56	0.54
iHg	[ng/L]	1.50	1.56	2.53	0.94	1.17	0.80	0.55	0.71	0.49	0.48
% MeHg	[]	5.1	18.8	16.5	14.5	10.0	11.5	10.4	17.0	12.8	10.6

*Additional analytes were measured by MnDNR in stream samples, but not used in this paper

**Appendix C

Table B.17. Lake McQuade Outlet Stream Raw Data (provided by MnDNR)

Sampling Date		5/16/2012	6/7/2012	6/28/2012	7/18/2012	7/31/2012	8/14/2012	8/27/2012	9/10/2012	9/24/2012	10/15/2012
In-situ measurements											
pH	[]	7.6	7.6	7.6	7.7	8.1	7.8	8.0	7.3	7.5	7.4
Temp	[^{o}C]	16.6	20.3	24.9	25.6	23.4	21.1	20.6	16.1	10.4	5.3
DO	[mg/L]	5.2	6.1	7.5	5.0	5.2	4.5	1.7	0.8	6.7	8.7
Conductivity	[µS/cm]	420	360	294	468	533	596	630	622	546	486
ORP	[mV]			0	74	315	205	172	209	117	174
*Analytes**											
Sulfate	[mM]	0.54	0.47	0.34	0.64	0.73	0.88	1.01	1.12	1.23	1.24
Nitrate	[mM]	0.094	0.013	0.006	0.009	0.010	0.004	0.004	0.001	0.002	0.001
Phosphate	[mM]										
Chloride	[mM]										
Ferrous Iron	[mM]	0.002	0.005	0.006	0.002	0.001	0.001	0.002	0.001	0.001	0.001
Sulfide	[mM]										
Ammonium	[mM]										
Mg	[mg/L]	31.4	26.2	20.1	37.6	41.7	49.8	57.2	54.8	63.7	64.9
DIC	[mg/L]										
DOC	[mg/L]	11.8	15.3	19.3	14.9	14.2	13.0	13.6	12.1	10.6	9.7
SUVA	[$Lm^{-1}mg^{-1}$]	2.8	3.4	3.7	3.7	3.4	3.3	2.8	2.8	2.7	2.8
*Mercury Analysis***											
MeHg	[ng/L]	0.18	0.29	0.39	0.35	0.16	0.20	0.35	0.26	0.05	0.05
THg	[ng/L]	0.96	2.70	3.24	1.95	1.16	0.62	0.68	0.60	0.63	0.39
iHg	[ng/L]	0.78	2.41	2.85	1.60	1.00	0.42	0.33	0.34	0.58	0.34
% MeHg	[]	18.8	10.7	12.0	17.9	13.8	31.6	51.3	43.9	8.2	13.9

*Additional analytes were measured by MnDNR in stream samples, but not used in this paper

**Appendix C

Table B.18(a). West Two River Wetland Pond (WTR) Sediment Porewater Raw Data (1 of 2)

Sample Label & Depth Interval	[cm]	7/24/2012						10/6/2012					
		A	A	A	B	C	**Average**	A	A	A	B	C	**Average**
		0-2	2-4	4-8	0-4	0-4	**0-4**	4-8	4-8	4-8	4-8	4-8	**0-4**
Analytes													
Sulfate	[mg/L]	0.8	0.5	0.5	5.5	0.8	**2.3**	2.1	1.0	0.9	0.5		**1.0**
Nitrate	[mg/L]	2.1	1.0	0.4	3.5	2.1	**2.4**	0.7	0.1	0.4	0.4		**0.4**
Phosphate	[mg/L]	1.3	2.7	2.5	2.0	0.4	**1.5**	0.0	0.8	0.2	0.0		**0.2**
Chloride	[mg/L]								1.9	1.7	1.828		**1.828**
Ferrous Iron	[mmol/L]	0.033	0.030	0.045	0.027	0.034	**0.031**	0.011	0.013	0.043	0.010	0.009	**0.010**
Sulfide	[µmol/L]	3.5	13.8	10.1	20.0	19.8	**16.1**	4.2	5.6	3.4	3.8	4.6	**4.5**
Ammonium	[mg/L]			6.3		3.9	**3.9**		2.7	2.5		1.7	**1.7**
DIC	[mg/L]	42.4	41.3	52.0	37.6	39.6	**39.7**		35.0	32.7	37.7	41.1	**39.4**
DOC	[mg/L]	22.8	23.5	21.7	22.0	24.4	**23.2**		18.2	17.5	18.9	21.7	**20.3**
SUVA	[$Lm^{-1}mg^{-1}$]	3.6	3.2	3.6	4.9		**4.2**		4.8	4.9	4.6	5.0	**4.8**
Mercury Analysis													
MeHg	[ng/L]	1.37	0.86	0.36	1.06	1.45	**1.21**	0.75	0.38	0.26	0.38	0.41	**0.45**
THg	[ng/L]	1.95	1.77	1.08	2.11	2.55	**2.17**	2.83	1.70	1.88	3.15	1.99	**2.47**
iHg	[ng/L]	0.6	0.91	0.72	1.06	1.10	**0.97**	2.08	1.32	1.62	2.76	1.58	**2.01**
% MeHg	[]	70.3	48.6	33.0	50.1	56.8	**55.5**	26.5	22.1	14.1	12.2	20.8	**18.4**

Table B.18(b). West Two River Wetland Pond (WTR) Sediment Porewater Raw Data (1 of 2)

Sample Label & Depth Interval	[cm]	6/3/2013 A 4-8	A 4-8	A 4-8	B 4-8	C 4-8	**Average 0-4**
Analytes							
Sulfate	[mg/L]	2.1	1.5	1.3	1.5	1.6	**1.6**
Nitrate	[mg/L]	6.5	2.3	2.2	7.2	0.2	**3.9**
Phosphate	[mg/L]	0.0	0.0	0.1	0.3	0.1	**0.1**
Chloride	[mg/L]	2.021	1.814	1.630	2.332	1.747	**1.999**
Ferrous Iron	[mmol/L]	0.027	0.053	0.056	0.060	0.122	**0.074**
Sulfide	[µmol/L]	4.0	11.3	11.0	7.4	4.4	**6.5**
Ammonium	[mg/L]	0.9	1.0	1.0	1.8	1.2	**1.3**
DIC	[mg/L]	42.0	30.1	33.5	40.6	28.8	**35.2**
DOC	[mg/L]	21.2	17.2	14.6	20.1	17.0	**18.8**
SUVA	[$Lm^{-1}mg^{-1}$]	4.3	4.4	4.4	4.8	4.6	**4.6**
Mercury Analysis							
MeHg	[ng/L]	0.52	0.50	0.29	0.34	0.18	**0.34**
THg	[ng/L]	2.14	1.85	1.82	1.72	1.44	**1.72**
iHg	[ng/L]	1.63	1.35	1.53	1.38	1.26	**1.38**
% MeHg	[]	24.2	27.1	15.8	19.8	12.2	**19.9**

Table B.19(a). West Two River Wetland Pond (WTR) Sediment Solid Phase Raw Data, Collected: 7/24/2012

Mercury Analysis

Sample Label & Depth Interval	[cm]	A 0-2	A 2-4	A 4-8	B 0-2	B 2-4	B 4-8	C 0-2	C 2-4	C 4-8	**Average 0-4**
MeHg	[ng/g]	0.8	0.7	0.8	3.7	1.9	0.8	3.8	1.1	1.1	**2.0**
THg	[ng/g]	80.2	91.6	143.4	79.1	84.4	149.0	83.1	117.5	188.7	**89.3**
iHg	[ng/g]	79.4	90.9	142.6	75.5	82.5	148.2	79.3	116.5	187.6	**87.4**
% MeHg	[]	1.01	0.78	0.56	4.62	2.25	0.53	4.53	0.91	0.60	**2.22**
log K_D^* (iHg)	[]										**4.96**
log K_D^* (MeHg)	[]										**3.22**
K_{meth}	[d^{-1}]	0.094	0.045	0.026	0.266	0.132	0.037	0.309	0.108	0.062	**0.159**
K_{demeth}	[hr^{-1}]	0.022	0.016	0.038	0.038	0.035	0.030	0.028	0.032	0.095	**0.029**
K_m/K_d	[]	4.24	2.76	0.69	7.00	3.77	1.23	10.88	3.44	0.65	**5.35**

Sediment Composition

Sample Label & Depth Interval	[cm]	A 0-2	A 2-4	A 4-8	B 0-4	C 0-4	**Average 0-4**
WEM - Iron	[g/kg]	10.7	9.0	7.7	12.5	8.2	**10.2**
AVS	[µmol/g]	137.6	87.7	43.2	101.5	55.9	**90.0**
%C-Organic	[]	49.6	50.1	49.9	51.0	50.3	**50.4**
%C-Calcite	[]	9.1	8.1	9.8	8.6	10.2	**9.2**
%C-Inorganic	[]	41.3	41.8	40.3	40.3	39.5	**40.5**
Dry density	[g/cc]	0.03	0.05	0.06	0.05	0.04	**0.04**
dry/wet	[]	0.03	0.05	0.05	0.05	0.04	**0.04**

Table B.19(b). West Two River Wetland Pond (WTR) Sediment Solid Phase Raw Data, Collected: 10/6/2012

Mercury Analysis

Sample Label & Depth Interval	[cm]	A 0-2	A 2-4	A 4-8	B 0-2	B 2-4	B 4-8	C 0-2	C 2-4	C 4-8	**Average 0-4**
MeHg	[ng/g]	2.8	1.0	0.9	1.9	1.1	0.8	2.5	1.3	0.9	**1.8**
THg	[ng/g]	172.5	198.6	195.7	141.9	160.4	197.1	147.4	153.3	216.9	**162.4**
iHg	[ng/g]	169.7	197.6	194.8	140.1	159.4	196.3	144.9	152.1	216.0	**160.6**
% MeHg	[]	1.61	0.52	0.47	1.31	0.67	0.42	1.70	0.82	0.43	**1.08**
log K_D^* (iHg)	[]										**4.90**
log K_D^* (MeHg)	[]										**3.59**
K_{meth}	[d^{-1}]	0.061	0.033	0.016	0.066	0.045	0.027	0.059	0.047	0.022	**0.052**
K_{demeth}	[hr^{-1}]	0.023	0.016	0.014	0.008	0.010	0.032	0.006	0.010	0.044	**0.012**
K_m/K_d	[]	2.65	2.09	1.10	8.56	4.38	0.84	10.70	4.58	0.50	**5.49**

Sediment Composition

Sample Label & Depth Interval	[cm]	A 0-2	A 2-4	A 4-8	B 0-4	C 0-4	**Average 0-4**
WEM - Iron	[g/kg]						
AVS	[µmol/g]	57.8	130.6	38.9	177.7	37.7	**103.2**
%C-Organic	[]	50.6	50.5	50.0	49.0	49.9	**49.8**
%C-Calcite	[]	11.2	10.8	11.0	11.1	10.7	**10.9**
%C-Inorganic	[]	38.3	38.7	38.9	39.9	39.3	**39.2**
Dry density	[g/cc]	0.03	0.03	0.04	0.03	0.04	**0.04**
dry/wet	[]	0.03	0.03	0.04	0.03	0.04	**0.04**

Table B.19(c). West Two River Wetland Pond (WTR) Sediment Solid Phase Raw Data, Collected: 6/3/2013

Mercury Analysis

Sample Label & Depth Interval	[cm]	A 0-2	A 2-4	A 4-8	B 0-2	B 2-4	B 4-8	C 0-2	C 2-4	C 4-8	**Average 0-4**
MeHg	[ng/g]	1.4	0.7	0.8	2.7	1.1	1.1	3.2	1.5	1.2	**1.8**
THg	[ng/g]	153.4	183.3	251.8	116.5	109.0	203.4	139.8	146.1	210.0	**141.3**
iHg	[ng/g]	152.0	182.5	251.0	113.8	107.9	202.3	136.7	144.5	208.8	**139.6**
% MeHg	[]	0.94	0.41	0.30	2.31	1.01	0.54	2.27	1.05	0.57	**1.26**
log K_D^* (iHg)	[]										**5.01**
log K_D^* (MeHg)	[]										**3.72**
K_{meth}	[d^{-1}]	0.049	0.026	0.014	0.104	0.075	0.040	0.107	0.065	0.033	**0.071**
K_{demeth}	[hr^{-1}]		0.017	0.027	0.006	0.028	0.059	0.013	0.042	0.037	**0.019**
K_m/K_d	[]		1.53	0.53	16.57	2.65	0.68	8.27	1.52	0.90	**7.16**

Sediment Composition

Sample Label & Depth Interval	[cm]	A 0-2	A 2-4	A 4-8	B 0-4	C 0-4	**Average 0-4**
WEM - Iron	[g/kg]						
AVS	[µmol/g]	77.9	81.5	33.6	50.0	152.7	**94.1**
%C-Organic	[]	49.6	50.0	47.7	50.5	46.7	**49.0**
%C-Calcite	[]	14.0	14.4	12.5	12.7	14.6	**13.8**
%C-Inorganic	[]	36.4	35.5	39.7	36.8	38.8	**37.1**
Dry density	[g/cc]	0.04	0.05	0.06	0.04	0.04	**0.04**
dry/wet	[]	0.04	0.05	0.06	0.04	0.04	**0.04**

Appendix C: Inter-lab Comparison of Mercury Analyses

Methods for water sample collection and Hg analysis differed between lake samples and stream samples. Lake water column samples were collected and filtered using a nominal 0.2 micron filter and were analyzed for Hg and MeHg at the University of Toronto laboratory, while samples of inlet and outlet streams were filtered using a nominal filter size of 0.45 microns and were analyzed for Hg and MeHg at the Gustavus Adolphus College laboratory. To compare Hg analysis between the two labs, concurrent water column samples were collected and filtered using both filter sizes and analyzed at the two labs (Table C.1). Measured concentrations across both lakes were correlated between the two labs for both MeHg ($R^2 = 0.66$) and THg ($R^2 = 0.66$) (Fig C.1 & C.2). The correlation remained for both THg and MeHg for each lake when analyzed individually (Fig C.1 & C.2).

Comparisons of the data show that as a general trend, MeHg concentrations were generally 30 to 80 % higher in the measurements made by the Gustavus Adolphus lab, which is consistent with the use of a larger filter size. There were, however, several exceptions to this in which MeHg quantified at Gustavus Adolphus were 4 to 8 times larger than those quantified at Toronto. Additionally, in Manganika surface waters, Gustavus consistently quantified concentrations lower than Toronto. Total mercury comparisons were less variable between labs, with values quantified at Gustavus typically falling between 50 and 150 % of those at Toronto, the surface waters of Lake Manganika again being an exception.

Modeling and MeHg mass flow analysis in Lake McQuade required use of measured data in the water column and in the inlet and outlet streams. Because of the difference in sampling method the measured data could not be compared directly. The inter-lab comparison was used to estimate a linear relationship between the two methods so that inlet and outlet data could be quantitatively "corrected" to the water column data and be used in the same equation. Excluding one outlier, the inter-lab comparison of MeHg measurements in Lake McQuade showed strong correlation ($R^2 = 0.87$) and a slope of 0.40 for the linear best fit line (Fig C.3). Thus, MeHg measurements in the inlet and outlet were multiplied by 0.4 when input into the Lake McQuade model.

Table C.1. Comparison of Gustavus Adolphus and U of Toronto mercury analysis in concurrently collected Lake McQuade water column samples

	MeHg [ng/L]			**THg [ng/L]**		
Site Location	Gustavus Adolphus	U of Toronto	Ratio	Gustavus Adolphus	U of Toronto	Ratio
McQ1 SW						
6/25/2012	0.31	0.21	1.47	3.38	2.78	1.22
7/10/2012	0.29	0.43	0.68		2.87	n/a
7/25/2012	0.36	0.13	2.69	1.97	1.52	1.30
8/7/2012	0.18	0.10	1.74		0.84	n/a
8/21/2012	0.13	0.08	1.62	0.93	0.67	1.39
9/6/2012	0.08	0.06	1.29	0.67	1.24	0.54
9/17/2012	0.09	0.05	1.60	0.78	1.20	0.65
10/4/2012	0.01	0.11	0.09	0.57	0.91	0.63
McQ2 SW						
6/25/2012	0.28		n/a	3.79		n/a
7/10/2012	0.35	0.24	1.47	2.46	2.43	1.01
7/25/2012	0.23	0.18	1.27	1.48	1.89	0.78
McQ1 BW						
7/25/2012	4.36	1.52	2.88	6.45	3.29	1.96
8/7/2012	5.09	6.50	0.78		8.08	n/a
8/21/2012	3.74	1.99	1.88	3.41	2.68	1.27
9/6/2012	2.74	0.68	4.01	3.21	2.39	1.34
9/17/2012	0.18	0.08	2.41	0.76	1.48	0.51
10/4/2012	0.03	0.12	0.25	0.70	0.89	0.79
McQ2 BW						
7/10/2012		1.32	n/a	5.83	3.45	1.69
7/25/2012	0.67	0.39	1.73	2.21	1.74	1.27

Table C.2. Comparison of Gustavus Adolphus and U of Toronto mercury analysis in concurrently collected Lake Manganika water column samples

	MeHg [ng/L]			**THg [ng/L]**		
Site Location	Gustavus Adolphus	U of Toronto	Ratio	Gustavus Adolphus	U of Toronto	Ratio
Mng1 SW						
6/25/2012	0.03	0.08	0.37	1.42	1.29	1.10
7/10/2012	0.05	0.50	0.10	1.21	2.32	0.52
7/24/2012		1.11	n/a	1.00	2.10	0.48
8/7/2012	0.06	0.11	0.55		0.43	n/a
8/21/2012	0.13	0.25	0.52	0.97	0.78	1.24
9/5/2012	0.03	0.11	0.26	0.56	1.71	0.32
9/17/2012	0.19	0.24	0.78	0.50	1.31	0.38
10/6/2012	0.13	0.09	1.41	0.44	1.39	0.32
Mng1 **B**W						
6/25/2012	2.33	1.45	1.61	3.40	4.75	0.72
7/10/2012	3.13	0.62	5.06	6.27	3.76	1.67
7/24/2012	1.43	1.28	1.12		5.02	n/a
8/7/2012	4.26	3.30	1.29		6.68	n/a
9/5/2012	3.24	1.14	2.84		4.01	n/a
9/17/2012	0.76	0.09	8.23	1.74	1.20	1.45
10/6/2012	0.03	0.15	0.21	0.46	0.96	0.48

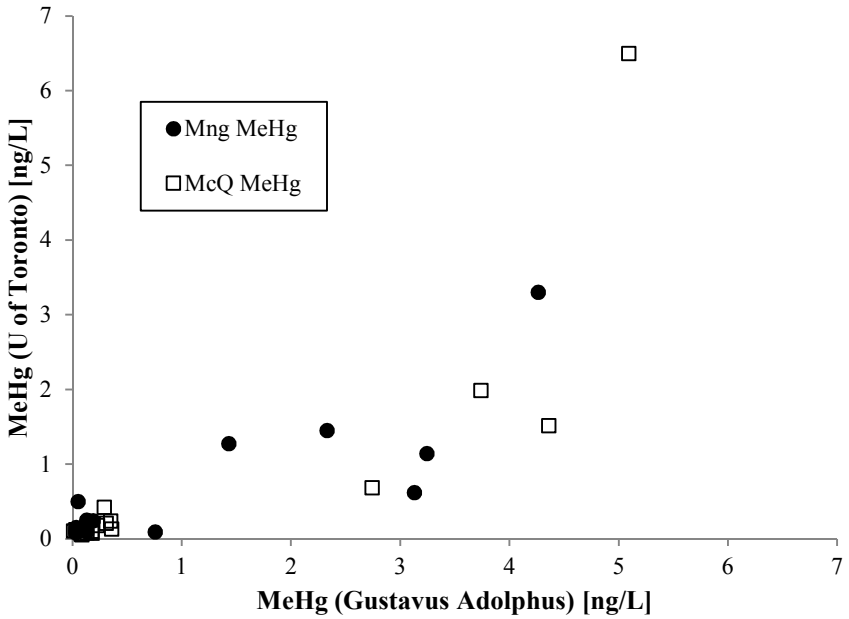

Fig C.1. Inter-lab comparison of MeHg measurements in concurrently collected water column samples.

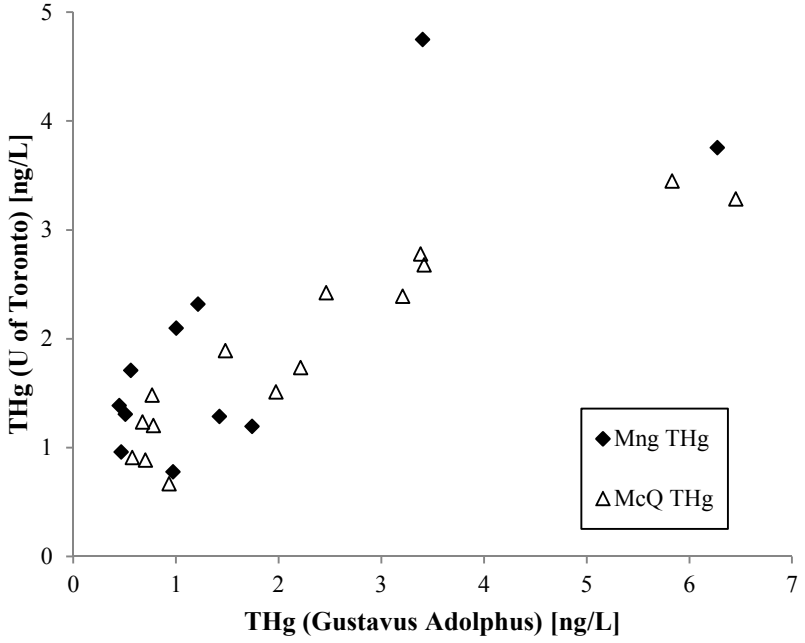

Fig C.2. Inter-lab comparison of THg measurements in concurrently collected water column samples.

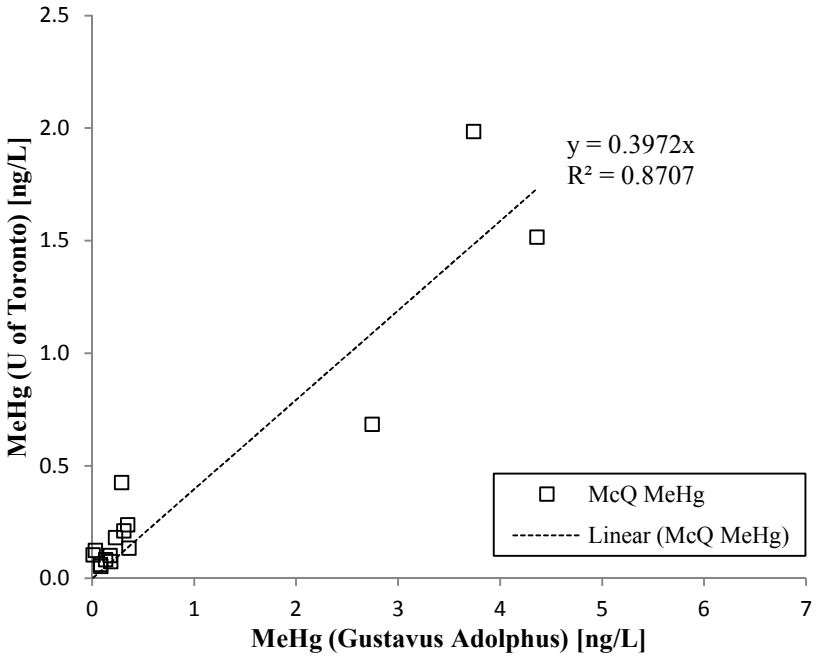

Fig C.3. Linear best-fit relationship of inter-lab comparison of MeHg measurements in Lake McQuade water column samples, collected concurrently by UMD/U of Toronto and MnDNR/Gustavus Adolphus.

Appendix D: Comparison of Mercury in Filtered & Unfiltered Samples

Quantification of MeHg and THg in the water column used filtered water samples, and therefore only describes the amount of dissolved MeHg and THg in the water column and not account for the total mass in the water column. In an effort to better understand the nature of the entire Hg pool, several raw (unfiltered) water samples were analyzed for MeHg and THg in addition to the filtered samples by the Gustavus Adolphus lab to determine the dissolved fraction of the THg and MeHg present in the water column (Table D.1 & D.2). In the waters of the mesotrophic Lake McQuade, 10 to 20 % of THg was present in the particulate (unfiltered minus filtered) phase. For MeHg, the particulate phase comprised 21% on average in the bottom water of Lake McQuade. In surface water samples, the fraction of MeHg on the particulate phase ranged from 24 to 70 %. However, concentrations of dissolved MeHg in the surface water were consistently low (<0.5 ng/L) throughout the sampling period (Fig 3.5g & 3.6g), thus the amount of particle-bound MeHg would also be small despite comprising a relatively high fraction of the epilimnetic MeHg pool.

Table D.1. Comparison of measured THg in filtered water samples (0.45 microns) and unfiltered (raw) samples collected at Lake McQuade

Site Location	Date	Dissolved phase conc. (filtered) [ng/L]	Total conc. (unfiltered) [ng/L]	Particulate fraction [%]
Total Mercury (THg)				
McQ1 SW	7/25/2012	1.97	2.00	1.5
	8/7/2012	n/a	n/a	n/a
	8/21/2012	0.93	0.98	5.1
	9/6/2012	0.67	0.66	*
	9/17/2012	0.78	0.76	*
	10/4/2012	0.57	0.79	27.8
McQ2 SW	7/25/2012	1.48	1.87	20.9
Surface Water Average				*9.2 +/- 12.1*
McQ1 BW	7/25/2012	6.45	8.00	19.4
	8/7/2012	n/a	n/a	n/a
	8/21/2012	3.41	4.16	18.0
	9/6/2012	3.21	3.46	7.2
	9/17/2012	0.76	0.90	15.6
	10/4/2012	0.70	1.00	30.0
McQ2 BW	7/25/2012	2.21	3.04	27.3
Bottom Water Average				*19.6 +/- 8.2*

*concentration in filtered sample measured higher than in unfiltered sample, though differences <10 %. Particulate phase fraction considered to be 0% when calculating averages

Table D.2. Comparison of measured MeHg in filtered water samples (0.45 microns) and unfiltered (raw) samples collected at Lake McQuade

Site Location	Date	Dissolved phase conc. (filtered) [ng/L]	Total conc. (unfiltered) [ng/L]	Particulate fraction [%]
Methylmercury (MeHg)				
McQ1 SW	7/25/2012	0.36	0.47	23.4
	8/7/2012	0.18	0.40	55.0
	8/21/2012	0.13	0.42	69.0
	9/6/2012	0.08	0.16	50.0
	9/17/2012	0.09	0.25	64.0
	10/4/2012	0.01	0.33	97.0
McQ2 SW	7/25/2012	0.23	0.46	50.0
Surface Water Average				*58.3 +/- 22.4*
McQ1 BW	7/25/2012	4.36	4.47	2.5
	8/7/2012	5.09	5.3	4.0
	8/21/2012	3.74	3.42	*
	9/6/2012	2.74	2.52	*
	9/17/2012	0.18	0.54	66.7
	10/4/2012	0.03	0.07	57.1
McQ2 BW	7/25/2012	0.67	0.81	17.3
Bottom Water Average				*21.1 +/- 28.6*

*concentration in filtered sample measured higher than in unfiltered sample, though differences <10 %. Particulate phase fraction considered to be 0% when calculating averages

Appendix E: Sediment Flux Estimates Method

Diffusive flux was estimated using equation E.1, which was derived from Fick's first law and assuming no bulk water movement (Equation E.1), where diffusive flux (J) is a function of the change in concentration across the sediment-water interface (SWI), sediment porosity (ϕ), tortuosity (θ^2), and the diffusion coefficient of the chemical in water (D_w). Water-only diffusion was corrected for temperature using measured bottom water temperature, following the method used in Li & Gregory 1974 and Boudreau 1997.

$$J = -\left(\frac{\varphi D_w}{\theta^2}\right)\frac{\partial C}{\partial z} \quad \text{(E.1)}$$

The concentration derivative was calculated using difference between filtered bottom water concentration and filtered porewater concentration of the composited 0-2 cm sediment sample, assuming 1 cm represented the change in depth between the two concentrations. Sediment porosity was calculated with equation E.2 using measured values for dry bulk density (ρ_b) and estimating particle density (ρ_s) using measured fractions of sediment composition (equation E.3):

$$\varphi = 1 - \left(\frac{\rho_b}{\rho_s}\right) \quad \text{(E.2)}$$

$$\rho_s = 1.1 f_{organic} + 2.72 f_{calcite} + 2.65 f_{inorganic} \quad \text{(E.3)}$$

Tortuosity was calculated based on the porosity relationship for unlithified fine-grained sediments proposed by Boudreau 1996 (equation E.4).

$$\theta^2 = 1 - \ln(\varphi^2) \quad \text{(E.4)}$$

A MeHg diffusion coefficient of 1.24 X 10^{-5} cm^{-2} s^{-1} was estimated for MeHg using equation E.5, based on the relationship with molar volume (V_m) for neutrally charged aqueous species (Hayduk & Laudie 1974; Schwarzenbach et al. 1993; Hammerschmidt et al. 2004). For the purpose of estimating diffusion coefficients, MeHg was assumed to be present in the form CH_3HgSH^0 (Dyrssen & Wedborg 1991; Hammerschmidt et al. 2004), a form of mercury hypothesized to be present in Lake Manganika and other sulfide rich waters of the region by Berndt & Bavin (2012b). Molar volume was calculated using the molecular weight and density of the CH_3HgSH^0 species (ATSDR 1999).

$$D_w = \left(\frac{2.3 \text{ X } 10^{-4}}{V_m{}^{0.71}}\right) \quad \text{(E.5)}$$

The diffusion coefficient of inorganic mercury was assumed to be 5.5 X 10^{-6} cm^{-2} s^{-1} based on values used in previous studies (Bothner et al. 1980; Gobeil & Costa 1993; Covelli et al. 1999).

Appendix F: Modeling Methods

Appendix F1: Model Operation

Modeling of chemical mass flows in both the epilimnion and hypolimnion of Lake McQuade were derived from the mass balance equations (Equation 3.2 & 3.3). These coupled equations contain first-order dependencies on C_e and C_h and therefore the linear equations can be written in vector notation as follows:

$$\begin{bmatrix} C_e' \\ C_h' \end{bmatrix} = \begin{bmatrix} a_{11} & a_{12} \\ a_{21} & a_{22} \end{bmatrix} \begin{bmatrix} C_e \\ C_h \end{bmatrix} + \begin{bmatrix} b_1 \\ b_2 \end{bmatrix} \quad \text{(F.1)}$$

Coefficient matrices a & b represent specific sources and sinks of each constituent. Several variables within the coefficient matrices are transient over time (ex: V_e, V_h, A_{ls}, k_z), which necessitates the model be solved numerically. Definitions of the coefficient matrices used for each chemical constituent modeled is included in Appendix F2, with individual variables defined in Appendix F3.

The modeling described in this thesis used a simple forward Euler method to calculate epilimnion and hypolimnion concentrations at each successive time-step (Δt). A time step of one day was utilized in each model. Smaller time-steps did not affect the accuracy or stability of the modeling results.

$$C_e^{n+1} = C_e^n + \Delta t(a_{11}^n C_e^n + a_{12}^n C_h^n + b_1^n) \quad \text{(F.2)}$$

$$C_h^{n+1} = C_h^n + \Delta t(a_{21}^n C_e^n + a_{22}^n C_h^n + b_2^n) \quad \text{(F.3)}$$

This method (initial value problem) requires initial concentrations to be known, therefore t_0 (day in which model is initiated) was set to a date when field samples were collected. Most parameters (physical dimensions and mixing rates) in the model were constrained by field observations (Appendix F5). The reaction parameters were varied to achieve the lowest least-squares error between modeled chemical concentrations and field measurements.

Equations 3.2 & 3.3 defining the model describe the lake under stratified conditions. Thus a change in the model is required when stratified conditions no longer exist. To account for lake mixing, lake turnover events were introduced. At a specified time step corresponding to an instantaneous and complete mixing event, a single, whole-lake concentration was calculated based on the previous mass inventory of the two layers:

$$C_{lake} = \frac{V_e C_e + V_h C_h}{V_{total}} \tag{F.4}$$

After lake turnover, the model will reflect one of two possible conditions: (1) re-stratification of the lake, in which the model reverts back to the initial Euler method, calculating the concentrations at the next time step using the value of C_{lake} for both C_e^n and C_h^n; or (2) persistence of well-mixed conditions, in which the model is changed to reflect the lake as a single, well-mixed system, with a single partial differential equation used to describe the concentration in the lake.

Appendix F2: Definition of Coefficient Matrices

Table F.1. Definition of coefficient matrices used in modeling equations

Constituent Modeled	**Mg**	**SO_4**
a_{11}	$-\left(\frac{Q}{V_e}+\frac{k_z A_{ls}}{V_e(z_{bw}-z_{ls})}\right)$	$-\left(\frac{Q}{V_e}+\frac{k_z A_{ls}}{V_e(z_{bw}-z_{ls})}\right)$
a_{12}	$\frac{k_z A_{ls}}{V_e(z_{bw}-z_{ls})}$	$\frac{k_z A_{ls}}{V_e(z_{bw}-z_{ls})}$
a_{21}	$\frac{k_z A_{ls}}{V_h(z_{bw}-z_{ls})}$	$\frac{k_z A_{ls}}{V_h(z_{bw}-z_{ls})}$
a_{22}	$-\left(\frac{k_z A_{ls}}{V_h(z_{bw}-z_{ls})}\right)$	$-\left(\frac{k_z A_{ls}}{V_h(z_{bw}-z_{ls})}\right)$
b_1	$\frac{Q}{V_e}C_{in}$	$\frac{Q}{V_e}C_{in}$
b_2	0	$-\dot{m}_L$

Appendix F3: Definition of Modeling Variables

C_e = concentration in epilimnion [mg/L or ng/L]

Field measurements of surface water concentrations at McQ1 and McQ2 were used as input data for C_e, with McQ1 and McQ2 data averaged together when on the same date. The model assumes a well-mixed epilimnion, thus C_e is constant at all depths within the epilimnion.

C_h = concentration in hypolimnion [mg/L or ng/L]

Field measurements of bottom water concentrations at McQ1 (deep site) were used as input data for C_h. Bottom water samples at McQ1 were collected at a depth of 15 ft, thus $C_h = C_{(z=15ft)}$

C_{in} = inlet concentration [mg/L or ng/L]

Inlet concentrations were represented in the model by two different time-constant values to describe the changes in inlet composition under high flow conditions (applied in the model from spring to early summer) and under dry, low flow conditions (applied in the model from mid-July to October). Over the duration of each flow regime, C_{in} was represented as constant with time in the model. This value was calculated using inlet stream sampling data (taken biweekly by MnDNR) were averaged over the appropriate time period for each regime.

Different collection methods were used for inlet and outlet samples collected for MeHg analysis than were used in for lake water column samples in Lake McQuade (Appendix

B). An inter-lab comparison of concurrent samples was used to establish an algebraic relationship between the two methods (Fig C.3, Appendix C). This relationship was used to correct inlet and outlet MeHg measurements so they would be compatible in the model with data from lake water column samples.

Q = inlet & outlet flow [m^3/d]

Flow rates of the inlet and outlet streams were not measured in this field study. Flow was defined in terms of lake residence time (τ) using the relationship $Q = V / \tau$. Residence time was estimated using the Mg model, with the estimated residence time during the summer stratified period used in the sulfate and MeHg models.

V_e = volume of epilimnion [m^3]

V_h = volume of hypolimnion [m^3]

A_{ls} = Surface area of the limnetic surface [m^2]

Volumes were estimated using geospatial bathymetry data of Lake McQuade, which was obtained from the Minnesota DNR. The surface area of each depth contour was calculated in ArcGIS, and used to interpolate the horizontal area at any given depth. The volume of a layer with upper bound at depth z_U and lower bound at z_L was estimated using equation F.5, with A_U and A_L representing the horizontal area corresponding to the depths of the upper and lower bound.

$$V = \frac{\frac{1}{2}(A_L + A_U)}{z_L - z_U} \quad \text{(F.5)}$$

The depth of the limnetic surface (z_{ls}) was defined using biweekly temperature depth profiles measured in Lake McQuade. Limnetic surface depth represents the lower bound of the epilimnion and the upper bound of the hypolimnion, with the upper bound of the epilimnion defined as the lake surface (z=0 ft) and the lower bound of the hypolimnion at the deepest point of the lake (defined in model as z=20 ft). A_{ls} was equal to the horizontal area at z_{ls} found with analysis of bathymetry data (as described above).

$A_{sed(e)}$ = surface area of sediment available for exchange with epilimnetic waters [m^2]

$A_{sed(h)}$ = surface area of sediment available for exchange with hypolimnetic waters [m^2]

$J_{sed(e)}$ = flux across the sediment-water interface into epilimnetic waters[$ng/m^2/d$]

$J_{sed(h)}$ = flux across the sediment-water interface into hypolimnetic waters[$ng/m^2/d$]

Flux across the sediment-water interface (SWI) was estimated as described in the Methods section. A discussion of the method used to estimate sediment flux of MeHg is included in Appendix E. Estimated MeHg flux at McQ1 was used to define flux into the hypolimnion in the model, while estimates at McQ2 were used to define flux into the epilimnion (Table 3.1).

Appendix F4: Estimating Flux across the Limnetic Surface

A heat-tracer method (Jassby & Powell 1975) was used to estimate flux across the limnetic surface. Mass transport by diffusion-like processes is defined by expressions analogous to Fick's first law of diffusion. In the absence of advective flow between layers, flux across the limnetic surface is driven by differences in concentration and mixing between the epilimnion and hypolimnion. C_h is defined by the concentration measured in the bottom waters and thus corresponds to the water column depth. Because C_e is constant throughout the epilimnion (due to the well-mixed assumption), the concentration immediately above the limnetic surface is equal to C_e. The concentration gradient term can then be written as: $\frac{C_e - C_h}{z_{ls} - z_{bw}}$

In many cases, the degree of vertical mixing in a lake water column is dictated by the lake's thermal structure. Since the same processes that move internal energy (heat) in the vicinity of the limnetic surface also carry dissolved constituents in the water, the eddy diffusivity of heat (K_z) can be used as an estimate for the vertical diffusion coefficient to estimate mass transport of dissolved constituents. In this study, K_z was estimated with thermal profile data using the flux-gradient method (Jassby & Powell 1975), simplified in equation F.6.

$$\frac{\partial T}{\partial t} = \frac{\partial}{\partial z}\left(K_z \frac{\partial T}{\partial z}\right) \tag{F.6}$$

The equation was simplified by removing terms accounting for heat sources and horizontal currents, which are believed to have little effect on thermal mixing in lake

hypolimnia (Powell & Jassby 1974). The $\partial T/\partial t$ term requires use of temperature profiles at two dates, thus the K_z value calculated with this method is input into the model at each time-step between the dates when temperature observations occurred. To account for the variation in K_z with depth, the diffusivity coefficient is integrated over the vertical range of the hypolimnion (Equation F.7). Depth-integrated K_z estimates varied throughout the year, ranging from 0.0017 – 0.0143 cm^2/s (Appendix F5).

$$\frac{\partial}{\partial z}\int_{z_{bw}}^{z_{ls}} K_z dz \tag{F.7}$$

Using the integrated K_z term as a diffusion coefficient yields equation F.8, which estimates flux across the limnetic surface.

$$J_{ls} = \left(\frac{1}{z_{ls} - z_{bw}}\right)(C_e - C_h)\int_{z_{bw}}^{z_{ls}} K_z dz \tag{F.8}$$

Appendix F5: Model Input Data

The following tables report the input data used to define the variables used for modeling of Lake McQuade (Appendix F). Two variables included in the coefficient matrices (Appendix G) were not defined by input data: Flow rate (Q), which was calculated using lake residence time. Lake residence time was allowed to be adjusted for the Mg model for optimization. The mass loss rate term in the sulfate model was not defined, but rather solved for using model optimization with measured field data.

Table F.2. Input data describing limnetic surface

date	thermocline depth (z_{ls}) [m]	K_z [cm^2/s]	A_{ls} [m^2]
6/5 - 6/14	3.5	0.0082	220,380
6/15 - 6/24	2.7	0.0143	363,980
6/25 - 7/2	2.7	0.0017	363,980
7/3 - 7/9	2.4	0.0019	424,300
7/10 - 7/16	2.4	0.0029	424,300
7/17 - 7/24	2.4	0.0029	424,300
7/25 - 7/31	2.4	0.0047	424,300
8/1 - 8/6	3.5	0.0031	220,380
8/7 - 8/14	3.5	0.0022	220,380
8/15 - 8/21	3.7	0.0023	192,620
8/22 - 8/29	3.7	0.0022	192,620
8/30 - 9/5	3.7	0.0022	192,620
9/6 - 9/10	3.7	turnover	192,620

Table F.3. Input data describing lake geometry

date	thermocline depth (z_{ls}) [m]	V_e [m^3]	V_h [m^3]	$A_{sed\|e}$ [m^2]	$A_{sed\|h}$ [m^2]
6/5 - 6/14	3.5	1,843,679	154,137	530,624	220,392
6/15 - 7/2	2.7	1,624,250	373,566	387,016	364,000
7/3 - 7/31	2.4	1,504,116	493,700	326,693	424,323
8/1 - 8/14	3.5	1,843,679	154,137	530,624	220,392
8/15 - 9/10	3.7	1,877,265	120,551	558,385	192,631

Table F.4. Input data describing inlet concentrations

date	C_{in} (Mg) [mg/L]	C_{in} (Sulfate) [mg/L]
6/5 - 7/5	30	60
7/6 - 10/15	72	143